Reduced-Complexity Transceiver Signal Processing Algorithms for Massive MIMO and mmWave Cellular Systems

by

Maliheh Soleimani

A thesis submitted in partial fulfillment of the requirements for the degree of

Doctor of Philosophy

in

Communications

Department of Electrical and Computer Engineering
University of Alberta

Abstract

Future broadband cellular networks will have to accommodate explosively growing demand for high bit rate data services. The adoption of multiple-input multiple-output (MIMO) designs with large antenna arrays (also known as massive MIMO) and the use of millimeter wave (mmWave) frequency bands are considered as two key techniques to satisfy these demands. The motivations of moving to mmWave frequencies and employing large antenna arrays are respectively the much wider bandwidths that become available and the higher spectral efficiencies that are enabled. While potentially providing great advantages, both of these technologies are still in an exploratory research stage, focused on developing efficient algorithms to address the challenges that their implementation faces. Issues such as channel estimation, radio frequency (RF) hardware constraints, computational complexity, cost and power consumption have yet to be fully addressed. The key objectives of this research are the design and performance evaluation of the following. First, a low complexity and simplified path selection algorithm, based on bipartite graphs for massive MIMO channel under sparsity condition in massive MIMO systems, is proposed and analyzed. Second, a joint design of user clustering and pre-processing algorithms that are suitable for spatially sparse massive MU-MIMO downlink channels is proposed where a two-layer beamforming scheme is performed to both minimize inter-beam and inter-user interference, and maximize spatial multiplexing gain. Third, a projection-based hybrid precoding algorithm for hybrid transceiver in mmWave MIMO systems is proposed for both fully-connected and

partially-connected structures. Finally, a robust precoder for massive MIMO systems employing single-RF-chain load-modulated transmitters that represents a promising alternative to hybrid digital-analog precoders to achieve reduced-complexity hardware implementation is studied.

Preface

This thesis contains contents that appear in the following publications.

In Chapter 3, we consider the downlink transmission over a sparse massive MIMO channel and propose a novel path selection algorithm to maximize sum rate. We introduce a bipartite graph, which connects angles of departure (AoDs) to users in the beam-space domain. Then, we formulate an optimization problem aiming to maximize sum rate by selecting edges in this graph in a greedy fashion. The content of Chapter 3 has been published in the following conference paper:

- M. Soleimani, M. Mazrouei-Sebdani, W.A. Krzymień, and J. Melzer, "A path selection algorithm for sparse massive MIMO channels," in *Proc. IEEE 50th Asilomar Conf. on Signals, Systems, and Computers*, Pacific Grove, USA, Nov. 2016, pp. 208–212.

In Chapter 4, we propose a two-layer beamforming scheme for downlink transmission over massive MIMO sparse beam-space channels. The first layer employs a bipartite graph to dynamically group users in the beam-space domain; the aim is to minimize inter-user interference while significantly reducing the effective channel dimensionality. In the second layer, a digital baseband linear MIMO precoding is performed to maximize spatial multiplexing gain and system throughput. The content of Chapter 4 has been published in the following journal paper:

- M. Soleimani, M. Mazrouei-Sebdani, R. C. Elliott, W. A. Krzymień, and J. Melzer, “Simplified user grouping algorithm for massive MIMO on sparse beam-space channels,” *IEICE Trans. Commun.*, vol. E102–B, no. 3, pp. 623–631, Mar. 2019.

In Chapter 5, we consider transmitter precoding and receiver combining in mmWave systems with large antenna arrays in a partially-connected structure, then we make use of projection algorithms to greatly simplify the design problem of digital baseband and analog radio frequency precoders into two optimization sub-problems, whose optimal solutions can be found. We also develop a channel estimation algorithm to estimate mmWave channel parameters via a codebook of beamforming vectors obtained through the discrete Fourier transform design. The content of Chapter 5 has been published in the following conference paper:

- M. Soleimani, R. C. Elliott, W. A. Krzymień, J. Melzer, and P. Mousavi, “Hybrid beamforming and DFT-based channel estimation for millimeter wave MIMO systems,” in *Proc. 28th Int. Symp. on Personal, Indoor and Mobile Radio Commun. (PIMRC)*, Montreal, Canada, Oct. 2017, pp. 1–7.

In Chapter 6, we propose a matrix factorization approach to tackle the problem of hybrid precoding-combining design while incorporating a simplified user clustering algorithm employing the discrete Fourier transform. The content of Chapter 6 has been published in the following journal paper:

- M. Soleimani, R.C. Elliott, W.A. Krzymień, J. Melzer, and P. Mousavi “Hybrid beamforming for mmWave massive MIMO systems employing DFT-assisted user clustering,” *IEEE Trans. Veh. Tech.*, vol. 69, no. 10, pp. 11646–11658, Oct. 2020.

In Chapter 7, we discuss the design of a precoder for massive MIMO with a single-RF-chain transmitter having an instantaneous total power constraint that is robust under channel uncertainty. The content of Chapter 7 has been published in the following journal paper:

- M. Soleimani, M. Mazrouei-Sebdani, R.C. Elliott, W.A. Krzymień, and J. Melzer, “Robust precoder design for massive MIMO with peak total power constrained single-RF-chain transmitters,” *IET Commun.*, vol. 11, no. 17, pp. 2667–2672, Nov. 2017.

Acknowledgment

First, and foremost, I would like to express my deep and sincere gratitude to my supervisor Dr. Witold A. Krzymień for his patience, encouragement, and technical guidance throughout my program. The truth is that this work would not have been done without his support on both the technical and personal levels. I would also like to express my deepest appreciation for my (deceased) co-supervisor Dr. Pedram Mousavi who tragically died (together with his wife and daughters) in the shootdown of the Ukraine International Airlines Flight 752.

I would also like to thank the members of my candidacy examination committee Dr. Ivan Fair, Dr. Masoud Ardakani, and Dr. Hai Jiang, as well as the members of my final PhD examination committee Dr. Tho Le-Ngoc from McGill University, Dr. Chintha Tellambura, Dr. Ivan Fair, and Dr. Hai Jiang for reviewing my thesis and their helpful comments.

I would like to express my gratitude for the financial support that I received from the Natural Sciences and Engineering Research Council (NSERC) of Canada, TR*Labs*, and DTI (Design, Test and Integration, a subsidiary of Testforce Systems Inc). This work has also been facilitated by the computing resources of Information Services and Technology (IST) at the University of Alberta, WestGrid, and Compute/Calcul Canada.

I would also like to express my thanks to Dr. Mahmoud Mazrouei-Sebdani and Dr. Robert C. Elliott for their consistent advice and guidance throughout my program. All of their comments and feedback have been tremendously beneficial and insightful.

Table of Contents

List of Figures

List of Symbols

x, X	Scalar (italics)
$\mathbf{x}$	Vector (lowercase boldface)
$\mathbf{X}$	Matrix (uppercase boldface)
$\mathbb{E}_{\mathbf{X}}\cdot$	Expected value / expectation over $\mathbf{X}$ (subscript may be omitted)
$\mathbf{I}_N$	$(N \times N)$ identity matrix (subscript may be omitted in general case)
$\mathbf{X}^*$	Conjugate of matrix $\mathbf{X}$ (note also smaller * than above)
$\mathbf{X}^T$	Transpose of matrix $\mathbf{X}$
$\mathbf{X}^H$	Hermitian (conjugate) transpose of matrix $\mathbf{X}$
$\mathbf{X}^{-1}$	Inverse of square matrix X
$\mathbf{X}^\dagger$	Moore-Penrose pseudoinverse of matrix $\mathbf{X}$
$\mathbf{X}^{1/2}$, $\mathbf{X}^{-1/2}$	Square root and inverse square root of $\mathbf{X}$
$\lvert\mathbf{X}\rvert$	Determinant of matrix $\mathbf{X}$
$\mathrm{Tr}\left(\mathbf{X}\right)$	Trace of matrix $\mathbf{X}$
$\mathrm{rank}\left(\mathbf{X}\right)$	Rank of matrix $\mathbf{X}$
$\lVert\mathbf{X}\rVert_F$	Frobenius norm of $\mathbf{X}$
$\lVert\mathbf{X}\rVert_F^2$	Squared Frobenius norm of $\mathbf{X}$
$\lVert\mathbf{X}\rVert_2^2$	Squared 2–norm of $\mathbf{X}$
$\mathbf{X} \succeq 0$	$\mathbf{X}$ is positive semidefinite
$\mathrm{blkdiag}\left(\mathbf{X}_1, \cdots\right)$	A block-diagonal matrix formed from the matrices $\mathbf{X}_1, \cdots$
$\mathcal{U}$	A set of numbers
$\mathcal{C}$	Set of complex numbers
$\lceil\cdot\rceil$	Ceiling function
$\left(\mathbf{X}\right)_{i,:}$	i$^{\text{th}}$ row of matrix $\mathbf{X}$
$\left(\mathbf{X}\right)_{i,j}$	Element (i, j) of matrix $\mathbf{X}$
$\lvert\mathcal{U}\rvert$	Cardinality of set
$\emptyset$	Empty set
$\otimes$	Kronecker product
$\circ$	Hadamard product
$\mathcal{O}\left(\cdot\right)$	"Big-O" ("order of") notation

List of Acronyms

4G	Fourth generation of cellular systems and networks
5G	Fifth generation of cellular systems and networks
ADC	Analog-to-digital converter
AoA	Angle of arrival
AoD	Angle of departure
BS	Base station
CoMP	Coordinated multipoint transmission/reception
CS	Compressed sensing
CSI	Channel state information
DAC	Digital-to-analog converter
DFT	Discrete Fourier transform
FDD	Frequency division duplexing
ICI	Inter-cell interference
IEEE	Institute of Electrical and Electronics Engineers
ISI	Inter-symbol interference
JSDM	Joint spatial division and multiplexing
LAN	Local Area Network
LTE	Long-Term Evolution of 3G cellular systems & networks standard
LTE-A	Long-Term Evolution Advanced of 3G cellular systems & networks standard (also known as 4G)
LOS	Line-of-sight
MIMO	Multiple-input multiple-output
MMSE	Minimum mean–square error
mmWave	Millimeter wave
MSE	Mean square error
MUI	Multiuser interference
MU-MIMO	Multiuser MIMO
NLOS	Non-line-of-sight
PAPR	Peak-to-average power ratio
QCQP	Quadratic constraint quadratic programming
RF	Radio frequency
SDP	Semi-definite programming
SISO	Single-input single-output
SNR	Signal-to-noise ratio
SINR	Signal-to-interference-and-noise ratio

SVD	Singular value decomposition
TDD	Time division duplexing
ULA	Uniform linear array
ZF	Zero-forcing

Chapter 1

Introduction

1.1 Motivation

The commercial wireless communication systems and standards have significantly advanced over the decades, since the first generation (1G) of cellular systems were introduced in 1970s. The 1G systems that were initially commercially deployed in 1979 were analog and provided only voice services. Faster than expected growth in the number of subscriptions throughout 1980s overwhelmed the capacity of 1G systems in North America. In other parts of the world (especially in Europe) a large number of incompatible 1G cellular systems became a big problem especially for international business. To overcome the limitations of 1G systems, the second generation (2G) digital cellular systems were developed in the early 1990s. The 2G systems offered voice and basic data services like short message service (SMS). The third generation (3G) cellular systems were first deployed in the early 2000s, to support simultaneous use of speech and data services and higher data rates. To meet ever-increasing data/video service demands, the fourth generation (4G) cellular systems were first launched in 2010 with mobile broadband Internet access. The gradual deployment of the fifth generation (5G) systems began in 2019. The objectives of 5G cellular systems are varied, however they are expected to support three major use cases: enhanced mobile broadband (eMBB), massive machine type communications (mMTC), and ultra-reliable-and-low-latency communications (uRLLC) [1]. Additionally, 5G systems are designed to be future-proof to address all the 5G use cases and rapidly customized services that cater to the needs of multiple industries. Network slicing technology is pivotal for the implementation of 5G networks. Network slicing allows multiple virtual networks to be created on top of a common shared physical infrastructure [2]. Functionally, this means that each virtual network can provide a specific subset of network capabilities and characteristics that serve the business requirements of a specific customer. Eventually, 5G networks will be designed to deliver the performance standard needed for massive IoT and enable a fully connected world [3]. The work in this thesis focuses mainly on the eMBB use case.

With its explosive growth, wireless communication technology has fundamentally changed the way we communicate, and has become an integral part of our everyday life with the total number of mobile subscriptions around 7.9 billion in the first quarter of 2019, and estimation of 8.3 billion subscribers by the end of 2024 [4]. As technology has advanced, the impact of wireless communication in different aspects of our lives such as work, education, and entertainment has immensely expanded. Nowadays, modern society finds itself immersed in wireless networking, as much of the population routinely uses cellular networks, wireless local area networks, and personal data networks, most of which have been developed and deployed over the past three decades. The remarkable popularity of these technologies causes device makers, infrastructure developers, and manufacturers to continually seek sophisticated and efficient techniques for more advanced product offerings. Cellular communications standards are evolving to accommodate the explosive increase in the number of devices, demanding high-speed wireless services, such as phones, tablets, sensors, connected vehicles, etc. The number of active mobile broadband subscriptions per 100 inhabitants continues to grow strongly, with an 18.4 percent year-on-year growth as of 2019 [5]. Meeting all these demands is a formidable task due to the following constraints. 1) radio resources such as available spectrum are limited especially in the most desirable spectrum below 6 GHz which is heavily congested; 2) the transmit power is a limiting factor in both users' battery devices, and the base station (BS) due to interference to adjacent cells. To improve the spectral efficiency and energy efficiency simultaneously, the wireless networks need to be significantly restructured.

1.1.1 MIMO Wireless Communications

To combat the limitation of radio resources to some degree, multiple-input multiple-output (MIMO) techniques were introduced where the transmitters and receivers are equipped with multiple antennas [6–8]. Development of MIMO systems is very promising, since the key additional gains in performance stem from the additional spatial degrees of freedom, which can be exploited in different ways. These additional degrees of freedom can be deployed as diversity solution to form more reliable links between the transmitter and the receiver. Diversity can be achieved by having antenna elements spaced far enough apart from each other to experience independent fading propagation paths, so that the copies of signals can be processed to create a stronger link. Spatial multiplexing is a more important way to take advantage of MIMO systems properties, where multiple data streams are sent from different antennas. This method increases the capacity of the system by taking advantage of rich scattering in the radio channel. The additional spatial degrees of freedom offer the opportunity to improve system capacity without increasing the required spectrum [9]. Roughly speaking, in a single-user MIMO (SU-MIMO) system where transmitter and receiver are equipped with N_t and N_r antennas, respectively, up to $\min(N_t, N_r)$-fold increase in capacity (bits per channel use) is possible. This performance is limited to richly scattering propagation environments.

Introduction of multiuser MIMO (MU-MIMO) systems further expanded potential network capacity gains due to MIMO spatial multiplexing [10]. Exploiting spatial multiplexing techniques makes it possible to serve multiple users within the same bandwidth and at the same time. In this system, the transmitter is equipped with N_t antennas, and there are K single-antenna users, which exhibit same behavior as SU-MIMO system in terms of capacity where $\min(N_t, K)$-fold increase in capacity can be achieved. However, MU-MIMO systems must overcome new challenges to deliver potential improvements. Since users are autonomous and normally do not cooperate with each other, data streams sent to them on the downlink channel must be separated at the BS transmitter via advanced signal processing techniques, known as precoding. This requires the transmitter to be aware of the channel state information (CSI) via some mechanisms such as channel estimation and feedback. Furthermore, usually there are more users requesting service than the available resources in the system to be served simultaneously. Therefore, user scheduling algorithms in addition to full CSI are necessary to achieve the spatial multiplexing gain of N_t, obtained by system sending data streams to N_t selected users out of $K(K > N_t)$ users. If each user is equipped N_k antennas, the total number of degrees of freedom for multiuser diversity is KN_k with extra gain of $\log\log(KN_k)$ [10].

As mentioned above, having knowledge of CSI is essential to achieve spatial multiplexing gain promised by MU-MIMO. However, such knowledge comes at a price, which is allocation of resources for channel estimation and feedback. Studies [11, 12] have shown that in MIMO transmission, where neither the transmitter nor the receiver know the channel, the spatial multiplexing gain is limited by $\min(N_t, N_r, T/2)$ where T is the fading coherence block over which the channel response can be approximated as constant and considered flat fading. This implies that increasing the number of antennas does not always increase the capacity, but is bounded by $T/2\log(SNR) + \mathcal{O}(1)$.

Finally, to achieve all the aforementioned advantages signal-to-interference-plus-noise ratios (SINRs) must be high enough at the mobile user and network node receivers. To establish high quality links, increasing transmit power is not an option due to the increased interference to the neighboring cells[1], which makes cellular systems interference limited. Hence, it is crucial to mitigate inter-cell interference (ICI). Since BSs are connected via high-speed backhaul links, coordinated multipoint transmission/reception (CoMP) techniques relying on coordination of BSs are considered to mitigate ICI, potentially resulting in great capacity improvement on the downlink of cellular networks [13–17].

Generally, exploiting MU-MIMO offers key advantages such as: i) better coverage through beamforming resulting in higher received signal power, ii) improved link reliability, through diversity schemes, iii) higher capacity, through spatial multiplexing, and iv) improved estimation of directional information, due to high resolution of antenna arrays. As a physical layer performance booster, the MIMO concept has been incorporated into wireless broadband standards such as IEEE 802.11n, IEEE 802.11ac, and Long-Term Evolution-Advanced (LTE-A). The latter allows for up to eight antennas at BS and two to four antennas at the user's device [18]. Fig. 1.1 shows examples of potential deployments of MIMO systems.

1.1.2 MIMO Precoding and Beamforming

Precoding and beamforming for MU-MIMO systems are solutions essential to provide reliable high data rate communication in wireless downlink channels. In these techniques, the downlink MIMO channel is decomposed into parallel independent single user MIMO channels so that the multiuser interference is canceled and then single user schemes can be applied over each independent channel. It is known that dirty paper coding (DPC) is the optimal algorithm that can achieve sum capacity by successively removing each user's interference on each other [21–23]. Therefore, no user will suffer from interference caused by prior users. However, this technique is highly complex and difficult to implement in practice. In practical situations suboptimal methods, compared to DPC, but less complex

[1]The signal power and the interference power both increase by about the same proportion, when increasing the transmit power. Therefore, in an interference-limited system, the SINR stays about the same.

a) b)

Figure 1.1: Examples of potential deployments of MIMO systems: a) A cellular BS tower with multiple transceiver antennas [19]. b) A wireless LAN router with multiple transceiver antennas [20].

are of interest. These suboptimal solutions can be linear or non-linear; e.g., Tomlinson Harashima [24, 25] and vector perturbation [26] are non-linear precoding methods, while zero-forcing (ZF) and block diagonalization (BD) [27] are linear.

1.2 MIMO Goes Massive

In both SU-MIMO and MU-MIMO, theoretically, the more antennas the transmitter and/or receiver are equipped with, the larger the scale on which the spatial domain can be exploited, meaning more degrees of freedom in the wireless channel. This can lead to better performance. In the last decade, massive MIMO (also known as large-scale antenna array) systems, which essentially are MU-MIMO systems with a much larger number of antennas at the network nodes (BSs) have been proposed [28–30]. This technology is capable of offering high spectral and energy efficiencies on a larger scale than conventional MU-MIMO systems by using many more antenna elements at the BSs (generally on the

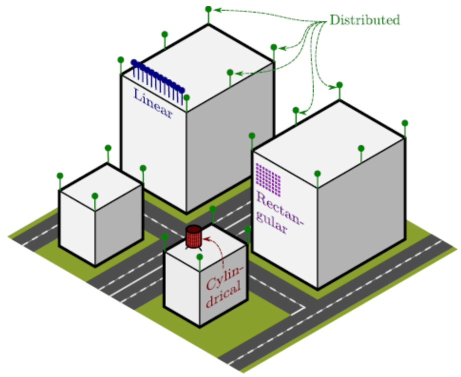

Figure 1.2: Illustration of possible deployments of massive MIMO antenna arrays [30].

order of hundreds) than the number of mobile users (by about an order of magnitude or more) that are sent data streams at any given time. Massive MIMO system involves a very large number of antennas at the BS simultaneously transmitting data streams to a smaller number of single-antenna mobile users. Antennas can be co-located in a linear, planar or cylindrical structure, or can be placed in a distributed manner, or possibly some combination thereof, as shown in Fig. 1.2.

In such setting, the number of users that can be served is limited, not by the number of BS antennas, but rather by our ability to acquire accurate and timely channel state information (CSI) for the large number of antennas that we have in the system. In general, the CSI is estimated through measurements of pilot sequences, and depending on the operating mode of the system different complications emerge. In massive MIMO, time division duplexing (TDD) operation seems a natural choice rather than frequency division duplexing (FDD) mode. This is driven by the fact that to estimate the downlink channel in the FDD mode, where uplink and downlink transmissions take place simultaneously in widely separated frequency bands, the number of pilot signals needs to be proportional to the number of antennas [31], which is unrealistic for the large scale arrays used in massive MIMO. It also creates an overwhelming amount of overhead in the uplink for feedback. Therefore, operation of massive MIMO systems in TDD mode is more realistic.

In the TDD mode reciprocity of radio channels at the same carrier frequency is exploited. If the coherence time of the radio channel is much larger than the frame duration of the transmitted digital signal, the uplink and downlink radio channels are essentially the same. Thus, massive MIMO systems use the acquired channel estimates on the uplink for both uplink combining and downlink precoding. In TDD mode, the number of orthogonal pilot sequences is proportional to the number of users, and they should fit in the frame duration of the signal. However, the length of this frame is limited by the coherence time of the radio channel, which limits the number of pilot sequences [31]. Also, when the same band of frequencies is reused among cells, of necessity the same orthogonal pilot sequences are also reused[2]. This results in so called pilot contamination that leads to channel estimation errors. There are numerous works in the literature that have studied different techniques to mitigate the interference due to pilot contamination [32–36].

Furthermore, the use of large antenna arrays at the BS introduces significant architectural and hardware implementation differences in the system design compared to conventional MU-MIMO systems. The current technology deploys a fully digital baseband precoder and a separate radio frequency (RF) chain, including a digital-to-analog (DAC) converter, mixer and a power amplifier (PA), for each antenna element. This leads to significant precoding processing complexity, power consumption and physical space challenges when the number of antennas is large. Hence, such deployment necessitates investigation of massive MIMO architectures and precoding algorithms that significantly reduce the number of RF chains and digital components to decrease the complexity and cost of the system. There exist many different promising solutions in the massive MIMO literature that will be discussed later in this chapter.

[2] The lack of sufficient orthogonal pilot sequences means that semi-orthogonal pilot sequences could be used as an alternative, but this leads to the same kinds of problems.

1.3 Millimeter Wave Massive MIMO

One obvious approach to increasing throughput of future wireless systems is to use much larger bandwidth for transmission. Not much additional bandwidth is available at frequencies below 6 GHz (the most desirable spectrum for wireless communications), but significant amounts of it are available in the millimeter wave (mmWave) range. Communication at mmWave carrier frequencies is receiving great interest from academia, industry, and government for future wireless systems (5G and beyond) [37]. In fact, mmWave technology is one of the promising candidates to facilitate future generation of cellular systems and address the available spectrum shortage. In mmWave communications, spectrum from about 30 GHz to 300 GHz with large available bandwidth potentially can be used, whereas most current commercial wireless systems operate at the carrier frequencies below 6 GHz. For instance, at operating frequency 28 GHz, channels with 800 MHz bandwidth are available, compared to bandwidths up to 20 MHz in LTE, and 100 MHz in LTE-Advanced (LTE-A) [38], [39]. Although the initial commercially available mmWave products are intended for short-range indoor communications, the potential of mmWave communications for cellular systems has been recognized [37], [40] and its capability to facilitate high throughput has been demonstrated. Also, a coverage range of more than 200 m even in non-line of sight (NLOS) situations has been reported in [38, 41, 42]. From a practical point of view, innovative signal processing techniques to make mmWave communications feasible are essential [43]. The reasons for this are: i) due to operation at higher frequencies and large bandwidths new hardware constraints emerge, ii) the mmWave channel characteristics are different, iii) to attain large beamforming gains, large antenna arrays need to be deployed, which introduces new circuit implementation and power consumption challenges.

In conventional MU-MIMO systems using a moderate number of antenna elements, precoding is typically done through digital precoders at baseband. This allows adjustment of both the amplitude and phase of the transmitted signal. Such precoding requires RF chain for each antenna element. Deploying such structures in large-array mmWave MIMO systems is not practical due to the very large number of antennas. Additionally, analog components like phase shifters are imperfect and their impairments need to be modeled and dealt with to yield good performance. Furthermore, channel models in mmWave frequencies are very different from those of lower frequency ones, due to the fact that the propagation environment has a different effect on smaller wavelength signals. At mmWave frequencies, path loss is much larger, the number of propagation paths is limited, and diffraction tends to be lower [43]; wireless channels become highly directional. Also, the size of the arrays discussed for mmWave communication may be large at both ends, which results in applying different MIMO communication techniques due to the different channel characteristics and hardware constraints. The combined complications of all these factors has a far-reaching impact on the design and signal processing of mmWave communication systems that are yet to be addressed. In the following, we aim to provide a brief overview of existing techniques to cope with these challenges.

Both massive MIMO and mmWave systems are intertwined with the concept of using large antenna arrays to deliver the potential improvements. However, the RF-related costs grow linearly with the number of antennas. To address the challenge of reducing the number of RF chains, extensive studies have been carried out on different structures. One possible structure is using only analog or RF beamforming where precoding is performed by a network of digitally controlled phase shifters that are connected to one RF chain, e.g. as in [44–47]. In such a structure, analog phase shifters, imposing a unit constant modulus constraint on the elements of the RF beamformer, are typically used. While the work in [44–47] does not consider massive MIMO systems, one can adopt the system model proposed there. The concept of selection of a subset of antennas can also result in reducing the number of RF chains for both massive MIMO and mmWave communications. In [48], the concept of antenna selection, which is implemented using analog switches, has been introduced for MIMO systems. Intuitively, antenna selection cannot achieve full spatial diversity gain in correlated environment due to the use of a subset of antennas/channels. A promising solution to these challenges lies in the concept of hybrid transceivers, which make use of analog beamformers in the RF domain, together with digital beamforming in baseband [49]. In this structure, the number of RF chains is only lower-limited by the number of data streams that are to be transmitted. Despite reducing the number of RF chains, even assuming full CSI at the BS, the design of the optimal analog and digital beamformers is difficult. The main difficulties are: i) coupling between the analog and digital beamformers at both ends, and ii) implementation of analog RF beamformers via phase shifters imposes constraints on the design of the elements of these matrices. In [50], a nearly-optimal low-complexity hybrid precoding scheme, in particular, RF precoding and combining algorithms for wideband multiuser mmWave systems has been proposed. The scheme is designed to maximize energy efficiency. In [51], an energy efficient user clustering hybrid precoding in non-orthogonal multiple access systems has been proposed where an enhanced K-means clustering algorithm has been deployed to achieve a fast convergence in user clustering. [52] contains a comprehensive overview of issues and challenges relevant to the hybrid transceivers for massive MIMO. It should be noted that hardware constraints for mmWave communication systems are not only limited to just the number of RF chains. Operating at higher frequencies and larger bandwidths requires new developments in the RF hardware designs of antennas, semiconductor device basics, and digital baseband issues related to analog-to-digital and digital-to-analog converters. [38] considers the hardware design challenges at mmWave carrier frequencies in more detail.

In [53, 54], joint spatial division and multiplexing (JSDM) technique has been introduced, in which precoding is implemented in two stages. In the first stage, by exploiting antenna correlation users are partitioned into groups, which have approximately the same channel covariances. This stage can be implemented in analog hardware. Then, the second stage performs a standard MU-MIMO precoding for spatial multiplexing on the effective channel obtained after the first stage. The MU-MIMO precoding stage can be implemented in standard digital baseband processing. Therefore, JSDM can lend itself to a hybrid beamforming implementation and possibly, in specific propagation environments, can enable FDD mode of operation for massive MIMO systems.

Additionally, in [55–58] a single-RF-chain transmitter for massive MIMO systems has been proposed to address the challenge of a large number of RF chains in implementation of large-antenna-array systems. This transmitter includes a single power amplifier and does not require any mixer. For each antenna element, data modulation is performed using adjustable two-port networks that control the currents on the individual elements. Unlike for the traditional voltage modulation, where the modulated signal drives the power amplifier, in this single-RF-chain setting the output of the power amplifier has a constant envelope, thus ensuring high power efficiency. In this new setting, unlike for voltage modulation, whatever arbitrary modulation desired is performed by adjusting the impedance of the loads. The load modulator network, which may consist of varactors or pin-diode switches, is configured such that the signals on the antenna elements become proportional to the desired signals. [59] has implemented a single-RF-chain transmitter with 4-port beam-space MIMO based on the load modulator technique. In [60], a minimum mean-square error (MMSE) precoding technique has been proposed for the single-RF-chain transmitter with load modulators. Obviously, deploying a single-RF-chain transmitter reduces the hardware cost, complexity and power consumption significantly.

1.4 Thesis Objectives and Organization

Massive MIMO and mmWave wireless systems are promising technologies that could allow the high capacity target of next generation cellular systems to be realized. Scaling up to large-antenna-arrays in massive MIMO design increases both power and spectral efficiencies, while mmWave wireless communication systems exploit a much wider bandwidth than sub 6 GHz systems. Unfortunately, the large number of antennas required by these technologies introduces new hardware constraints, potentially prohibitive hardware cost and energy consumption, and CSI acquisition issues.

This thesis focuses on the development of reduced-complexity transmitter/receiver signal processing techniques and algorithms for future broadband cellular systems. Particular attention is devoted to the development of cost-efficient implementable signal processing techniques for massive MIMO that can cope with implementation imperfections and channel uncertainty. These advances were facilitated by the completion of four research objectives : 1) analysis of a low complexity and linear precoding method based on bipartite graphs under sparsity condition in massive MIMO systems; 2) joint design of user clustering and pre-processing algorithms that are suitable for spatially sparse massive MIMO channels; 3) development of hybrid precoding-combining algorithms for partially-connected and fully-connected transceivers that make implementation of massive MIMO feasible; 4) investigation of robust precoding algorithms for single-RF-chain transmitters for massive MIMO systems.

In this section, the organization of the thesis is discussed and we outline the contributions of each chapter.

- Chapter 2 begins by examining the background and details of MIMO systems more closely. We discuss single-user and multiuser MIMO systems, including details of linear precoding methods to handle multiuser interference. We also give an overview of massive MIMO concepts and advantages and disadvantages of massive MIMO in more detail.

- In Chapter 3, we propose a novel path selection algorithm for sparse massive MIMO channels, where each user receives its signal via only a few resolvable paths. With a uniform linear array consisting of a large of number of antenna elements and discrete Fourier transform (DFT) beamforming, we have considered a virtual channel representation in the beam-space domain to capture channel sparsity, where each user's path lies within a bin of angles of departure. We have associated a sparse bipartite graph with this multiuser setting, where independent user and angular bin nodes are connected by edges, if there are physical signal paths between a given user and the transmitter at the angle(s) of departure in question. Next we have formulated an optimization problem aiming to maximize sum rate by selecting edges in this graph in a greedy fashion. Unlike coarse user selection algorithms, our fine path selection algorithm is able to take advantage of available multipath and multiuser diversity more efficiently, thus resulting in higher throughput.

- In Chapter 4, we tackle the problem of user grouping for sparse beam-space massive MIMO channels. First of all, we have no prior knowledge of the possible number of user groups/clusters, and secondly choosing an arbitrary number of groups can limit the performance of the system without considering multiuser and inter-beam interference. Herein, we propose a novel and simplified user grouping scheme, which is our primary contribution. Inspired by the concept of path selection and the bipartite graph introduced in Chapter 3 we partition the set of users into groups corresponding to the angular bins that they occupy. In this approach, we examine each angular bin, which is connected to a set of user nodes via edges (resolvable paths). Users that receive a signal from the same angular bin are grouped together. Our proposed algorithm takes advantage of the sparsity of massive MIMO channels to achieve spatial multiplexing and cope with the interference resulting from overlapping multipath components. Specifically, the MIMO pre-processing at the BS is partitioned into a DFT beamforming layer and a linear MU-MIMO precoding layer. The DFT beamformer creates orthogonality among groups of users in the beam-space domain to combat inter-beam interference, while the linear MU-MIMO precoder achieves spatial multiplexing within groups of users. In this algorithm, the size of user groups is not fixed. In fact, users will be dynamically partitioned into groups corresponding to the angular bins that they occupy. This simplified user grouping and two-layer pre-processing algorithm offers the possibility of a hybrid implementation, where the DFT beamformer is implemented in the analog RF domain via phase shifters, while the MU-MIMO precoder is implemented digitally. Complexity of the latter is significantly reduced compared to a precoder implemented fully in the digital domain as in conventional MU-MIMO systems.

- In Chapter 5, we describe a projection hybrid precoding algorithm for a hybrid precoding-combining transceiver in mmWave massive MIMO systems. The algorithm is designed for the partially-connected structure since it employs fewer phase shifters, which is attractive in terms of complexity and energy efficiency. Inspired by the principle of matrix factorization, we have made use of projection algorithms to greatly simplify the design problem of digital baseband and analog RF precoders into two optimization subproblems whose optimal solutions can be found. In the same chapter, we propose an efficient channel estimation algorithm for mmWave systems with hybrid architectures. Leveraging the mmWave channel characteristics, we develop a sparse formulation of the mmWave channel estimation problem. Based on this formulation, we propose a DFT-based channel training algorithm that estimates the defining parameters of the multi-path mmWave channels.

- We then extend the proposed projection hybrid precoding-combining algorithm to a multiuser massive MIMO system at mmWave frequencies in Chapter 6. We also formulate the design problem for frequency-selective channels using an orthogonal frequency division multiplexing (OFDM). The problem of hybrid precoding design is formulated in part as a DFT-assisted user clustering problem to solve the overall problem for both fully-connected and partially-connected structures incorporating their respective limitations.

- As a solution to the implementation complexity of massive MIMO systems, in Chapter 7, we propose the design of a precoder for massive MIMO with a single-RF-chain transmitter having an instantaneous total power constraint that is robust under channel uncertainty. To reflect realistic restrictions in our design, we consider the peak total transmitted power rather than the average power constraint. Also, we consider imperfect CSI and model the uncertainty region as a bounded one, which is a reasonable assumption. In this transmitter structure, there is only one power amplifier and load modulation rather than voltage modulation is used to generate the desired signals on the antenna elements. We demonstrate that when a very simple fixed equalizer is used at all user terminals, the problem of minimizing the mean-square error of the received signals at user terminals under the worst-case channel uncertainty can be transformed into a convex optimization problem.

- Finally, in Chapter 8 we summarize the contributions of the thesis and give some directions for possible future work.

Chapter 2

Background

Although the focus of this thesis is on massive MIMO systems, understanding the MU-MIMO theory is instrumental in understanding the fundamental nature and limits of gains associated with deploying large number of antennas in wireless communication systems. Hence, we begin with the concept of MIMO and build upon that concept to formulate the challenges associated with massive MIMO systems.

2.1 MIMO Systems

Let us begin with a simple SU-MIMO system, as shown in Fig. 2.1, where a BS equipped with N_t antennas communicates with a single user that has N_r antennas. Accordingly, the received signal at the user terminal can be written as:

$$\mathbf{y} = \mathbf{H}\mathbf{x} + \mathbf{n}, \tag{2.1}$$

where $\mathbf{x} = [x_1, x_2, \cdots, x_{N_t}]^T$ is the transmitted signal vector, $\mathbf{y} = [y_1, y_2, \cdots, y_{N_r}]^T$ is the received signal vector, and $\mathbf{H} \in \mathcal{C}^{N_r \times N_t}$ is the channel matrix between the transmit and receive antennas. $\mathbf{n} \in \mathcal{C}^{N_r \times 1}$ is the noise vector with independent and identically distributed (i.i.d.) elements, circularly symmetric, complex Gaussian random variables with zero mean and variance of σ_n^2. Furthermore, the channel matrix $\mathbf{H}$ is composed of

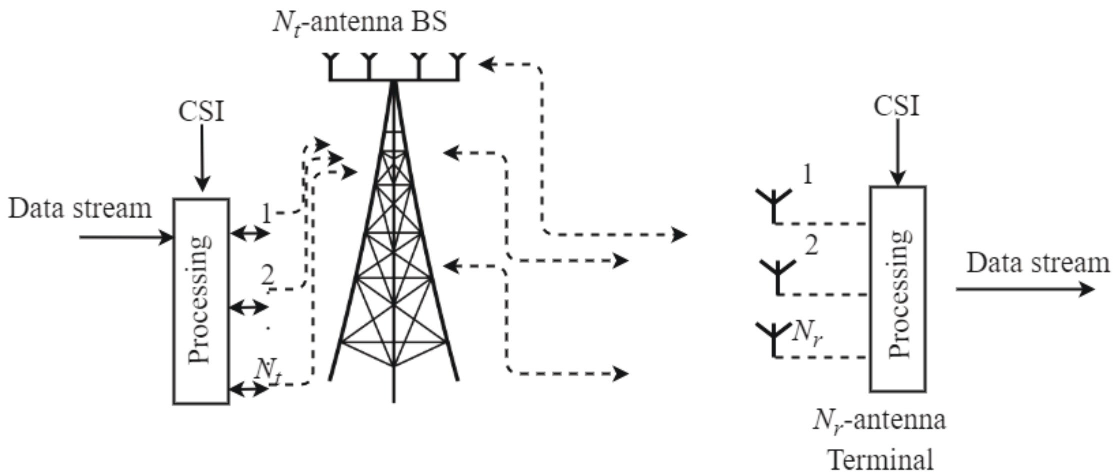

Figure 2.1: An illustration of a $N_t \times N_r$ single-user MIMO system.

elements $h_{i,j}$ which are the complex channel coefficients between the i^{th} receive antenna and the j^{th} transmit antenna. The capacity of the channel when the transmitted signal is Gaussian distributed, and the full CSI is available at both transmitter and receiver, can be expressed as [9]:

$$C = \sum_{i=1}^{n_{\min}} \left(\log_2 \left(1 + \frac{P_i^* \lambda_i^2}{\sigma_n^2} \right) \right) = \log_2 \prod_{i=1}^{r} \left(1 + \frac{P_i^* \lambda_i^2}{\sigma_n^2} \right). \tag{2.2}$$

In (2.2), the λ_i terms are the singular values of the channel matrix $\mathbf{H}$, and $n_{\min}$ is the rank of the channel matrix, which equals $\min(N_t, N_r)$ in a rich scattering propagation environment. The values of $P_1^*, \cdots P_{n_{min}}^*$ are the waterfilling power allocations:

$$P_i^* = \max \left(\mu - \frac{\sigma_n^2}{\lambda_i^2}, 0 \right) \tag{2.3}$$

where μ is chosen to satisfy the total power constraint $\sum_i P_i^* = P$.

In scenarios where the CSI is only available at the receiver, the channel capacity is reduced and can be achieved by allocating equal power to each of the transmit antennas. Hence, the capacity is [9]:

$$C = \log_2 \prod_{i=1}^{r} \left(1 + \frac{P \lambda_i^2}{N_t \sigma_n^2} \right), \tag{2.4}$$

where r is the rank of the channel.

As noted above, the capacity of MIMO channel can be measured by the rank of the matrix $\mathbf{H}$. In particular, in rich scattering environment where channel coefficients are i.i.d. circularly symmetric complex Gaussian (which implies their envelopes are independent Rayleigh), the channel capacity increases by a factor of $\min(N_t, N_r)$ in comparison to the SISO case. Since the channel matrix $\mathbf{H}$ is random, the *ergodic* capacity of the channel is a proper measure, which is the expected value of the capacity with respect to the channel, i.e., $C_E = \mathbb{E}_{\mathbf{H}}\{C\}$.

The situation with MU-MIMO is quite different from SU-MIMO as it requires use of more sophisticated signal processing techniques to allow users spatial sharing of the channel. In MU-MIMO, downlink and uplink channels are referred to as broadcast channel (BC) and multiple access channel (MAC), respectively. Fig. 2.2, illustrates a MU-MIMO communication system in which the BS with N_t antennas is serving K independent users, where user k is equipped with $N_{r,k}$ antennas.

Let $\mathbf{x} = [x_1, x_2, \cdots, x_{N_t}]^T$ be the downlink transmitted signal from the BS to the K users. Then, the received signal at user k is:

$$\mathbf{y}_k = \mathbf{H}_k^{\text{BC}}\mathbf{x} + \mathbf{n}_k. \tag{2.5}$$

Here, $\mathbf{H}_k^{\text{BC}}$ with $k = 1, 2, \cdots, K$ is the $N_{r,k} \times N_t$ downlink channel between the BS and the k^{th} user, and $\mathbf{n}$ is the $N_{r,k} \times 1$ noise vector. Furthermore, the overall received downlink signals can be represented in a vector format as:

$$\begin{bmatrix} \mathbf{y}_1 \\ \mathbf{y}_2 \\ \vdots \\ \mathbf{y}_K \end{bmatrix} = \begin{bmatrix} \mathbf{H}_1^{\text{BC}} \\ \mathbf{H}_2^{\text{BC}} \\ \vdots \\ \mathbf{H}_K^{\text{BC}} \end{bmatrix} \mathbf{x} + \begin{bmatrix} \mathbf{n}_1 \\ \mathbf{n}_2 \\ \vdots \\ \mathbf{n}_K \end{bmatrix}. \tag{2.6}$$

Assuming a unit variance for the noise, it is known that the capacity region for a given

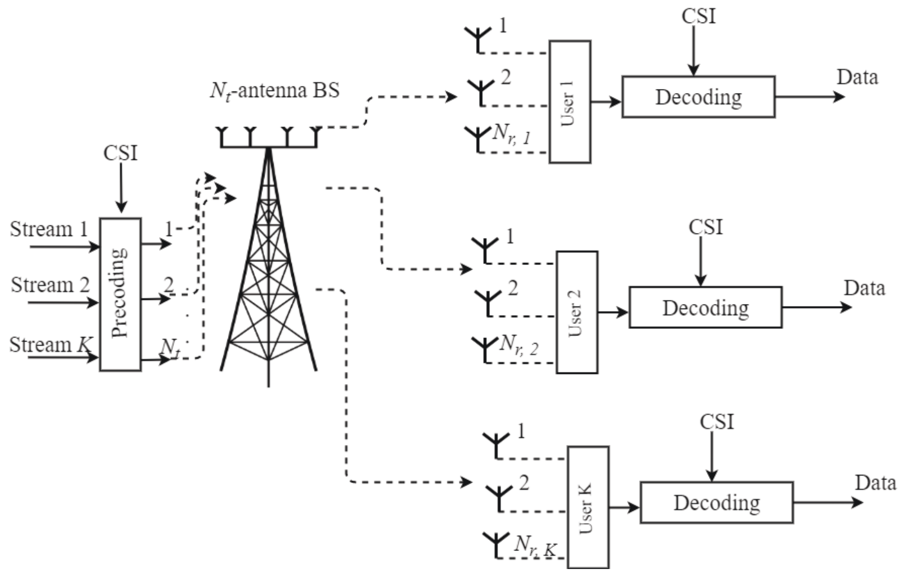

Figure 2.2: An illustration of a multiuser MIMO system.

matrix channel realization can be expressed as [61]:

$$\mathcal{C}_{\text{BC}} = \cup_{P_1,\cdots,P_K s.t. \sum_k P_k = P} \left\{ (R_1, \cdots, R_K) \in \mathbb{R}^{+K}, R_i \le \log_2 \frac{\det \left| \mathbf{I} + \mathbf{H}_i (\sum_{j \ge i} \mathbf{Q}_j) \mathbf{H}_i^H \right|}{\det \left[\mathbf{I} + \mathbf{H}_i (\sum_{j > i} \mathbf{Q}_j) \mathbf{H}_i^H \right]} \right\}, \tag{2.7}$$

where $\mathbf{Q}_k = \mathbb{E}\left\{\mathbf{x}_k \mathbf{x}_k^H\right\}$, with $\text{Tr}\left\{\mathbf{Q}_k\right\} = P_k$ is covariance of the transmitted signal to user k and the expressions is optimized over each possible user ordering, this is explained in more details in the following. Note that in contrast to single user systems where the capacity is one-dimensional, the capacity of a multiuser system with K users is characterized by a K-dimensional rate region, where each point is a vector of achievable rates by all the K users simultaneously.

On the MAC, let $\mathbf{x}_k = [x_1, x_2, \cdots, x_{N_{r,k}}]^T$ be the uplink transmitted signal to the BS from the k^{th} user. Then the $N_t \times 1$ received signal at the BS from the K users is:

$$\mathbf{y}_{\text{MAC}} = \mathbf{H}_1^{\text{MAC}} \mathbf{x}_1 + \mathbf{H}_2^{\text{MAC}} \mathbf{x}_2 + \cdots + \mathbf{H}_K^{\text{MAC}} \mathbf{x}_K + \mathbf{n} \tag{2.8}$$

$$= \left[\mathbf{H}_1^{\text{MAC}}, \mathbf{H}_2^{\text{MAC}}, \cdots, \mathbf{H}_K^{\text{MAC}}\right] \begin{bmatrix} \mathbf{x}_1 \\ \mathbf{x}_2 \\ \vdots \\ \mathbf{x}_K \end{bmatrix} + \mathbf{n}. \tag{2.9}$$

Here $\mathbf{H}_k^{\text{MAC}}$ with $k = 1, 2, \cdots, K$ is the $N_t \times N_{r,k}$ uplink channel between the BS and the k^{th} user. It has been shown that the BS with successive interference cancellation (SIC) achieves the best total rate among all the receiver structures [9]. That is, after one user is decoded, its signal (or interference) is subtracted from the aggregate received signal before decoding the next user. This is particularly significant when the received power of one user is much larger than that of the other; basically by decoding and subtracting the signal of the stronger user first, the weaker users can get a much higher data rate when the interference is reduced. This means that the order of decoding has an impact on the rates each user receives. Although the individual rates change, the sum rate remains the same. Let $\{\pi(K), \pi(K-1), \cdots, \pi(1)\}$ denote the order of decoding, where $\pi(1)$ is decoded *last*, the achievable sum rate is:

$$R_{\text{MAC}} = \log_2 \left| \mathbf{I} + \sum_{i=1}^{K} \mathbf{H}_{\pi(i)}^{\text{MAC}} \mathbf{Q}_{\pi(i)} \left(\mathbf{H}_{\pi(i)}^{\text{MAC}}\right)^H \right|. \tag{2.10}$$

On the downlink channel, the BS transmits several data streams with its multiple antennas to several users in the same time-frequency resource block using spatial multiplexing. Usually, different data streams are transmitted to different users. Hence, multiple transmissions interfere with each other, resulting in multiuser interference (MUI). The number of antennas at individual multiple users is normally smaller (or much smaller) than the number of different data streams (and different users receiving them) and therefore each user does not have enough degrees of freedom to cancel all MUI it receives. Additionally, in the MU-MIMO system users cannot cooperate to form a sufficiently large antenna array in order to cancel MUI. Hence, the BS needs to perform precoding to mitigate MUI. In [22, 23], it has been shown that in case of having perfect non-causal channel knowledge at the MU-MIMO downlink transmitter, it can encode the data accounting for interference without any power penalty, as if there were no interference. This precoding technique is called dirty paper coding (DPC), based on the original SISO technique [62] that Costa considered analogous to "writing on dirty paper" using a different colour of ink. DPC considers a user ordering map and assumes that the data of the first user is detected using a capacity achieving code. As the interference caused by the data signal transmitted to this user in known, the transmitter encodes the data of the second user in such a way that it does not receive any interference from the first user. The same approach is done to subsequent users, thus the interference caused by the signal to user j on the signal intended for user k, where $j < k$, is removed. This is similar to the SIC method on the MAC link, keeping similar user encoding order as SIC (where $\pi(1)$ is encoded *first*), the achievable rate for each user is equal to [63]:

$$R^{\text{BC}}_{\pi(k)} = \log_2 \frac{\left|\mathbf{I} + \mathbf{H}^{\text{BC}}_{\pi(k)}(\sum_{j\geq k}\mathbf{P}_{\pi(j)})\left(\mathbf{H}^{\text{BC}}_{\pi(k)}\right)^H\right|}{\left|\mathbf{I} + \mathbf{H}^{\text{BC}}_{\pi(k)}(\sum_{j> k}\mathbf{P}_{\pi(j)})\left(\mathbf{H}^{\text{BC}}_{\pi(k)}\right)^H\right|}, \tag{2.11}$$

where this is achievable for all the positive semi-definite covariance matrices $\mathbf{P}_k$ subject to the power constraint $\sum_{\forall k}\text{Tr}\left(\mathbf{P}_k\right) \leq P$, and possible encoding order. Since DPC is the optimal solution to achieve sum rate capacity in downlink MU-MIMO system, based on our signal model, we can write capacity of the channel as:

$$C^{\text{BC}}_{\text{DPC}} = \max_{\mathbf{P}_1,\mathbf{P}_2,\cdots,\mathbf{P}_K} \log_2\left|\mathbf{I} + \frac{1}{\sigma_n^2}\sum_k\left(\mathbf{H}^{\text{BC}}_{\pi(k)}\right)^H\mathbf{P}_{\pi(k)}\mathbf{H}^{\text{BC}}_{\pi(k)}\right|, \text{ s.t. } \mathbf{P}_k \succeq 0\,\forall k, \sum_{k=1}^{K} P_k = P. \tag{2.12}$$

The challenge of finding the capacity region of the MU-MIMO BC, and characterizing the DPC capacity region have been extensively studied in several research works. It has been shown that there is a duality between the MAC and BC capacity regions; and DPC can deliver the maximum possible sum rate of the MU-MIMO BC [64–66]. Although computation of the DPC capacity region and user rates is difficult on its own, it is facilitated by exploiting this MAC-BC duality, with $\mathbf{H}_k^{\text{MAC}} = \left(\mathbf{H}_k^{\text{BC}}\right)^H$. The BC region can be calculated through the union of regions of the dual MAC with all uplink power allocation vectors meeting the sum power constraint P [63]. Calculation of the MAC regions is a much simpler convex problem. The capacity-achieving individual BC user rates for users encoded in the order $\{\pi(1), \pi(2), \cdots, \pi(K)\}$ are the same as for users on the dual MAC decoded $\{\pi(K), \pi(K-1), \cdots, \pi(1)\}$. In [67] a water-filling solution to above power allocation problem has been proposed to maximize the sum rate.

Despite being the optimal precoding technique, DPC is highly complex and of a nonlinear nature. It also requires non-causal knowledge of the channel (which means the knowledge of the future state of the channel) at the transmitter, which is not feasible. Hence, more practical, but suboptimal methods were introduced to reduce the interference between users. In particular, linear precoding techniques are of interest due to their lower complexity compared to DPC and other non-linear techniques such as vector perturbation. In linear precoding users are assigned different precoding matrices at the transmitter. In other words, transmitted data is precoded (pre-processed) as follows:

$$\mathbf{x} = \sum_k \mathbf{x}_k = \sum_k \mathbf{F}_k \mathbf{d}_k, \tag{2.13}$$

$$\mathbf{y}_k = \mathbf{H}_k \mathbf{F}_k \mathbf{d}_k + \mathbf{H}_k \sum_{l=1, l\neq k}^{K} \mathbf{F}_l \mathbf{d}_l + \mathbf{n}_k, \tag{2.14}$$

where $\mathbf{y}_k$ is the received signal, $\mathbf{d}_k \in \mathcal{C}^{d_k \times 1}$ is the data symbols vector, and $\mathbf{F}_k \in \mathcal{C}^{N_t \times d_k}$ is the precoding matrix for the k^{th} user. Let $\mathbf{H} = \left[\mathbf{H}_1^T, \mathbf{H}_2^T, \cdots, \mathbf{H}_K^T\right]^T$ denotes the vertical concatenation of K users' channels, where $\mathbf{H}_k \in \mathcal{C}^{N_{r,k} \times N_t}$ and $N_t \geq K$. We assume that user k has $N_{r,k}$ antennas, and will decode $d_k \leq N_{r,k}$ data streams containing its data. The goal is to design $\{\mathbf{F}_k\}_{k=1}^K$ based on the channel matrix knowledge, so a given performance metric is maximized for each stream. In the following, we mainly focus on methods that maximize the system sum rate under a power constraint.

In the precoding process the amplitudes and phases of the transmitted signals are suitably adjusted. Commonly-used linear schemes include matched filtering (MF), zero-forcing (ZF) and minimum-mean-squared-error (MMSE) filtering. We focus on linear precoding in the downlink (assuming $N_{r,k} = d_k = 1 \; \forall k$ for simplification), and corresponding linear detection in the uplink can be derived in a similar fashion.

With linear precoding the simplest approach is MF or maximum ratio transmission (MRT), which aims at maximizing the received SNR at each user. Finding MF precoding matrix involves solving the following optimization problem:

$$\mathbf{F}_{k,\text{MF}} = \arg\max_{\mathbf{F}_k} \frac{\mathbb{E}\left\{\mathbf{d}_k^H \mathbf{y}_k\right\}}{\sigma_n^2}. \tag{2.15}$$

The solution to above optimization problem is the Hermitian transpose of the channel matrix as follows [68]:

$$\mathbf{F}_{k,\text{MF}} = \mathbf{H}_k^H, \tag{2.16}$$

which maximizes the received signal power for the user, but cross-talk still exists. The effective signal for the k^{th} user becomes:

$$\mathbf{y}_k = \left[\mathbf{H}\mathbf{H}^H\right]_{k,k} \mathbf{d}_k + \sum_{l=1, l\neq k}^{K} \left[\mathbf{H}\mathbf{H}^H\right]_{k,l} \mathbf{d}_l + \mathbf{n}_k. \tag{2.17}$$

Due to the maximization of the receive SNR at each user, MF is suitable for noise-limited scenarios. At high SNRs, MF performance will be limited by inter-user interference, in which case, ZF precoding is superior to MF.

ZF precoding nulls out the inter-user interference, and is the solution to the following optimization problem:

$$\mathbf{F}_{\text{ZF}} = \arg\max_{\mathbf{F}} \mathbb{E}\left\{\|\mathbf{F}\mathbf{d}\|^2\right\}, \tag{2.18}$$

where $\mathbf{F} = [\mathbf{F}_1, \cdots, \mathbf{F}_K] \in \mathcal{C}^{N_t \times K}$, and $\mathbf{d} = \left[\mathbf{d}_1^T, \cdots, \mathbf{d}_K^T\right]^T \in \mathcal{C}^{K \times 1}$ are the joint precoding and data matrices of K users. The solution completely removes the interference with minimum transmit energy, and is the Moore–Penrose pseudoinverse of the channel [68], i.e.,

$$\mathbf{F}_{\text{ZF}} = \mathbf{H}^{\dagger} = \mathbf{H}^H \left(\mathbf{H}\mathbf{H}^H\right)^{-1}. \tag{2.19}$$

By deploying ZF as precoding at the BS, we can perfectly cancel inter-user interference by creating a set of orthogonal and non-interfering channels. However, this solution is only suitable when the propagation environment is richly scattering; when the Gram matrix $\mathbf{H}_k \mathbf{H}_k^H$ is full rank and diagonally dominant.

So far, we have shown that ZF is suitable for interference-limited scenarios, while MF outperforms it in noise-dominant ones. However, there are schemes that mitigate both interference and noise. MMSE precoding is one example. The idea is, if the noise covariance is estimated at the receiver and fed back to the transmitter, we can design a better precoder for the entire SNR range. MMSE is obtained through the optimization:

$$\mathbf{F}_{\text{MMSE}} = \arg\min_{\mathbf{F}} \mathbb{E} \left\|\mathbf{y} - \mathbf{d}\right\|^2 = \arg\min_{\mathbf{F}} \mathbb{E} \left\|\left(\mathbf{H}\mathbf{F} - \mathbf{I}\right)\mathbf{d} + \mathbf{n}\right\|^2 \tag{2.20}$$

where $\mathbf{y} = \left[\mathbf{y}_1^T, \cdots, \mathbf{y}_K^T\right]^T \in \mathcal{C}^{K \times 1}$, $\mathbf{n} = \left[\mathbf{n}_1^T, \cdots, \mathbf{n}_K^T\right]^T \in \mathcal{C}^{K \times 1}$ are the corresponding joint received signal and noise of K users. Here, we try to minimize the mean-square error (MSE) between the received and transmit signals. One possible solution is ZF, if the available transmit power can be arbitrary high. With limited transmit power, we need to consider the noise covariance $\sigma_n^2 \mathbf{I}$ which results in MMSE solution [69] as follows:

$$\mathbf{F}_{\text{MMSE}} = \mathbf{H}^H \left(\mathbf{H}\mathbf{H}^H + \alpha \mathbf{I}\right)^{-1}, \tag{2.21}$$

where $\alpha = \frac{K\sigma_n^2}{P}$. This solution is also called regularized ZF, and α is the regularization parameter.

One generalization of ZF beamforming is finding the optimal transmit vectors $\mathbf{F}_k$ such that all multiuser interference is zero. Since the resulting product $\mathbf{H}_l\mathbf{F}_k$ will be block-diagonal, the algorithm is referred to as block diagonalization (BD). Note that when $N_{r,k} = 1$ for all users, this simplifies to a complete diagonalization, which can be achieved using a pseudo-inverse of the channel (ZF). While complete diagonalization could also be applied when $N_{r,k} > 1$ and would have the advantage of simplifying the receiver (each antenna would receive only one signal), it comes at the cost of reduced throughput or requiring higher power at the transmitter, particularly when there is significant spatial correlation between the antennas at the receiver.

To eliminate all multiuser interference in (2.14), we impose the constraint $\mathbf{H}_l\mathbf{F}_k = 0$, $\forall l \neq k$, thus $\mathbf{y}_k = \mathbf{H}_k\mathbf{F}_k\mathbf{s}_k + \mathbf{n}_k$. If we define $\hat{\mathbf{H}}_k$ as:

$$\hat{\mathbf{H}}_k = \left[\mathbf{H}_1^T \cdots \mathbf{H}_{k-1}^T \mathbf{H}_{k+1}^T \cdots \mathbf{H}_K^T\right]^T, \tag{2.22}$$

then any suitable $\mathbf{F}_k$ lies in the null space of $\hat{\mathbf{H}}_k$. Let the singular value decomposition (SVD) of $\hat{\mathbf{H}}_k$ be:

$$\hat{\mathbf{H}}_k = \hat{\mathbf{U}}_k \hat{\mathbf{D}}_k \left[\hat{\mathbf{V}}_k^{(1)} \hat{\mathbf{V}}_k^{(0)}\right]^H, \tag{2.23}$$

where $\hat{\mathbf{U}}_k$ and $\hat{\mathbf{D}}_k$ are left singular vector matrix and the diagonal matrix of singular values of $\hat{\mathbf{H}}_k$, respectively, and $\hat{\mathbf{V}}_k^{(1)}$ and $\hat{\mathbf{V}}_k^{(0)}$ denote the right singular matrices each corresponding to non-zero singular values and zero singular values, respectively. Any precoder $\mathbf{F}_k$ that is a linear combination of the columns of $\hat{\mathbf{V}}_k^{(0)}$ will satisfy the null constraint. This definition allows us to define the dimension condition necessary to guarantee that all users can be accommodated under the zero-interference constraint. Data can be transmitted to user k if the null space of $\hat{\mathbf{H}}_k$ has a rank greater than 0. This is satisfied when $\text{rank}(\hat{\mathbf{H}}_k) < N_t$. So for any $\mathbf{H}$, block diagonalization is possible if $N_t > \max\left\{\text{rank}(\hat{\mathbf{H}}_1), \text{rank}(\hat{\mathbf{H}}_2), \cdots, \text{rank}(\hat{\mathbf{H}}_k)\right\}$. Assuming that $\mathbf{H}_k$ is full rank, the transmitter requires that $\sum_{j\neq k} N_{r,j} < N_t, \forall k$ to satisfy the dimensionality constraint required to cancel interference for each user [70]. Under the BD constraint, $\mathbf{F}_k$ can be further optimized by waterfilling of power. If excess antennas are available, eigenmode selection or antenna subset selection can be used to further improve performance [71].

From a practical perspective, the key performance indicators of a communication system are error probability, sum rate, signal-to-interference-plus-noise (SINR) ratio, etc. It has been shown that in MU-MIMO systems with linear precoding algorithms, as the number of active users in the system increases, the sum capacity also increases. This leads to the resource allocation problem that is: how many and which users should effectively be served at any given time slot. This issue is also known as the user scheduling problem; we will not discuss it in this thesis.

2.2 Massive MIMO Systems

In massive MIMO, the number of antennas N_t at the BS becomes much larger than the number of users served. Theoretically, the sum rate capacity of a MU-MIMO system grows with $\min(N_t, K)$, the minimum of the number of antennas at the BS and the number of users. When both N_t and K become large the rank of $\mathbf{H}\mathbf{H}^H$ grows which results in a large increase in the sum rate capacity. For a fixed number of users K and $N_t \gg K$ the array gain becomes very large. In this system, the inter-user interference significantly reduces which leads to a large sum capacity. Fig. 2.3 illustrates a massive MIMO system.

2.2.1 Advantages of Massive MIMO

Large Array gain

With more antennas at the BS, there are more degrees of freedom available for signal processing [72]. For example, coherently combining the transmit and receive signals can improve SNR as compared to that in single antenna system. This is known as array gain.

As N_t grows, the channel matrix $\mathbf{H}$ becomes long, and the value of $\left[\mathbf{H}\mathbf{H}^H\right]_{i,i}$ where

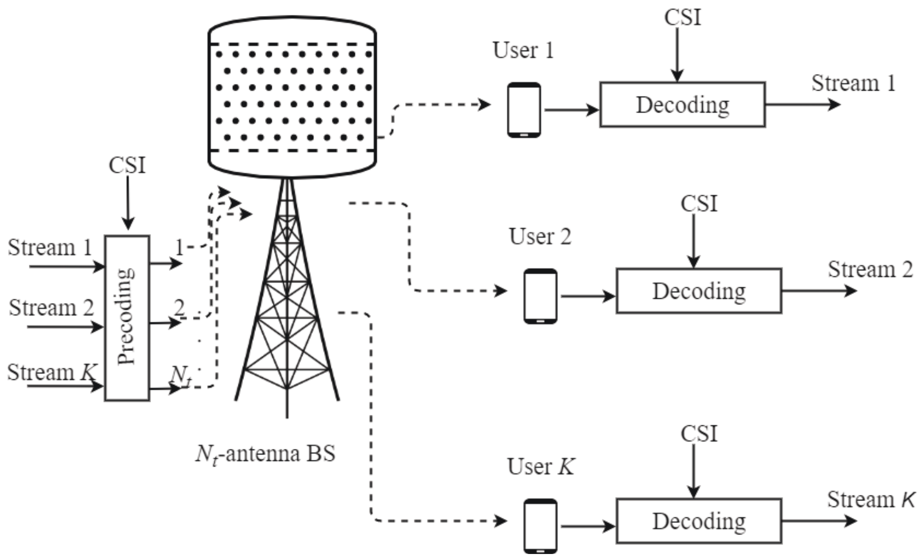

Figure 2.3: An illustration of a massive MIMO system.

$i = 1, 2, \cdots, K$ increases. Hence, as shown with MF precoding, the received signal strength for the intended user becomes higher. This is achieved without any increase in transmit power. A similar result can be shown for precoding with ZF and MMSE; thus inter-user interference becomes small resulting in higher capacity. Basically, for all the linear precoding schemes, when SINR increases higher data rates can be achieved. In massive MIMO, the effect of array gain is much more significant than in smaller-scale MU-MIMO systems.

Additionally, having large array gain can improve link quality and coverage. Usually, higher SINR in a system means higher data rates since higher order modulation can be used. However, large dynamic range in signal strength and higher modulation order requires a higher precision analog-to-digital-converter (ADC) which can increase the cost of hardware [72].

Massive MIMO Inter-User Interference Reduction

Assume that the elements of channel matrix $\mathbf{H}$ are zero mean i.i.d with complex Gaussian coefficients, $\mathcal{CN}(0, \sigma_h^2), \sigma_h^2 < \infty$. In massive MIMO regime, as N_t grows the diagonal elements $\left[\mathbf{HH}^H\right]_{i,i}$ become larger, while the off-diagonal elements $\left[\mathbf{HH}^H\right]_{i,j}$ where $i \neq j$ grow far slower compared to diagonal elements. This leads to the phenomenon that users' channels become orthogonal, inter-user interference vanishes, and the BS can communicate with several users at higher data rates.

We examine the diagonal elements of the Gram matrix as follows:

$$\frac{1}{N_t}\left[\mathbf{HH}^H\right]_{i,i} = \frac{1}{N_t}\sum_{n=1}^{N_t}\left|\mathbf{H}_{i,n}\right|^2, \tag{2.24}$$

and the off-diagonal elements are

$$\frac{1}{N_t}\left[\mathbf{HH}^H\right]_{i,j} = \frac{1}{N_t}\sum_{n=1}^{N_t}\mathbf{H}_{i,n}\mathbf{H}_{j,n}^*, i \neq j. \tag{2.25}$$

According to the central limit theorem, the average of n independent samples from a distribution having finite variance σ^2 and mean μ, when $n \to \infty$ is asymptotically normally distributed according to $\mathcal{N}\left(\mu, \frac{\sigma^2}{n}\right)$ [73]. Thus, given the nature of $\mathbf{H}$ elements the distributions of both diagonal and off-diagonal elements converge to Gaussian distributions,

$$\frac{1}{N_t}\left[\mathbf{HH}^H\right]_{i,i} \xrightarrow{d} \mathcal{N}\left(\mu_0, \frac{\sigma_0^2}{N_t}\right), \tag{2.26}$$

and

$$\frac{1}{N_t}\left[\mathbf{HH}^H\right]_{i,j} \xrightarrow{d} \mathcal{N}\left(\mu_1, \frac{\sigma_1^2}{N_t}\right), i \neq j, \tag{2.27}$$

where $\mu_0 = \mathbb{E}\left\{\left|\mathbf{H}_{i,n}\right|^2\right\}$, $\sigma_0^2 = \mathrm{var}\left\{\left|\mathbf{H}_{i,n}\right|^2\right\}$, $\mu_1 = \mathbb{E}\left\{\mathbf{H}_{i,n}\mathbf{H}_{j,n}^*\right\}$, and $\sigma_1^2 = \mathrm{var}\left\{\mathbf{H}_{i,n}\mathbf{H}_{j,n}^*\right\}$, and $\xrightarrow{d}$ means convergence in distribution. As $N_t \to \infty$, $\frac{\sigma_0^2}{N_t}$ and $\frac{\sigma_1^2}{N_t}$, variances of both distributions approach zero. In addition, the terms $|\mathbf{H}_{i,n}|^2$ follow a chi-squared distribution with two degrees of freedom and mean of $\mu_0 = \sigma_h^2$, whereas the off-diagonal elements $\mu_1 = \mathbb{E}\left\{\mathbf{H}_{i,n}\right\}\mathbb{E}\left\{\mathbf{H}_{j,n}^*\right\} = 0$ since the channel coefficients for different users are independent random variables. Thus,

$$\frac{1}{N_t}\left[\mathbf{H}\mathbf{H}^H\right]_{i,i} \to \sigma_h^2\mathbf{I}, \tag{2.28}$$

as N_t grows [74].

Linear Precoding and Beamforming

As shown above, as the number of antennas at the BS grows, the users' channels become highly orthogonal. This is of great importance since it means that simple linear precoding and beamforming algorithms are sufficient to be used in massive MIMO systems [72]. As a comparative demonstration, in the massive MIMO regime, we can rewrite the sum rate capacity achieved by DPC from (2.12) as follows:

$$C_{\text{DPC}} = \max_{\mathbf{P}_1,\mathbf{P}_2,\cdots,\mathbf{P}_K} \log_2\left|\mathbf{I} + \frac{N_t\sigma_h^2}{\sigma_n^2}\mathbf{P}_{\text{DPC}}\right| \text{s.t.}\mathbf{P}_k \succeq 0\ \forall k, \sum_{k=1}^{K} P_k = P, \tag{2.29}$$

where equal power allocation of $P_k = \frac{P}{K}$ is the optimal solution. Thus,

$$C_{\text{DPC}} = K\log_2\left(1 + \frac{N_t\sigma_h^2 P}{\sigma_n^2 K}\right), \tag{2.30}$$

is the sum rate capacity of DPC, with N_t as array gain, and K as the multiplexing gain. With linear precoding at the transmitter, since the interference among users vanishes, the sum rate capacity achieved by ZF, MF, and MMSE will be equal to DPC. Hence, as N_t increases the inter-user interference reduces and simple linear precoding methods achieve the capacity achieved by the infeasible DPC technique.

Channel Hardening

From (2.26) and (2.27), it can be observed that the fluctuation in the elements of $\frac{1}{N_t}\left[\mathbf{H}\mathbf{H}^H\right]$ decrease rapidly relative to their respective means, as N_t grows large. This effect is called channel hardening [75]. Note that channel hardening does not mean the variation in the channel $\mathbf{H}$ becomes small, but is an effect that stabilizes the outputs of signal processing phases. Other impacts of channel hardening phenomenon include:

- The effect of small-scale fading disappears. If we scale down the transmit power with the number of antennas, e.g., $P = \frac{\rho K}{N_t}$ (ρ is the SNR), then the receive SINRs at the users become more stable in the sense that they do not fluctuate with small-scale fading in the channel, for all the precoding schemes MF, ZF and MMSE.

- Resource allocations can be performed on a slower time scale. For example, the transmit power does not need to be updated with variations in the small-scale fading of the propagation environment, but only to the large-scale fading characteristics of the channel.

- The variation in sum-rates becomes small. The SINRs at the users' receivers do not vary with small-scale fading, as a result, the sum rate stays relatively constant. The probability that we have a rate much lower than the ergodic average rate becomes very small.

- Precoders and detectors become more stable. Due to interference reduction and channel hardening, the power variation in the precoded signal $\mathbf{x}$, i.e., the variation in $\|\mathbf{x}\|^2$, becomes small and stable, when the transmit symbols in $\mathbf{d}$ vary.

In addition, the effects of channel hardening on transmission schemes and system performance have been studied, e.g., in [76, 77]. As the number of antennas increases, channel conditions that were random before, now start to be deterministic.

Sharply-Focused Digital Beamforming into Smaller Regions in Space

With an antenna array, we can perform analog beamforming that steers directional beams by adjusting the phases of RF signals at each antenna. Depending on the number of antennas and the size of the array, multiple beams can be formed to serve different users. In full-dimension MIMO (FD-MIMO) [78, 79], 3D beams can be formed to serve users in different azimuths and elevations. With more antennas, beams can be made narrower, resulting in a better separation of user signals. With analog beamforming, the number of simultaneous users is typically limited by the number of orthogonal beams that can be formed, and is fixed by the number of deployed RF chains.

Linear precoding, as discussed earlier, works in a different way. It can be seen as digital beamforming, performed in the baseband by tuning the phases and amplitudes of transmitted signals across all antennas. Without steering actual beams into the channel, signals add up in phase at the intended users and out of phase at other users. With increasing number of antennas, this effect is more significant: the signal strength at the intended user location gets higher, while causing lower interference to the other users.

Digital beamforming in massive MIMO provides a more flexible and dynamic way of spatial multiplexing, as the number of users can vary [72]. Whereas, analog beamforming methods depend on array calibration, whose complexity grows with the number of antennas.

2.2.2 Challenges of Massive MIMO

With the theoretical advantages of massive MIMO described above, the question is what challenges we may face in practice, and to what extent the theoretically demonstrated advantages can be captured in reality.

Propagation Channel

In Subsection 2.2.1 we have assumed, we assume i.i.d. Rayleigh channels where the number of base station antennas $N_t \to \infty$. This leads to interference-free transmission and optimal performance achieved by linear precoding and detection. In practice however, the number of antennas is limited and propagation channels are not i.i.d. Rayleigh. Channels from antenna elements in a large array are often spatially correlated and this spatial correlation may be due to different reasons. For example, the propagation environment may produce more multipath components from the BS in some spatial directions than in others; also, the polarization and propagation pattern of antennas can impact the small-scale signal statistics [80].

In massive MIMO literature, there is a commonly-used term called favorable propagation [72]. Many theoretical studies are based on this propagation condition, assuming that user channels become orthogonal as the number of antennas increases. Although Rayleigh channels provide favorable propagation, for channel gains to be Rayleigh distributed, it requires very rich and complex propagation environment which does not always exist in real-life scenarios.

Hardware Complexity

A crucial challenge of massive MIMO is hardware complexity. As the number of antennas increases, the number of RF transceiver chains including components like RF amplifier, mixer and ADC/DAC, also grows well beyond that in conventional small-scale MU-MIMO. To deal with large channel matrices, the complexity in baseband processing will also significantly increase, as more operations are needed.

High hardware complexity often leads to low efficiency in terms of cost and energy. Antennas are usually cheap and easy to deploy, but RF chains can be relatively expensive. Due to large array gains, massive MIMO is energy efficient in terms of radiated power. However, energy consumption in hardware can be quite high and may dominate massive MIMO energy consumption [74].

To implement massive MIMO in practice, many studies are focused to simplify the hardware implementation. Among those, hybrid transceivers [52] and single-RF [58] chain transceiver have been considered in this thesis, as a direct solution that reduces the number of RF chains without a significant reduction in performance.

Hardware Imperfections

Since massive MIMO hardware tends to be very complex with many antennas and transceiver chains, it is important to make them as inexpensive as possible. However, the cheaper the hardware, the more imperfection imperfections are typically expected. With massive MIMO, we may allow many of the imperfections to be quite large, since the averaging effect due to many antennas helps to reduce the impact of imperfections on system performance [81]. This opens up the possibility to use inexpensive hardware, such as nonlinear amplifiers, high IQ-imbalance mixers, low-precision ADC/DACs, and so on.

Another issue is reciprocity calibration[1] in TDD massive MIMO. Ideally, precoding for the downlink transmission is computed based on the CSI feedback in the uplink. Although radio channels in TDD are reciprocal, transmit and receive RF chains are typically not. In order to make use of channel reciprocity, we need to estimate and compensate for the differences between the transmit and receive RF chains. There are many calibration methods, e.g., in [82], in which mutual coupling among base station antennas is used.

Mutual Coupling in Antenna Arrays

In [82], it is shown that strong mutual coupling between antennas is good for reciprocity calibration. However, mutual coupling can also degrade massive MIMO performance, primarily due to power loss when many antennas are packed into a small physical space [29]. Study in [83] provides a thorough systematic review on the impact of mutual coupling between antenna elements in MIMO systems, and presents some decoupling techniques and mutual coupling reduction algorithms through antenna array design and post-processing.

[1]Strictly speaking, the problem of reciprocity calibration for TDD systems is not unique to massive MIMO.

Channel Estimation

As discussed earlier, massive MIMO relies on the availability of CSI at the base station to coherently process the signals, i.e., to perform precoding and detection. However, there are challenges associated with CSI acquisition. Channel variations, due to the movement of users and scatterers, determine how often we need to update the CSI [84]. Accurate and timely CSI acquisition can be challenging, especially in high mobility scenarios. In FDD mode, massive MIMO faces the issue of training overhead, since channels from all base station antennas to all the users' antennas need to be estimated and fed back [31]. While in TDD massive MIMO can rely on channel reciprocity, reference signals (pilot sequences) may occupy a large fraction of the coherence interval if the channel varies fast. Hence, the number of orthogonal pilot sequences is limited by the channel coherence interval and therefore pilot sequences have to be reused from cell to cell. This causes pilot contamination, which means that channel estimates may contain interference due to adjacent cells using the same pilots for the estimation of their channels. The resulting inaccurate channel estimates will obviously deteriorate performance of massive MIMO [31].

2.3 Millimeter Wave Systems

As discussed in Chapter 1, one obvious approach to increase future wireless systems' throughput is to use a much large bandwidth for transmission. Currently, practically no radio spectrum is available for allocation in the sub-6 GHz frequency range. However, a significant amount of bandwidth is available in the mmWave frequency range. Precisely speaking this frequency range extends from 30 to 300 GHz, but already wireless systems operating at frequencies above 20 GHz are commonly understood as operating in the mmWave range.

The key benefits of operating in the mmWave range of frequencies are as follows

[38, 40]:

- the abundance of radio frequency bandwidth available for transmission;
- a large number of antennas can be packed in a small physical space;
- highly directional beams can be generated to reduce multiuser interference and overcome increased path loss;
- an inherently increased privacy and security in mmWave communication due to the reduced scattering and range of transmission.

Despite the advantages associated with operating in the mmWave band, there are a number of challenges that need to be addressed such as [38, 41]:

- increased power consumption due to the need to deploy large antenna arrays;
- significantly greater path loss and increased susceptibility to weather conditions;
- from hardware implementation point of view, mmWave systems suffer from increased nonlinear distortions and phase noise;
- serving mobile users is a challenge due to significantly reduced channel coherence time resulting from significantly increased Doppler spread caused by a much higher carrier frequency.

Chapter 3

A Path Selection Algorithm for Sparse Massive MIMO Channels

Massive MIMO channels at mmWave frequencies are sparse, which means that amongst all the multipath components that contribute to signal transmission only few carry significant power. Inspired by the sparse nature of these channels, in [85] computationally efficient way of optimizing performance of a massive MIMO system on a mmWave channel is introduced. We start by introducing a bipartite graph, which connects angle of departure (AoD) to users in the beam-space domain that conveniently reveals the sparsity of the channel. This model can be implemented in practice using DFT beamforming especially when the number of transmit antennas is large. Next we formulate an optimization problem aiming to maximize sum rate by selecting edges in our sparse bipartite graph in a greedy fashion.

3.1 System Model

We consider the downlink of a mmWave massive MIMO system, where the base station (BS) is equipped with N_t antennas and serves K single-antenna users. Symbol-to-symbol independent quasi-static Rayleigh fading is assumed to model the channel. The sparse nature of mmWave massive MIMO channels makes beam-space or virtual representation of the channels a natural choice [86]. Hence, the channels are resulting from the sum of the contributions from discrete multipath components N_p, which further assumed to be one single propagation path between the BS and users. Let $\mathbf{h}_k \in \mathcal{C}^{1\times N_t}$ denote the downlink channel vector of user k which has entries of zero-mean complex Gaussian random variables. Under such model, for a N_t-element uniform linear arrays (ULA) the steering vector $\mathbf{a}(N_t, \theta) \in \mathcal{C}^{N_t\times 1}$ at the angle θ is given by

$$\mathbf{a}(N_t, \theta) = \frac{1}{\sqrt{N_t}} \left[1, e^{jqd\sin(\theta)}, ..., e^{jqd(N_t-1)\sin(\theta)}\right]^T, \tag{3.1}$$

where $q = \frac{2\pi}{\lambda}$, λ is the wavelength, and d is the distance between two adjacent antenna elements. Given the steering vectors, the MIMO channel vector $\mathbf{h}_k$ for user k can be described by a multipath model of the form

$$\mathbf{h}_k = \sum_{p=1}^{N_p} \rho_{k,p}\mathbf{a}^H(\theta_{k,p}), \tag{3.2}$$

where $\theta_{k,p}$ and $\rho_{k,p}$ denote the angle of departure (AoD) and complex channel gain for path p of user k, respectively. N_p is the number of multipath components between the BS to the user k, and each user is assumed to receive the same number of paths. The channel gains $\rho_{k,p}$ are independent zero-mean complex Gaussian random variable with variance $1/N_p$. From (3.2) and the assumptions made about complex channel gains $\rho_{k,p}$, we can conclude that $\mathbb{E}[\|\mathbf{h}_k\|^2] = 1$. Let $\mathbf{x} \in \mathcal{C}^{N_t\times 1}$ be the transmitted signal vector, then to satisfy the power constraint at the transmitter, the inequality $\mathbb{E}[\|\mathbf{x}\|^2] \leq P$ must hold, where P is the available power budget at the transmitter. Thus, the received signal y_k at the user terminal k is given by

$$y_k = \mathbf{h}_k\mathbf{x} + n_k, \tag{3.3}$$

where $n_k \sim \mathcal{CN}(0,1)$ is an additive Gaussian noise at the user terminal k. Consequently, the average signal-to-noise ratio (SNR) for each user is represented by SNR $= P$.

In [54], it has been shown that discrete Fourier transform (DFT) beamforming is near-optimal in terms of maximizing throughput when the size of ULA N_t is large. Without loss of generality, we assume that AoDs lie in the the interval $[-\pi/3, \pi/3]$. We divide this angular spread into N_t equal disjoint intervals, which we call angular bin. For example, the angular bin j for $0 \leq j \leq N_t - 1$ is the interval

$$\mathcal{B}_j = \left\{ \theta \Big| -\frac{\pi}{3} + \frac{2\pi}{3}\frac{j}{N_t} \leq \theta \leq -\frac{\pi}{3} + \frac{2\pi}{3}\frac{j+1}{N_t} \right\}. \tag{3.4}$$

With ULA, we quantize the AoDs such that if it lies in the angular bin j it would be represented by the central angle $\hat{\theta}_j = -\frac{\pi}{3} + \frac{\pi}{N_t} + \frac{2\pi}{3}\frac{j}{N_t}$ for that bin. Now, we can define the beamforming vector $\mathbf{f}_j$ for each angular bin j as $\mathbf{f}_j = \mathbf{a}(\hat{\theta}_j)$. As $N_t \to \infty$ the quantization effect diminishes and we get very narrow beams to separate users from each other. This DFT beamforming has the following orthogonality property, which is useful for inter-beam interference cancellation:

$$\mathbf{f}_i \mathbf{f}_j^H = 0 \text{ for } i \neq j. \tag{3.5}$$

Given the beamforming vector of each angular bin, the transmitted signal vector $\mathbf{x}$ can be obtained as $\mathbf{x} = \sum_{j=0}^{N_t-1} \mathbf{f}_j d_j$ where d_j is the transmitted data stream at each beam/angular bin j, which is generated from a given constellation. Obviously, when there is no data on a particular beam, the data stream vector d_j will be equal to zero.

3.2 Path Selection Algorithm and Problem Formulation

Definition 1 (System Topology Graph). Define the *topology graph* of the mmWave massive MIMO cellular system as a bipartite graph $\mathcal{G} = \{\mathcal{B}, \mathcal{U}, \mathbf{C}\}$, where $\mathcal{B}$ denotes the set of all angular bins, $\mathcal{U}$ denotes the set of all user nodes, and $\mathbf{C}$ is the connectivity

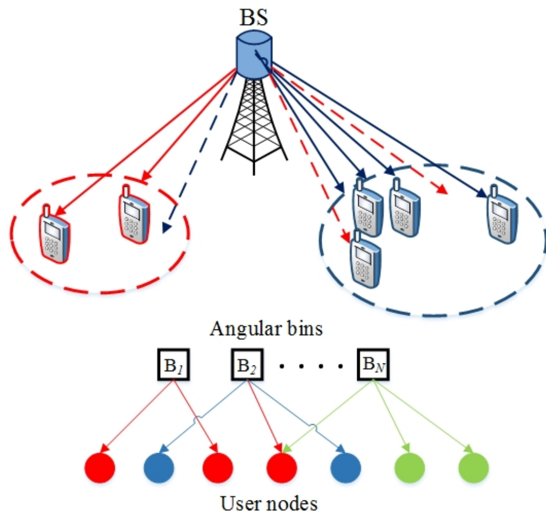

Figure 3.1: The model of sparse massive MIMO channel

matrix and includes all the edges between the BS and users. The dimension of this matrix is $K \times N_t$ and its (i, j) element denoted by $c_{i,j}$ is either 0, if there is no edge between user i and angular bin j, or 1 otherwise. Each edge $(i, j) \in \mathbf{C}$ is associated with a channel complex gain $\rho_{i,j}$, which represents the complex gain of the path between the angular bin j and user i. Fig. 3.1 illustrates the system topology graph.

We also define the selection matrix $\mathbf{S}$ of dimension $K \times N_t$, where element $s_{i,j} \in \{0, 1\}$ denote the selection variable for the path between user i and angular bin j in our optimization problem described later in this subsection. In particular, for an existing path with $c_{i,j} = 1$, $s_{i,j} = 1$ means that we select that path and $s_{i,j} = 0$ means that we do not select that path in the current channel use. Naturally, when there is no path between user i and angular bin j, $s_{i,j}$ becomes zero. With the assumption of one stream per beam, the following constraints on selection variables are enforced:

$$s_{i,j}s_{i',j} = 0, \forall i' \neq i, \text{ or equivalently} \tag{3.6}$$

$$\sum_{i=1}^{K} s_{i,j} \in \{0,1\} \tag{3.7}$$

$\sum_{i=1}^{K} s_{i,j}$ in (3.7) actually indicates whether or not beam j is selected. Therefore, the number of angular bins out of N_t that are selected for transmission is equal to $\sum_{j=1}^{N_t}\sum_{i=1}^{K} s_{i,j}$. With DFT beamforming and its resulting orthogonal beams, the power allocated to beam j is given by

$$\gamma_j = \sum_{i=1}^{K} s_{i,j} \times \frac{P}{\sum_{j'=1}^{N_t}\sum_{i'=1}^{K} s_{i',j'}}. \tag{3.8}$$

Now, the rate for user i is given by

$$R_i = \log\left(1 + \frac{\sum_j s_{i,j}|\rho_{i,j}|^2\gamma_j}{1+\sum_j |\rho_{i,j}|^2 c_{i,j}\gamma_j \times \left(\sum_{i'\neq i} s_{i',j}\right)}\right), \tag{3.9}$$

and consequently sum rate is expressed as $R_{\text{sum}}(\mathbf{S}) = \sum_{i=1}^{K} R_i$. Note that in (3.9), the numerator shows the desired signal power, and the denominator shows the power of inter-beam interference plus noise. The goal of path selection algorithm is to select variables $\{s_{i,j}\}$ in a way that sum rate is maximized. Casting sum rate with constraints on selection variables yields the following optimization problem

$$\mathcal{P} = \begin{cases} \max & \sum_{i=1}^{K} \log\left(1 + \frac{\sum_j s_{i,j}|\rho_{i,j}|^2\gamma_j}{1+\sum_j |\rho_{i,j}|^2 c_{i,j}\gamma_j\times\left(\sum_{i'\neq i} s_{i',j}\right)}\right) \\ \text{s.t.} & s_{i,j} \in \{0,1\}, \forall i,j \;\text{ and }\; s_{i,j}s_{i',j} = 0, \forall i' \neq i, \end{cases} \tag{3.10}$$

which is not convex and it is in the category of integer programming and computationally complex. In the following, we resort to greedy approach to solve this problem, summarized as follows:

- **Step 1**: Initialize $R_0 = 0$, $\mathbf{S}_0 = \mathbf{0}$ of dimension $K \times N_t$ and $\mathcal{L} = \{(i,j)|c_{i,j} = 1\}$. Let $\mathbf{E}_{(i,j)}$ denote a matrix of dimension $K \times N_t$ whose elements are all zero except the element at (i,j) which is one, i.e. $e_{i,j} = 1$.

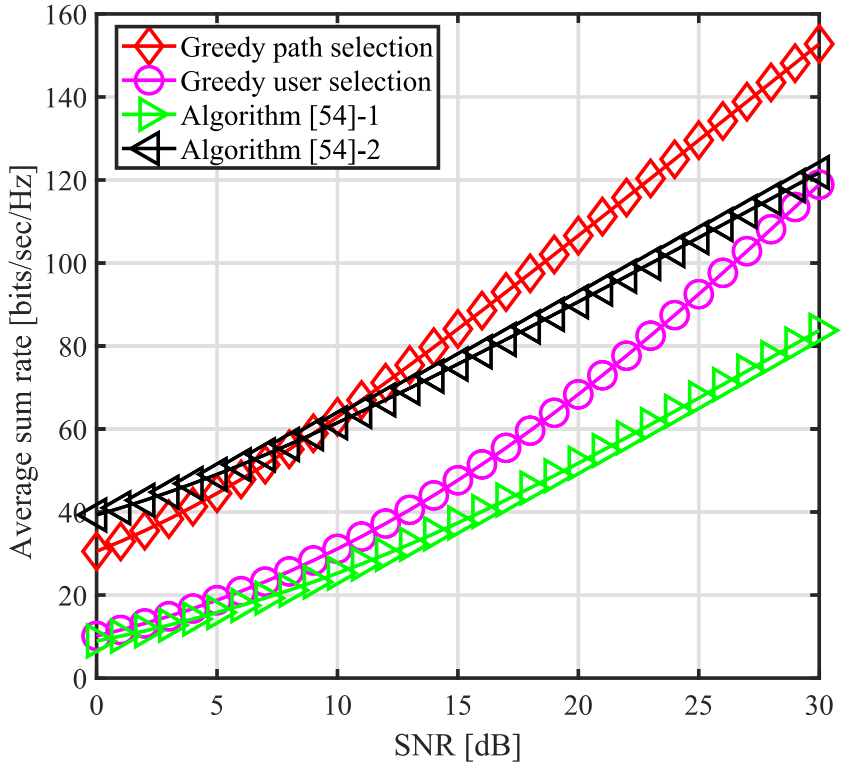

Figure 3.2: Average sum rate vs. SNR; $N_t = 40$, $N_p = 2$ and $K = 10$.

- **Step 2**: Let $(i^\star, j^\star) = \text{argmax}_{(i,j)\in\mathcal{L}} R_{\text{sum}}(\mathbf{S}_0 + \mathbf{E}_{(i,j)})$.

- **Step 3**: Set $\mathcal{D} = \{(i,j)|(i,j) \in \mathcal{L}, j = j^\star\}$.

- **Step 4**: Update $\mathcal{L} := \mathcal{L} \setminus \mathcal{D}$.

- **Step 5**: If $R_{\text{sum}}(\mathbf{S}_0 + \mathbf{E}_{(i^\star,j^\star)}) > R_0$ update $\mathbf{S}_0 := \mathbf{S}_0 + \mathbf{E}_{(i^\star,j^\star)}$ and $R_0 := R_{\text{sum}}(\mathbf{S}_0 + \mathbf{E}_{(i^\star,j^\star)})$. Otherwise output $\mathbf{S}_0$ as the selection matrix.

- **Step 6**: If $\mathcal{L} \neq \emptyset$ go to step 2. Otherwise output $\mathbf{S}_0$ as the selection matrix.

In step 1 we initialize the selection matrix and define $\mathcal{L}$ as the set of all edges in the bipartite graph. In step 2, we add candidate edges to the set of already selected paths and

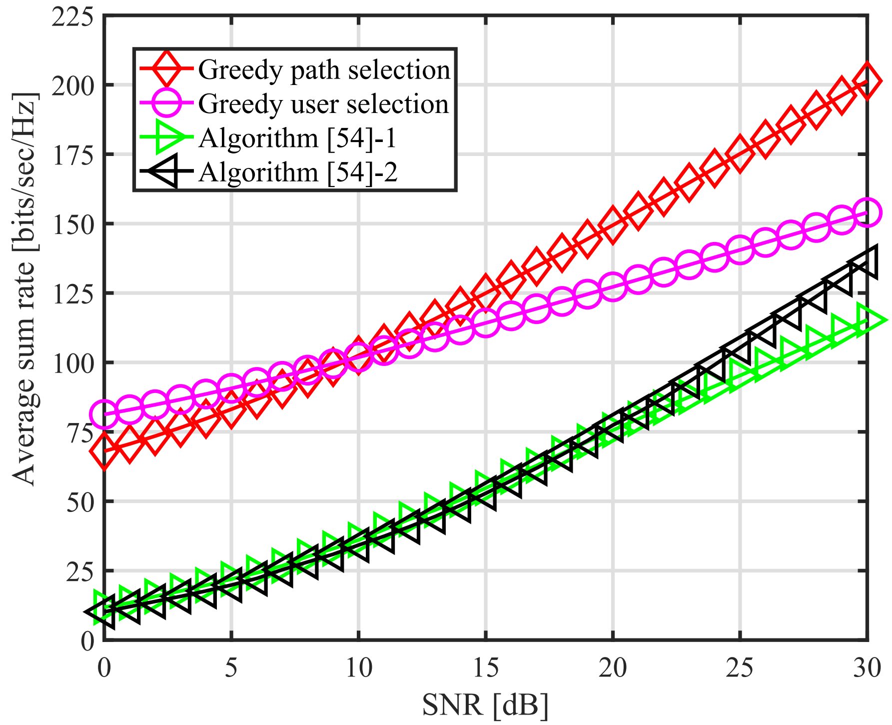

Figure 3.3: Average sum rate vs. SNR; $N_t = 40$, $N_p = 2$ and $K = 20$.

find which one maximizes sum rate. In steps 3 and 4 we remove the currently found edge along with those edges which violate constraint (3.7). If the currently found edge makes sum rate higher than its old value we update the selection matrix. Otherwise we output the current selection matrix. Finally, if there are still edges in the candidate set, we repeat the process.

For the sake of comparison, we have also considered two user selection algorithms proposed in [54], which are also applicable in highly directional channel as those observed in sparse massive MIMO channels. The following explain the way these two algorithms select users. In order to have a fair comparison, we assume that similarly to our path selection algorithm at most one data stream is sent over each angular bin when using these selection algorithms.

Algorithm [54]-1: This algorithm, firstly, removes all those angles of departure that overlap in beam-space domain. Then over the remaining angles of departure, it chooses the users that maximize the total coverage area in the beam-space domain.

Algorithm [54]-2: In contrast to Algorithm [54]-1, Algorithm [54]-2 aims to maximize the number of served users who have at least one non-overlapping angle of departure in the beam-space domain.

For example, consider two users, whose angles of departure lie in the following angular bins $B_1 = (-0.1, 0.1) \cup (0.2, 0.25)$ and $B_2 = (-0.1, 0.1) \cup (-0.4, -0.3)$. Applying Algorithm [54]-1 results in the selection of only user 2, while with Algorithm [54]-2 both users will be selected.

3.3 Simulation Results

Here, we present simulation results demonstrating the performance of the proposed path selection algorithm. Fig. 3.2 shows the average sum rate for different algorithms as a function of SNR. "Algorithm [54]-1" and "Algorithm [54]-2" refer to the selection algorithms described above. "Greedy path selection" refers to our proposed algorithm described above, and "Greedy user selection" is a typical user selection approach, which aims to maximize the sum rate by successively adding users one by one to the set of candidate users in a greedy fashion. As it can be seen the proposed path selection algorithm outperforms other three algorithms particularly at reasonably high SNRs. Fig. 3.3 presents the the same trend as Fig. 3.2, but for the case of $K = 20$. Note that in this case when the number of users has been doubled, at low-SNR regime fine selection of paths does not result in higher throughput compared to coarse user selection which is due to increase in inter-beam interference. This causes our algorithm to not select a number of paths that cause interference to other angular bins.

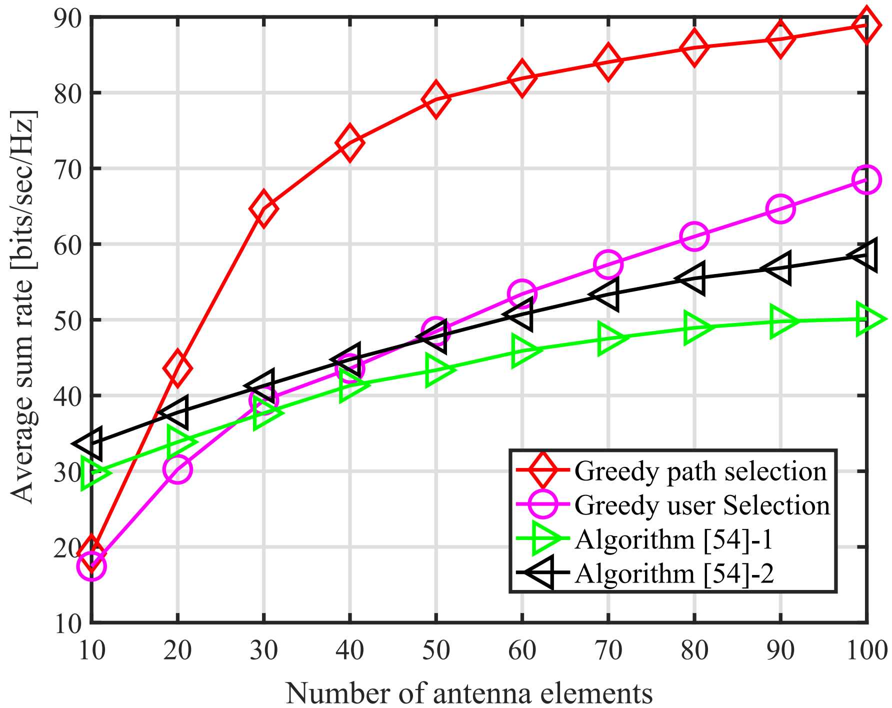

Figure 3.4: Average sum rate vs. number of antenna elements N_t; SNR $= 18$ dB , $N_p = 2$ and $K = 20$.

In Fig. 3.4, average sum rate versus the number of antenna elements N_t is shown. As the number of antenna elements increases, the greedy path selection algorithms shows its advantage over other algorithms. The reason is that number of angles of departure increases and multipath components are distributed over a larger set of angular bins. Thus, greedy path selection algorithm can take advantage of available multipath and multiuser diversity more flexibly. Fig. 3.5 shows average sum rate versus the number of multipath components N_p. It is interesting that as N_p increases greedy path selection algorithm is able to select proper paths and use available multipath diversity in order to maximize sum rate due to its fine selection strategy. However, as N_p increases the other three algorithms are not able to cope with the interference resulting from overlapping multipath components

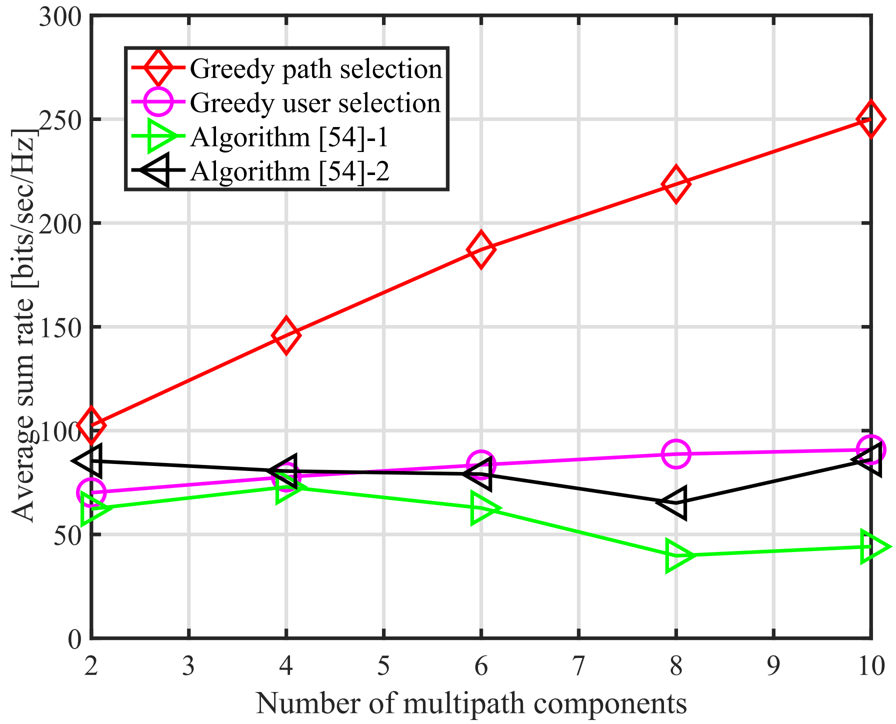

Figure 3.5: Average sum rate vs. number of multipath components N_p; $N_t = 100$, SNR $= 18$ dB and $K = 20$.

as efficiently as the greedy path selection.

3.4 Summary

In this chapter, we have introduced a path selection algorithm for sparse massive MIMO channels, where each user receives its signal via only a few propagation paths. With uniform linear array consisting of a large number of antenna elements and DFT beamforming, we have considered a virtual channel representation in the beam-space domain to capture channel sparsity, where each user's path lies within a bin of angles of departure. We have associated a sparse bipartite graph with this multi-user setting, where independent user and angular bin nodes are connected by edges, if there are physical paths between them. Next we have formulated an optimization problem aiming to maximize sum rate by selecting edges in this graph in a greedy fashion. Unlike coarse user selection algorithms, our fine path selection algorithm is able to take advantage of available multipath and multiuser diversity more efficiently, thus resulting in higher throughput.

Chapter 4

Simplified User Grouping Algorithm for Massive MIMO on Sparse Beam-Space Channels

In this chapter, we tackle the problem of user grouping for sparse beam-space massive MIMO channels. First of all, we have no prior knowledge of the possible number of user groups/clusters, and secondly choosing an arbitrary number of groups can limit the performance of the system without considering multiuser and inter-beam interference. Herein, we propose a novel and simplified user grouping scheme, which is our primary contribution. Inspired by the concept of path selection and the bipartite graph introduced in [85], we partition the set of users into groups corresponding to the angular bins that they occupy. In this approach, we examine each angular bin, which is connected to a set of user nodes via edges (resolvable paths). Users that receive a signal from the same angular bin are grouped together. In [87], we have proposed a two-layer beamforming scheme for massive multiuser MIMO (MU-MIMO) downlink channels. The first layer employs a bipartite graph to dynamically group users in the beam-space domain; the aim is to minimize inter-user interference while significantly reducing the effective channel dimensionality. Then, with a focus on maximizing spatial multiplexing gain and system throughput, the second layer performs MU-MIMO linear precoding using a precoding matrix determined by the effective channel within each group. Our proposed algorithm takes advantage of the sparsity of massive MIMO channels to achieve spatial multiplexing and cope with the interference resulting from overlapping multipath components.

4.1 Problem Formulation

In this work, we create groups of users that maximize the system throughput by minimizing the inter-user interference in the beam-space domain, derived from the concept of the path selection algorithm introduced in [85]. Given the connectivity matrix $\mathbf{C}$, we have the knowledge that enables us to perform user grouping. Inspired by the concept of path selection introduced in [85], we adopt the bipartite graph representation and simply categorize users into groups according to the angular bins that they occupy. Therefore, by investigating each angular bin and the paths that connect it to a set of user nodes, we can partition users into groups. Obviously, in most cases a user could be allocated to one of several candidate groups (recall each user receives data over N_p multipath components that can originate from at most N_p different angular bins). In such cases, we consider adding the user to each candidate group and evaluate the objective function for each case. Among all the candidate groups, the one that results in the highest performance (or the largest objective function value) will be selected.

Suppose that the K user terminals are grouped into G groups, where K_g users are in group g. The algorithm groups users such that each user in a given group g has overlapped angular bins with at least one other user in the group (provided that $K_g > 1$). We define $\mathcal{U}_g$ as the discrete set of users in group g, therefore $|\mathcal{U}_g| = K_g$ indicates its cardinality; we also enforce the constraint that a user can only belong to one group. Let ψ_k indicate the set of angular bins that user k occupies, and $|\psi_k|$ be equal to the number of angular bins over which user k receives its signal from the BS. Now, we can define the rank condition for each group as follows:

$$K_g \leq \left| \bigcup_{k \in \mathcal{U}_g} \psi_k \right| = \beta_g, \tag{4.1}$$

where β_g is the rank of group g, and it is related to the number of dominant eigenmodes for group g. This condition defines the number of users that can be spatially multiplexed in group g. In this notation, we denote user k in group g by the index g_k, and its channel vector is given by $\mathbf{h}_{g_k}$. Consider $\mathbf{H}_g = \left[\mathbf{h}_{g_1}^T, \ldots, \mathbf{h}_{g_{K_g}}^T\right]^T \in \mathcal{C}^{K_g \times N_t}$ as the aggregate concatenated channel matrix of users in group g.

Similar to the previous chapter, we quantize the AoD such that if it lies in the angular bin j, it would be represented by the central angle $\hat{\theta}_j = -\frac{\pi}{3} + \frac{\pi}{3N_t} + \frac{2\pi}{3}\frac{j}{N_t}$ for that bin. Now, we can define the beamforming vector $\mathbf{f}_j$ for each angular bin j as

$$\mathbf{f}_j = \mathbf{a}(N_t, \hat{\theta}_j). \tag{4.2}$$

As $N_t \to \infty$ the quantization effect diminishes and we get very narrow beams to separate users from each other. Note also that these DFT beamforming vectors are orthogonal, i.e. $\mathbf{f}_i^H \mathbf{f}_j = 0$ for $i \neq j$, which is useful for inter-beam interference cancellation.

In order to achieve spatial multiplexing within a group g, we employ zero-forcing (ZF) linear precoding. The ZF precoding matrix $\mathbf{W}_g \in \mathcal{C}^{\beta_g \times K_g}$ is a simple pseudo-inverse given by

$$\mathbf{W}_g = \xi_g^2 \tilde{\mathbf{H}}_g^H (\tilde{\mathbf{H}}_g \tilde{\mathbf{H}}_g^H)^{-1}, \tag{4.3}$$

where ξ_g^2 is the power normalization factor, $\tilde{\mathbf{H}}_g = \mathbf{H}_g \mathbf{F}_g \in \mathcal{C}^{K_g \times \beta_g}$ is the effective channel, and $\mathbf{F}_g \in \mathcal{C}^{N_t \times \beta_g}$ is the DFT beamforming matrix of group g. $\mathbf{F}_g$ is formed from the beamforming vectors $\mathbf{f}_j$ for all bins j belonging to group g, given by $\bigcup_{k \in \mathcal{U}_g} \psi_k$. The number of users K_g in group g that can be spatially multiplexed cannot be larger than the rank of the equivalent channel, given by β_g.

Now, focusing only on the received signal $\mathbf{y}_g \in \mathcal{C}^{K_g \times 1}$ for users in group g, we have

$$\mathbf{y}_g = \tilde{\mathbf{H}}_g \mathbf{W}_g \mathbf{d}_g + \left(\sum_{\ell=1, \ell \neq g}^{G} \mathbf{H}_g \mathbf{F}_\ell \mathbf{W}_\ell \mathbf{d}_\ell \right) + \mathbf{n}_g, \tag{4.4}$$

where $\mathbf{d}_g \in \mathcal{C}^{K_g \times 1}$ is the vector of transmitted data streams to users in group g, and $\mathbf{n}_g \in \mathcal{C}^{K_g \times 1}$ is an additive white Gaussian noise vector with i.i.d. entries $\sim \mathcal{CN}(0, 1)$. The bracketed term denotes the inter-group interference. The achievable sum rate within a group g can be expressed as follows:

$$R_g = \log_2 \frac{\det\left(\mathbf{I} + \tilde{\mathbf{H}}_g \mathbf{W}_g \mathbf{d}_g \mathbf{d}_g^H \mathbf{W}_g^H \tilde{\mathbf{H}}_g^H \right)}{\det\left(\mathbf{I} + \sum\limits_{\ell=1, \ell \neq g}^{G} \mathbf{H}_g \mathbf{F}_\ell \mathbf{W}_\ell \mathbf{d}_\ell \mathbf{d}_\ell^H \mathbf{W}_\ell^H \mathbf{F}_\ell^H \mathbf{H}_g^H \right)}. \tag{4.5}$$

The sum rate of the system will be equal to $R_{\text{sum}} = \sum_{g=1}^{G} R_g$. Furthermore, by appropriate user grouping and DFT beamforming, it is possible to approximately eliminate the inter-group interference by enforcing the condition

$$\mathbf{H}_g \mathbf{F}_\ell \approx \mathbf{0}, \text{ for all } \ell \neq g. \tag{4.6}$$

Algorithm 4.1 provides pseudocode of the proposed user grouping algorithm. The algorithm first initializes the connection matrix $\mathbf{C}$. Then, it investigates each angular bin j, finds all the user node indices $i \in \{1, 2, \ldots, K\}$ connected to bin j, and stores them in temporary user group $\mathcal{D}$. For each user node $\mathcal{D}^{(i)}$, it inspects the possibility that the user has been previously put in another group $\mathcal{U}_l \in \mathcal{S}$, resulting in two cases. If not yet in a group, the user will be allocated to the user group associated with bin j (called $\mathcal{U}_g$). Otherwise, the objective function (4.4) will be evaluated for both the user's previously assigned group and the group for the current bin. The user will be assigned (or reassigned) to the group that yields the higher rate. Once all the user nodes $\in \mathcal{D}$ are investigated for all the previously created groups, the group associated with bin j will be added to the set $\mathcal{S}$, if that group is not empty. The entire process is repeated for all the angular bins.

4.1.1 Complexity

In this subsection, we briefly discuss the complexity of the proposed user grouping and two-layer beamforming algorithm. Before discussing the user grouping itself, we consider the complexity of converting to the sparse beam-space representation of the users' channels. Nominally, performing the DFT operation can be considered a multiplication between the channel matrix and the DFT beamforming matrix. However, the DFT can be performed with less complexity via a fast Fourier transform with complexity order $\mathcal{O}(N_t \log(N_t))$ [88, 89]. This must be done for each user, for a total complexity of $\mathcal{O}(KN_t \log(N_t))$. Note that some of this complexity could be potentially reduced depending on the hardware used. For instance, the DLA antenna as used in [90] approximates the ULA and the DFT operation together in one. The $K \times N_t$ binary connectivity matrix $\mathbf{C}$ must then be constructed, i.e. to determine if an edge exists between user i and angular bin j, $\forall i, j$. This process is of order $\mathcal{O}(KN_tQ)$, where Q is the complexity of whatever calculation is used to determine if an edge exists. The specifics of this process are mostly outside the scope of this study, but as an example, one could use a a channel estimation algorithm to estimate massive MIMO sparse beam-space channel parameters (i.e. the gains and AoDs of the paths), like that in [91] where a compressed sensing algorithm was used to estimate the sparse channel's parameters via a codebook of beamforming vectors obtained through the discrete Fourier transform design.

On the user grouping itself, the selection process in our algorithm is an exhaustive search. However, at this point one no longer needs to consider the "full" channel matrix, but rather the sparse beam-space representation, which has a limited number of paths. Therefore, the computational complexity of the group selection will be moderate, since one no longer has to deal with computations on the order of N_t. Considering the user grouping problem, there is a bipartite graph with a number of vertices (from the sets of user nodes and angular bins) and a number of paths among these vertices. The graph has

$N_t + K$ vertices and $N_t K$ edges in total. However, we are able to exploit the sparsity of the graph, since we are only interested in edges with a value of 1 in the connectivity matrix $\mathbf{C}$. (At this point, determining the value is just a simple binary check, whose relatively simple complexity compared to other floating-point operations can easily be neglected.) From our system model, there are only KN_p edges with a value of 1 in $\mathbf{C}$; the rest are zero.

The main complexity of the user grouping algorithm is in the evaluation of (4.5), i.e. the rate of group g, which is dependent on the effective channel matrix $\tilde{\mathbf{H}}_g \in \mathcal{C}^{K_g \times \beta_g}$. More specifically, we are mostly concerned with calculating the numerator of (4.5); from the approximate elimination of inter-group interference by the condition in (4.6), the denominator of (4.5) approximately reduces to 1. The rate calculation involves matrix (pseudo-)inverses, multiplications, and determinant operations. The pseudo-inverse in (4.3) can be found with $\mathcal{O}(\beta_g K_g^2)$ complex operations to find $\tilde{\mathbf{H}}_g \tilde{\mathbf{H}}_g^H$, then $\mathcal{O}(K_g^3)$ operations for the matrix inverse $(\tilde{\mathbf{H}}_g \tilde{\mathbf{H}}_g^H)^{-1}$ by LDL decomposition [74]. $\tilde{\mathbf{H}}_g \mathbf{W}_g = \xi_g^2 \tilde{\mathbf{H}}_g \tilde{\mathbf{H}}_g^H (\tilde{\mathbf{H}}_g \tilde{\mathbf{H}}_g^H)^{-1}$ can be found by reusing the above $\tilde{\mathbf{H}}_g \tilde{\mathbf{H}}_g^H$ calculation and doing an order $\mathcal{O}(K_g^3)$ matrix multiplication of two $K_g \times K_g$ matrices [74, 92]. Similarly, the multiplications $\tilde{\mathbf{H}}_g \mathbf{W}_g \mathbf{d}_g$ and then $\tilde{\mathbf{H}}_g \mathbf{W}_g \mathbf{d}_g \mathbf{d}_g^H \mathbf{W}_g^H \tilde{\mathbf{H}}_g^H$ can be performed with order $\mathcal{O}(K_g^2)$. Finally, the matrix determinant can be calculated with order $\mathcal{O}(K_g^3)$ by means of LU decomposition [92].[1] The total complexity clearly depends on the value of K_g and β_g for each group. However, the total number of rate calculations should be at most about $2KN_p$; for each connected edge in $\mathbf{C}$, a rate is generally calculated twice, once for determining whether the user-bin pair represented by the edge should become part of a new group, and once to see if it should stay as part of its old group. Rate calculations for the latter could potentially be reused to reduce complexity in some cases.

Considering hardware complexity, in conventional multiuser MIMO systems precoding is typically done through digital precoders at baseband, which requires a

[1] With square $n \times n$ matrices, multiplication, and by extension inverses and determinants [89], can in fact potentially be done with as low a complexity as $\mathcal{O}(n^{2.373})$ [93].

separate RF chain, including digital-to-analog converters, mixers, and power amplifiers, for each of the N_t antenna elements. Deploying such structures in massive MIMO systems is not practical due to the very large number of antennas. However, in a hybrid architecture the precoding and combining processes are jointly implemented in analog and digital domains. In such a structure the hardware complexity of transceiver is significantly reduced, which makes it an attractive alternative for implementation of massive MIMO systems. For our scheme, when using the hybrid architecture, the DFT beamforming can be implemented in the analog domain. Transformation to the beam-space representation can be done for each user with an analog DFT, requiring $\lceil \log_2(N_t) \rceil$ stages of 4-port hybrid directional couplers and $\lceil \log_2(N_t) \rceil - 1$ stages of phase shifters [94], where $\lceil \cdot \rceil$ is the ceiling function; each stage contains $\lceil N_t/2 \rceil$ components. However, for the actual downlink transmission, once the DFT beamforming matrices $\mathbf{F}_g$ for each group have been determined, fewer components are required. In transmitting K streams (one to each of the K users), the digital ZF precoder portion then only requires a total of K RF chains. Meanwhile, the analog beamforming portion would use just $K \times N_t$ phase shifters, assuming a fully-connected structure [52].

4.2 Simulation Results

In this section, we present simulation results demonstrating the performance of our proposed two-layer beamforming algorithm. In order to gain interesting insights into the operation of our proposed algorithm, we run the algorithm for different values of parameters N_t, K, N_p, and SNR. The number of RF chains is assumed to be equal to the number of users K. We assume equal power allocation to all the downlink data streams, and define SNR $= P$, where P is the total transmit power at the BS. In this work, we assume that the BS has access to imperfect CSI subject to channel estimation error, e.g. as in [95]. We set the estimation variance parameter τ from [95] to be 0.1.

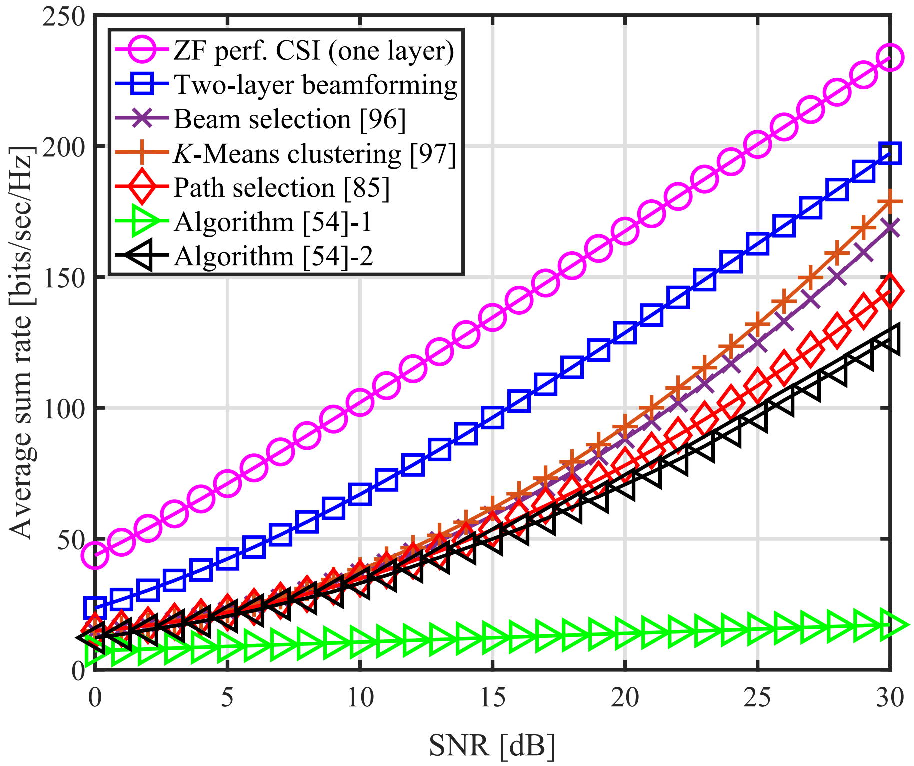

Figure 4.1: Average sum rate vs. SNR; $N_t = 100$, $N_p = 2$, and $K = 20$.

Fig. 4.1 shows the average sum rate for different algorithms as a function of SNR for $N_t = 100$, $N_p = 2$, and $K = 20$. “ZF perf. CSI (one layer)” shows the performance obtained using linear zero-forcing beamforming with perfect CSI and a conventional (one-layer) fully digital baseband precoder. “Two-layer beamforming” is our proposed algorithm, “Beam selection” refers to the proposed beam selection algorithm in [96], and “K-means clustering” is the proposed user selection algorithm in [97] with ZF within each group. “Path selection” refers to the algorithm described in [85], in which only DFT beamforming is used and only one user is served per beam/ angular bin, and “Algorithm [54]-1” and “Algorithm [54]-2” refer to selection algorithms that have been proposed in [54]. Our two-layer beamforming scheme and the algorithms from [96] and [97] all

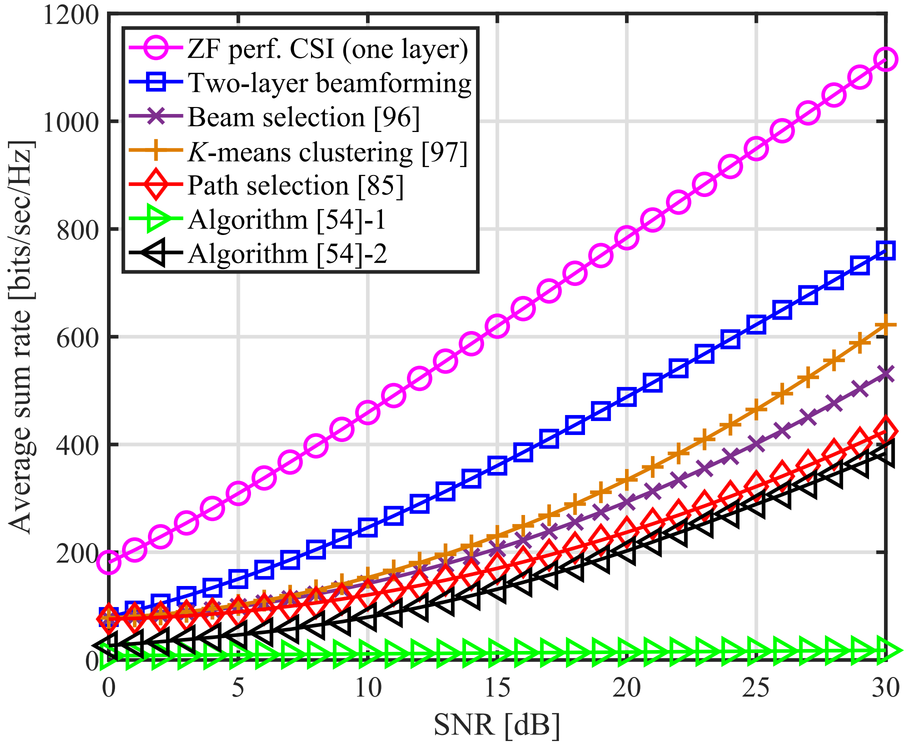

Figure 4.2: Average sum rate vs. SNR; $N_t = 400$, $N_p = 2$, and $K = 100$.

perform user grouping on beams/bins, and thus can be reasonably compared. In contrast, our path selection from [85] and the two algorithms from [54] only assign one user per beam/path. They therefore are not on the same footing as the user grouping schemes, but can reasonably be compared with each other.

As it can be seen in Fig. 4.1, the proposed two-layer beamforming algorithm outperforms the other algorithms at all SNR values. The path selection algorithm from [85] also outperforms Algorithms [54]-1 and [54]-2. In [97], the target number of groups is not known beforehand and choosing an arbitrary number of clusters can have severe impact on the performance of the system. On top of that, appropriate chordal distance thresholds are hard to predict in the clustering process. Our proposed algorithm dynamically categorizes users into groups while keeping the inter-group interference almost zero. In [96], the algorithm allocates only one beam/bin to each user; therefore in cases where two or more users have the same strongest beam, at most one of them is assigned to use it. However, in our algorithm that same beam/bin can be shared among multiple users. Also, in [96] ZF precoding is used to cancel interference between beams, whereas in our work it cancels interference within a group; in our proposed scheme, inter-group interference cancellation is handled by the DFT beamformer.

The performance at $N_t = 400$, $K = 100$, and $N_p = 2$ versus SNR is illustrated in Fig. 4.2. As seen, as the number of antennas at the BS and the number of users both grow, the superior performance gain of our algorithm becomes somewhat higher relative to that of the other algorithms at higher SNRs. This is due to the fact that the greedy path selection (DFT beamformer) enables us to partition the set of users into groups in a finer fashion in the beam-space domain. In addition, “Algorithm [54]-1” and “Algorithm [54]-2” do not select some of the users due to their selection criteria, which results in lower spectral efficiency.

As expected, by increasing the number of antennas the number of angular bins grows as well. This results, amongst other things, in having more user groups (due to better angular resolution in the beam-space domain), which enables us to cope with both inter-group and inter-user interference better. Hence, the average sum rate of the system goes up as N_t increases[2], while other parameters remain constant. In particular, at SNR = 20 dB, $N_t = 400$, and $K = 20$, the average sum rate is about 200 bits/sec/Hz, which is about 55% higher than 129 bits/sec/Hz with $N_t = 100$ seen in Fig. 4.2.

In Fig. 4.3, the average sum rate versus the number of multipath components N_p is illustrated. It is interesting that as N_p increases the proposed algorithm is able to

[2]However, it should be noted that increased angular resolution is not the only effect of increasing the number of antennas; for example, spatial diversity also increases. Unfortunately, the effect of angular resolution on the system performance cannot be isolated by itself, since the number of angular bins is tied to the number of antennas.

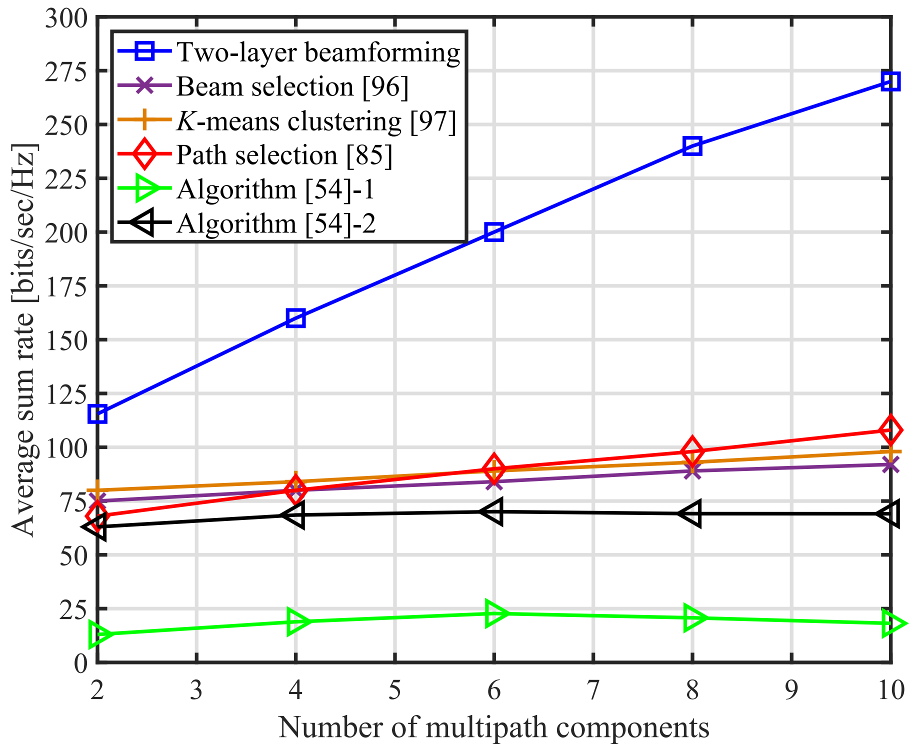

Figure 4.3: Average sum rate vs. number of multipath components N_p; $N_t = 100$, SNR $=$ 18 dB, and $K = 20$.

achieve a higher throughput. However, as N_p increases the two algorithms in [54] and the path selection algorithm are not able to cope with the interference resulting from overlapping multipath components. "Algorithm [54]-1" simply removes those users that have overlapped angular bins, and "Algorithm [54]-2" just allows users with only one overlapped angular bin. The beam selection method of [96] defines only two user groups, interfering and non-interfering, and only assigns one beam per user. Increasing the number of multipath components means more interference, which results in a rapidly decreasing likelihood of users belonging to the "non-interfering" group if the power on more than one of those paths is approximately equal. This also makes it more difficult to assign one

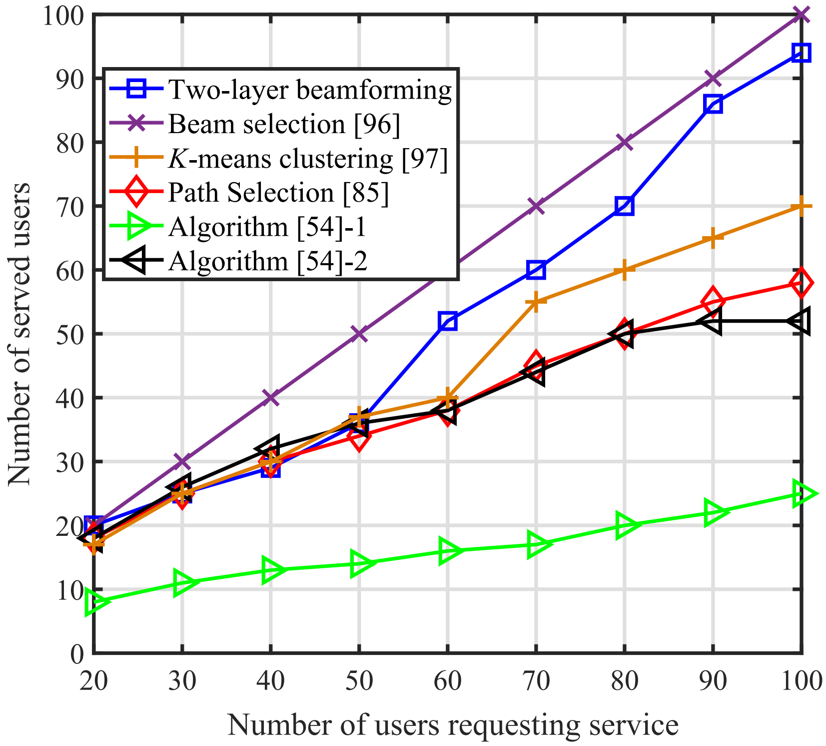

Figure 4.4: Comparison of the number of served users vs. the number of users requesting service K; $N_t = 400$, SNR $= 20$ dB, and $N_p = 2$.

"best" beam and perform ZF precoding among those users. In the case of the K-means clustering algorithm proposed in [97], we can see that increasing the number of multipath components degrades the accuracy of the iterative algorithm to partition users into a fixed number of groups. In this situation, users' channel covariances in different groups will have non-empty intersection, or inter-group interference will not be under control.

We also investigate the average number of users being simultaneously served versus varying numbers of users requesting service when the number of BS antennas is $N_t = 400$, as plotted in Fig. 4.4. Contrary to what is observed in [54], it can be seen that by grouping together users who have the same angular bins and serving them using ZF beamforming, we are able to achieve high spatial multiplexing. In other words, our algorithm is capable of serving more users by grouping them based on the angular bins that they occupy while channels are sparse in the beam-space domain. In [96], the authors guarantee that their proposed beam selection algorithm will serve all the users; however the number of served users is lower limited by the number of RF chains. In comparison to our proposed algorithm, which aims to serve as many users as possible via all the existing paths, the beam selection method of [96] serves all the users through only a limited number of beams that satisfy a sum rate maximization criterion. Our proposed user selection algorithm serves more users than the K-means clustering algorithm of [97], which is due to inter-user and inter-group interference limitations of the latter.

4.3 Summary

In this chapter, we have proposed a two-layer MU-MIMO beamforming algorithm for sparse massive MU-MIMO downlink channels that contain few discrete multipath components. Such sparse channels are particularly common at mmWave frequencies, though sub-6 GHz massive MIMO channels are also highly directional. By assuming a ULA as the transmitter antenna array and DFT beamforming, we have adopted a virtual channel representation in the beam-space domain to capture channel sparsity, where each user's paths lie within bins of AoDs. In the first layer of the scheme, a considerable dimensionality reduction of the channel matrix occurs due to user grouping; users that overlap angular bins in the beam-space domain are assigned to the same group. In the second layer, simple MU-MIMO linear precoding is performed using the reduced-dimension effective channel. We have demonstrated the superior performance of our proposed two-layer beamforming algorithm for different parameter values in comparison to some other algorithms described in the literature.

Algorithm 4.1: User Grouping Algorithm

Initialize the connectivity matrix $\mathbf{C}$ of dimension $K \times N_t$, temporary user group $\mathcal{D} = \emptyset$, and the set that contains all the user groups
$\mathcal{S} = \{\mathcal{U}_g | g = 1, ..., G\} = \emptyset$;
for $j = 1$ to N_t **do**
  $\mathcal{D} = \{i | c_{i,j} \neq 0\}$;
  $\mathcal{U}_g = \emptyset$;
  for each $\mathcal{D}^{(i)} \in \mathcal{D}$ **do**
    if $\mathcal{D}^{(i)} \notin \mathcal{S}$ **do**
      Update group $\mathcal{U}_g = \mathcal{U}_g \cup \mathcal{D}^{(i)}$;
    else
      Define temporary set $\mathcal{U}_{gt} = \mathcal{U}_g \cup \mathcal{D}^{(i)}$;
      Calculate R_g using the users in $\mathcal{U}_{gt}$ and (4.5);
      Find the set $\mathcal{U}_l \in \mathcal{S}$ for which $\mathcal{D}^{(i)} \in \mathcal{U}_l$;
      Calculate R_l using the users in $\mathcal{U}_l$ and (4.5);
      if $R_g > R_l$,
        $\mathcal{U}_g = \mathcal{U}_{gt}$;
        $\mathcal{U}_l = \mathcal{U}_l \setminus \mathcal{D}^{(i)}$;
        if $|\mathcal{U}_l| = 0$,
          $\mathcal{S} = \mathcal{S} \setminus \mathcal{U}_l$;
        end if
      end if
    end if
  end for
  if $|\mathcal{U}_g| > 0$,
    $\mathcal{S} = \mathcal{S} \cup \mathcal{U}_g$;
  end if
end for

Chapter 5

Hybrid Beamforming and DFT-Based Channel Estimation for Millimeter Wave Large-Scale MIMO Systems

Hybrid beamforming architecture facilitates implementation of large-scale MIMO systems making them somewhat more practical. This architecture, shown in Fig. 5.1, splits the precoding process between analog and digital domains. In general, hybrid precoding architectures may employ two different signal mapping structures between the RF chains and antennas [43]. The first structure is fully-connected, with all the RF chains connected to each antenna element. The signals from the digital precoder are sent to all the antenna elements through RF chains. In contrast, in the partially-connected structure only N_t/N_{RF}^t antennas are connected to each of N_{RF}^t RF chains at the transmitter. The fully-connected structure enjoys full beamforming gain, while the partially-connected structure offers lower implementation complexity in return for losing some beamforming gain [98]. Both structures are shown in Fig. 5.2.

In [91], assuming a partially-connected structure, we describe a matrix factorization approach to tackle the problem of hybrid precoding-combining design as two separate optimization problems. We also introduce a channel estimation algorithm with beamforming reference vectors derived using the discrete Fourier transform (DFT) approach. This method exploits channel sparsity present at mmWave frequencies when estimating the channel parameters and delivers better beamforming patterns for channel estimation compared to the existing algorithm in [99].

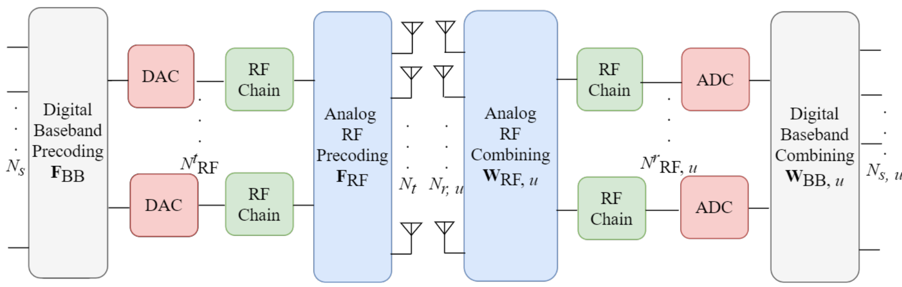

Figure 5.1: MIMO architecture for a mmWave system using hybrid analog-digital precoding and combining (DAC = digital-to-analog converter, ADC = analog-to-digital converter).

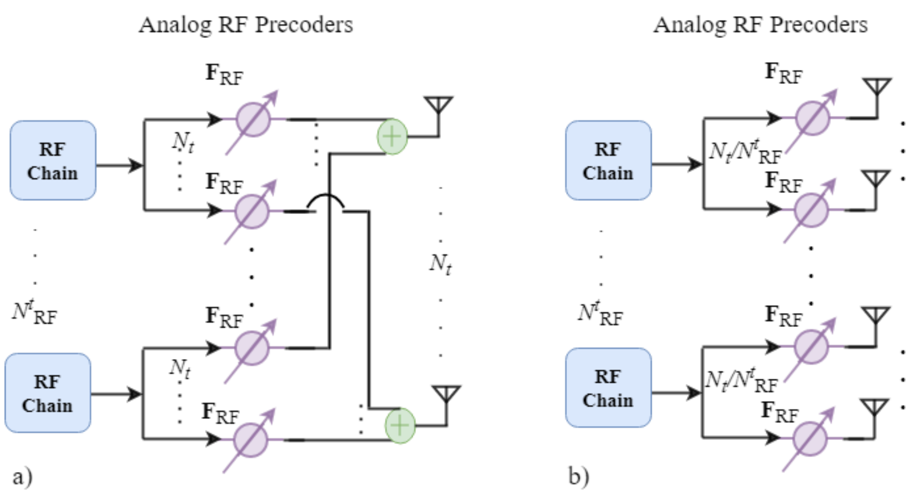

Figure 5.2: Analog processing for hybrid precoding transmitters. a) Fully-connected structure. b) Partially-connected structure.

5.1 System Model

Consider a mmWave MIMO system with N_t antennas at the BS collecting and sending N_s data streams to a single user with N_r antennas. To enable multistream transmission and reception, the transmitter and receiver are equipped with N_{RF}^t and N_{RF}^r RF chains, respectively, such that $N_s \leq N_{\text{RF}}^t \leq N_t$ and $N_s \leq N_{\text{RF}}^r \leq N_r$ hold. Focusing solely on the downlink transmission, the transmitted signal can be written as

$$\mathbf{x} = \mathbf{F}_{\text{RF}}\mathbf{F}_{\text{BB}}\mathbf{s}, \tag{5.1}$$

where $\mathbf{s} \in \mathcal{C}^{N_s \times 1}$ is the symbol vector such that $\mathbb{E}[\mathbf{s}\mathbf{s}^H] = \frac{1}{N_s}\mathbf{I}_{N_s}$. The transmitter is assumed to apply a digital baseband precoder $\mathbf{F}_{\text{BB}} \in \mathcal{C}^{N_{\text{RF}}^t \times N_s}$ followed by an analog RF precoder $\mathbf{F}_{\text{RF}} \in \mathcal{C}^{N_t \times N_{\text{RF}}^t}$. The total transmit power constraint is given by $\|\mathbf{F}_{\text{RF}}\mathbf{F}_{\text{BB}}\|_F^2 = N_s$.

For simplicity, we adopt a narrowband[1] block fading propagation channel. The receiver uses an analog RF combining matrix $\mathbf{W}_{\text{RF}} \in \mathcal{C}^{N_r \times N_{\text{RF}}^r}$, and a digital baseband decoder $\mathbf{W}_{\text{BB}} \in \mathcal{C}^{N_{\text{RF}}^r \times N_s}$ to obtain the received signal $\mathbf{y} \in \mathcal{C}^{N_s \times 1}$:

$$\mathbf{y} = \sqrt{\rho}\mathbf{W}_{\text{BB}}^H\mathbf{W}_{\text{RF}}^H\mathbf{H}\mathbf{F}_{\text{RF}}\mathbf{F}_{\text{BB}}\mathbf{s} + \mathbf{W}_{\text{BB}}^H\mathbf{W}_{\text{RF}}^H\mathbf{n}, \tag{5.2}$$

where ρ stands for the average transmitted power, $\mathbf{H} \in \mathcal{C}^{N_r \times N_t}$ is the channel matrix, and $\mathbf{n} \sim \mathcal{CN}(\mathbf{0}, \sigma^2\mathbf{I})$ is the $N_r \times 1$ Gaussian noise vector corrupting the received signal. Considering a Gaussian distribution for transmitted symbols, the achievable spectral efficiency can be expressed as follows:

$$\begin{aligned} R = \log\det(\mathbf{I}_{N_s} + \frac{\rho}{\sigma^2 N_s}&(\mathbf{W}_{\text{RF}}\mathbf{W}_{\text{BB}})^\dagger\mathbf{H}\mathbf{F}_{\text{RF}}\mathbf{F}_{\text{BB}} \\ &\times\mathbf{F}_{\text{BB}}^H\mathbf{F}_{\text{RF}}^H\mathbf{H}^H(\mathbf{W}_{\text{RF}}\mathbf{W}_{\text{BB}})). \end{aligned} \tag{5.3}$$

[1]In the case of a wideband multicarrier system, the bandwidth is split into several sub-bands, with narrowband subchannels. A similar channel model then applies to each of the subchannels.

In the hybrid precoding design, the analog RF precoder $\mathbf{F}_{\text{RF}}$ and combining matrix $\mathbf{W}_{\text{RF}}$ are implemented using analog phase shifters, which only adjust the phases of the transmitted signals. Such implementation requires unit modulus for all non-zero elements of the matrices $\mathbf{F}_{\text{RF}}$ and $\mathbf{W}_{\text{RF}}$.

One of the main features of mmWave channels is the presence of high free-space path loss leading to limited spatial selectivity scattering. Additionally, the use of large tightly-packed antenna arrays in mmWave transceivers results in high antenna correlation. The existence of such high correlation in the sparse multipath scattering environment at mmWave frequencies makes most of the statistical fading channel models used in conventional MIMO systems inaccurate and irrelevant. The highly directional nature of propagation at mmWave frequencies and the high dimensionality of MIMO channels with large antenna arrays can be modeled by beam-space or virtual channel representation [86]. Considering an environment with limited useful scattering paths, we adopt a virtual channel representation in which the mmWave channel results from the sum of N_p discrete multipath components, each of which is further assumed to be one single propagation path between the BS and a given user. Based on this model, the mmWave channel matrix $\mathbf{H}$ can be expressed as follows:

$$\mathbf{H} = \sqrt{\frac{N_t N_r}{\gamma}} \sum_{p=1}^{N_p} \alpha_p \mathbf{a}_r(\theta_p^r) \mathbf{a}_t(\theta_p^t)^H, \tag{5.4}$$

where γ is the average path loss between the BS and a given user, α_p is the complex gain of the p^{th} path, and θ_p^r and θ_p^t are the azimuth angle of arrival (AoA) and angle of departure (AoD) of that path, respectively. In addition, $\mathbf{a}_r(\theta_p^r)$ and $\mathbf{a}_t(\theta_p^t)$ represent the receive and transmit antenna array response vectors at the corresponding angles of arrival and departure. In this investigation, we consider that α_p for $p = 1, 2, \ldots, N_p$ are i.i.d $\mathcal{CN}(0, \sigma_\alpha^2)$ where σ_α^2 represents the average power gain, which is equal for each path.

The receive and transmit antenna array response vectors $\mathbf{a}_r(\theta_p^r)$ and $\mathbf{a}_t(\theta_p^t)$ are a function of the receive and transmit antenna array structure. Given an N-element uniform linear array (ULA) composed of isotropic antenna elements, the array response vector can be written as:

$$\mathbf{a}_{\text{ULA}}(\theta) = \frac{1}{\sqrt{N}}[1, e^{jkd\sin(\theta)}, ..., e^{jkd(N-1)\sin(\theta)}]^T, \tag{5.5}$$

where $k = \frac{2\pi}{\lambda}$, λ is the wavelength, and d is the distance between two adjacent antenna elements.

In this work, we propose a DFT beamforming vector codebook for the training stage of channel that is only applicable to ULAs, on account of the similarity between the ULA response vector and the complex exponential terms used in the inverse DFT. If a ULA is assumed, the receive and transmit antenna array response vectors $\mathbf{a}_r(\theta_p^r)$ and $\mathbf{a}_t(\theta_p^t)$ can be written as

$$\mathbf{a}_r(\theta_p^r) = \frac{1}{\sqrt{N_r}}[1, e^{jkd\sin(\theta_p^r)}, ..., e^{jkd(N_r-1)\sin(\theta_p^r)}]^T, \tag{5.6}$$

$$\mathbf{a}_t(\theta_p^t) = \frac{1}{\sqrt{N_t}}[1, e^{jkd\sin(\theta_p^t)}, ..., e^{jkd(N_t-1)\sin(\theta_p^t)}]^T. \tag{5.7}$$

5.2 Hybrid Precoding for Partially-Connected Structure

Here, the goal is to design a set of hybrid precoders and combiners that maximizes the spectral efficiency expression given in (5.3). As it can be seen, the solution to this problem seeks a joint optimization over four matrices, namely $\mathbf{F}_{\text{RF}}, \mathbf{F}_{\text{BB}}, \mathbf{W}_{\text{RF}}$ and $\mathbf{W}_{\text{BB}}$. However, the global optimum for such an optimization problem due to similar joint constraints is often found to be intractable [100], [101]. For the sake of simplicity in transceiver design, we decouple the joint optimization of the transmitter and receiver, and for now only focus on the design of the hybrid precoders $\mathbf{F}_{\text{RF}}$ and $\mathbf{F}_{\text{BB}}$ of the transmitter. Hereafter, we will mainly focus on designing the precoders, however the proposed algorithm is applicable to the decoder/combiner design at the receiver side.

With the focus only on the design of the hybrid precoders, the new optimization function that we seek to maximize is

$$\mathrm{I}(\mathbf{F}_{\text{RF}}, \mathbf{F}_{\text{BB}}) = \log\det(\mathbf{I}_{N_s} + \frac{\rho}{\sigma^2 N_s}\mathbf{H}\mathbf{F}_{\text{RF}}\mathbf{F}_{\text{BB}}\mathbf{F}_{\text{BB}}^H\mathbf{F}_{\text{RF}}^H\mathbf{H}^H). \tag{5.8}$$

In [49], it has been shown that maximizing the mutual information expression given above is approximately equivalent to minimization of

$$\mathbb{F} = \begin{cases} \min_{\mathbf{F}_{\text{RF}},\mathbf{F}_{\text{BB}}} & \|\mathbf{F}_{\text{opt}} - \mathbf{F}_{\text{RF}}\mathbf{F}_{\text{BB}}\|_F^2 \\ \text{s.t.} & \mathbf{F}_{\text{RF}} \in \mathcal{A} \\ \text{s.t.} & \|\mathbf{F}_{\text{RF}}\mathbf{F}_{\text{BB}}\|_F^2 = N_s, \end{cases} \tag{5.9}$$

where $\mathcal{A}$ is the set of feasible analog RF precoders, $\mathbf{F}_{\text{opt}}$ is the optimal precoder, while $\mathbf{F}_{\text{RF}}$ and $\mathbf{F}_{\text{BB}}$ respectively are the analog RF and digital precoders to be determined. It is known that the transceiver architecture that achieves single-user capacity can be derived from the channel's ordered singular value decomposition (SVD), i.e. $\mathbf{H} = \mathbf{U}\mathbf{\Sigma}\mathbf{V}^H$. Accordingly, the precoder (decoder) can be comprised of the first N_s columns of unitary matrix $\mathbf{V}(\mathbf{U})$.

Although the objective function given in (5.3) has been simplified to (5.8), optimization of problem $\mathbb{F}$ involving two variables simultaneously is not straightforward. However, optimization with respect to one variable while keeping the other one fixed is often easier and sometimes possible analytically. Accordingly, we can consider the optimization problem in (5.9) a matrix factorization problem consisting of solving the original optimization problem over two variables, namely $\mathbf{F}_{\text{RF}}$ and $\mathbf{F}_{\text{BB}}$. Then, the projection algorithm will be adopted as an auxiliary tool to solve the problem. The iterative nature and simplicity of the algorithm has made it as a powerful tool in many applications such as signal processing, information theory, control, and finance. As mentioned earlier, we consider a partially-connected structure for the hybrid precoding transceiver which will be applied henceforth. While the fully-connected structure provides full beamforming gain for each RF chain, the partially-connected structure deploys markedly fewer phase shifters and automatically results in a considerably higher energy efficiency, which is quite attractive in mmWave MIMO systems. In this structure, the output of each RF chain is only connected to N_t/N^t_{RF} antennas, which means less beamforming gain is available. Furthermore, the analog RF precoder $\mathbf{F}_{\text{RF}}$ is block-diagonal and composed of a set of vectors $\mathcal{A}_p = \{\mathbf{p}_1, \mathbf{p}_2, \ldots, \mathbf{p}_{N^t_{\text{RF}}}\}$, each with length N_t/N^t_{RF}. These vectors have elements with unit modulus that are essentially the phase of each phase shifter. Thus, the analog RF precoder $\mathbf{F}_{\text{RF}}$ is given by

$$\mathbf{F}_{\text{RF}} = \text{diag}[\mathbf{p}_1, \mathbf{p}_2, \ldots, \mathbf{p}_{N^t_{\text{RF}}}] = \begin{bmatrix} \mathbf{p}_1 & \mathbf{0} & \ldots & \mathbf{0} \\ \mathbf{0} & \mathbf{p}_2 & \ldots & \mathbf{0} \\ \vdots & \vdots & \ddots & \vdots \\ \mathbf{0} & \mathbf{0} & \ldots & \mathbf{p}_{N^t_{\text{RF}}} \end{bmatrix}, \tag{5.10}$$

where $\mathbf{p}_i = \left[\exp\left(j\phi_{(i-1)\frac{N_t}{N^t_{\text{RF}}}+1}\right), \ldots, \exp\left(j\phi_{i\frac{N_t}{N^t_{\text{RF}}}}\right)\right]^T$, and ϕ_k is the phase of the k^{th} phase shifter. The special structure of the analog RF precoder $\mathbf{F}_{\text{RF}}$ leads to the following power constraint for the optimization problem $\mathbb{F}$:

$$\|\mathbf{F}_{\text{RF}}\mathbf{F}_{\text{BB}}\|_F^2 = \frac{N_t}{N^t_{\text{RF}}}\|\mathbf{F}_{\text{BB}}\|_F^2 = N_s. \tag{5.11}$$

Now, the optimization problem for the analog RF precoder design can be written as follows:

$$\mathbb{F}_{\text{RF}} = \begin{cases} \min_{\mathbf{F}_{\text{RF}}} & \|\mathbf{F}_{\text{opt}} - \mathbf{F}_{\text{RF}}\mathbf{F}_{\text{BB}}\|_F^2 \\ \text{s.t.} & \mathbf{F}_{\text{RF}} = \text{diag}[\mathbf{p}_1, \mathbf{p}_2, \ldots, \mathbf{p}_{N^t_{\text{RF}}}] \\ \text{s.t.} & \mathbf{p}_i \in \mathcal{A}_p, i = 1, 2, \ldots, N^t_{\text{RF}}, \end{cases} \tag{5.12}$$

Given the structure of the analog RF precoder $\mathbf{F}_{\text{RF}}$ in (5.10), the problem in (5.12) can also be written as

$$\mathbb{F}_{\text{RF}} = \min_{\phi_i} \|(\mathbf{F}_{\text{opt}})_{i,:} - \exp(j\phi_i)(\mathbf{F}_{\text{BB}})_{l,:}\|_2^2, \tag{5.13}$$

where $i = 1, 2, \ldots, N_t$ and $l = \lceil iN^t_{\text{RF}}/N_t \rceil$. Problem $\mathbb{F}_{\text{RF}}$ is equivalent to finding those non-zero elements of $\mathbf{F}_{\text{RF}}$ whose phases are equal to

$$\arg\{(\mathbf{F}_{\text{RF}})_{i,l}\} = \arg\{(\mathbf{F}_{\text{opt}})_{i,:}(\mathbf{F}_{\text{BB}})^H_{l,:}\}. \tag{5.14}$$

As it can be seen in (5.14), the design of the analog RF precoder $\mathbf{F}_{\text{RF}}$ is only dependent on the phase of the phase shifters, therefore the unit modulus constraint (mentioned below (5.3)) does not cause any intractability in the problem and is met in the partially-connected structure.

Now, we can design the digital baseband precoder $\mathbf{F}_{\text{BB}}$. Based on (5.11), the design problem can be written by

$$\mathbb{F}_{\text{BB}} = \begin{cases} \min_{\mathbf{F}_{\text{BB}}} & \|\mathbf{F}_{\text{opt}} - \mathbf{F}_{\text{RF}}\mathbf{F}_{\text{BB}}\|_F^2 \\ \text{s.t.} & \|\mathbf{F}_{\text{BB}}\|_F^2 = \frac{N_s N_{\text{RF}}^t}{N_t}, \end{cases} \tag{5.15}$$

Obviously, the objective function and the constraint in the optimization problem in (5.15) are both quadratic. This means that the design of digital baseband precoder $\mathbf{F}_{\text{BB}}$ is a quadratic constraint quadratic programming (QCQP) problem and a non-convex optimization problem [102].

In the literature, different methods have been proposed to solve a non-convex QCQP problem. In [103], it has been shown that by applying the S-lemma, the following homogeneous QCQP formula is achieved:

$$\mathbb{F}_{\text{BB}} = \begin{cases} \min_{\mathbf{F}} & \text{tr}(\mathbf{A}\mathbf{F}) \\ \text{s.t.} & \text{tr}(\mathbf{A}_1\mathbf{F}) = \frac{N_s N_{\text{RF}}^t}{N_t}, \\ \text{s.t.} & \text{tr}(\mathbf{A}_2\mathbf{F}) = 1, \\ \text{s.t.} & \text{rank}(\mathbf{F}) = 1, \\ \text{s.t.} & \mathbf{F} \succeq \mathbf{0}. \end{cases} \tag{5.16}$$

In the problem in (5.16), we try to find a square $n \times n$ matrix $\mathbf{F}$ where $n = N_{\text{RF}}^t N_s + 1$, $\mathbf{F} = \mathbf{f}\mathbf{f}^H$, $\mathbf{f} = [\{\text{vec}(\mathbf{F}_{\text{BB}})\}^T, z]^T$ with an auxiliary variable z, $\mathbf{g} = \text{vec}(\mathbf{F}_{\text{opt}})$, and

$$\mathbf{A}_1 = \begin{bmatrix} \mathbf{I}_{n-1} & \mathbf{0} \\ \mathbf{0} & 0 \end{bmatrix}, \tag{5.17}$$

$$\mathbf{A}_2 = \begin{bmatrix} \mathbf{0}_{n-1} & \mathbf{0} \\ \mathbf{0} & 1 \end{bmatrix}, \tag{5.18}$$

$$\mathbf{A} = \begin{bmatrix} (\mathbf{I}_{N_s} \otimes \mathbf{F}_{\text{RF}})^H (\mathbf{I}_{N_s} \otimes \mathbf{F}_{\text{RF}}) & -(\mathbf{I}_{N_s} \otimes \mathbf{F}_{\text{RF}})^H \mathbf{g} \\ -\mathbf{g}^H (\mathbf{I}_{N_s} \otimes \mathbf{F}_{\text{RF}}) & \mathbf{g}^H \mathbf{g} \end{bmatrix}. \tag{5.19}$$

When solving the problem in (5.16), the most difficult constraint to satisfy is the rank constraint. However, this can be relaxed by a semi-definite programming (SDP) relaxation [104], as follows:

$$\mathbb{F}_{\text{BB}} = \begin{cases} \min_{\mathbf{F}} & (\mathbf{AF}) \\ \text{s.t.} & (\mathbf{A}_1\mathbf{F}) = \frac{N_s N_{\text{RF}}^t}{N_t}, \\ \text{s.t.} & (\mathbf{A}_2\mathbf{F}) = 1, \\ \text{s.t.} & \mathbf{F} \succeq \mathbf{0}. \end{cases} \tag{5.20}$$

ll Now, we can iteratively solve the relaxed SDP optimization problem in (5.17) using Algorithm 5.1 to find the digital baseband precoder $\mathbf{F}_{\text{BB}}$. This problem can be solved by standard convex optimization tools such as those described in [102]. Algorithm 5.1 provides a step-by-step pseudocode summary of the proposed projection algorithm. The algorithm alternates between fixing $\mathbf{F}_{\text{RF}}$ and solving for $\mathbf{F}_{\text{BB}}$, then fixing $\mathbf{F}_{\text{BB}}$ and solving for $\mathbf{F}_{\text{RF}}$. The iterations continue until $\|\mathbf{F}_{\text{opt}} - \mathbf{F}_{\text{RF}}\mathbf{F}_{\text{BB}}\|_F^2$ drops below some specified convergence threshold ϵ.

In the proposed algorithm, the digital precoders are updated by the relaxed optimization problem in (5.17), which is a computationally efficient approximation approach to a QCQP problem and has polynomial-time complexity in the problem size $n = N_{\text{RF}}^t N_s + 1$. Updating the RF analog precoder is realized by a phase extraction of the matrix $\mathbf{F}_{\text{opt}}\mathbf{F}_{\text{BB}}^H$ of dimension $N_t \times \lceil iN_{\text{RF}}^t/N_t \rceil$ for $i = 1, 2, \ldots, N_t$.

In conventional MIMO orthogonal frequency division multiplexing (OFDM) systems with sub-6 GHz carrier frequencies, digital precoding is performed in the frequency domain for every narrowband subcarrier. Similar OFDM methodology can be employed at mmWave frequencies, splitting the larger total bandwidth into narrow subbands to avoid frequency selective channel gains. Note though that digital precoding would be followed by an inverse fast Fourier transform (IFFT) operation, which combines the signals of all the subcarriers together. However, since the analog precoding in our hybrid transmitter

Algorithm 5.1: Precoder Optimization for Partially-Connected Hybrid Precoding-Combining Transceivers

Calculate SVD $\mathbf{H} = \mathbf{U}\mathbf{\Sigma}\mathbf{V}^H$;
Set $k = 0$ and $\mathbf{F}_{\text{opt}} =$ first N_s columns of $\mathbf{V}$;
Set value of threshold ϵ;
Construct $\mathbf{F}_{\text{RF}}^{(0)}$ with random phases uniformly distributed in interval $[0, 2\pi)$;
Repeat
  Fix $\mathbf{F}_{\text{RF}}^{(k)}$, find $\mathbf{F}_{\text{BB}}^{(k)}$ using convex optimization tool (see e.g. [105]) and relaxed SDP problem in (5.20);
  Fix $\mathbf{F}_{\text{BB}}^{(k)}$, find $\mathbf{F}_{\text{RF}}^{(k+1)}$ using (5.14);
  $k = k + 1$;
Until $\|\mathbf{F}_{\text{opt}} - \mathbf{F}_{\text{RF}}\mathbf{F}_{\text{BB}}\|_F^2 < \epsilon$

architecture is a post-IFFT processing, the signals of all the subcarriers can only share one common analog precoder $\mathbf{F}_{\text{RF}}$.

Algorithm 5.1 assumes a narrowband channel model. To adopt it to a wideband multicarrier system, in the initialization, a separate $\mathbf{F}_{\text{opt}}$ would be found for each subband. During the "Repeat" loop, first the digital precoders $\mathbf{F}_{\text{BB}}$ for all the subcarriers can be updated in parallel, while holding the common $\mathbf{F}_{\text{RF}}$ fixed. Then, all $\mathbf{F}_{\text{BB}}$ would be held fixed while updating the common matrix $\mathbf{F}_{\text{RF}}$. The stop criterion in the last line would have to be satisfied for each subband.

5.3 Problem Formulation of Channel Estimation

As mentioned earlier, mmWave channels are expected to have few significant scattering paths, which makes these channels sparse in nature, and thus they can be modeled via a virtual channel representation as shown in (5.4). Assuming discrete multipath components contributing to the mmWave channel model in (5.4), to estimate the channel, we need to estimate different parameters of the N_p propagation paths, namely the AoA, the AoD, and the gain of each path. Here, we propose a DFT codebook design for the training precoders and combiners in a hybrid precoding transceiver. Then, similarly to [99], inspired by adaptive compressed sensing (CS), the training precoding and measurement matrices are adaptively determined based on the output of the earlier stages.

Considering the mmWave channel model described in (5.4), if the BS uses a beamforming matrix $\bar{\mathbf{F}} = \bar{\mathbf{F}}_{\text{RF}}\bar{\mathbf{F}}_{\text{BB}} = \left[\bar{\mathbf{f}}_1, \bar{\mathbf{f}}_2, \cdots, \bar{\mathbf{f}}_{M_t}\right]$ of size $N_t \times M_t$, and the user employs a measurement matrix $\bar{\mathbf{W}} = \bar{\mathbf{W}}_{\text{RF}}\bar{\mathbf{W}}_{\text{BB}} = [\bar{\mathbf{w}}_1, \bar{\mathbf{w}}_2, \cdots, \bar{\mathbf{w}}_{M_r}]$ of size $N_r \times M_r$ to combine the received signal, the resulting matrix representation of the training signal after combining can be written as

$$\mathbf{Y} = \bar{\mathbf{W}}^H\mathbf{H}\bar{\mathbf{F}}\mathbf{S} + \mathbf{Q}, \tag{5.21}$$

where $\mathbf{Q} \in \mathcal{C}^{M_r \times M_t}$ is the noise matrix, and $\mathbf{S} = \mathbf{I}_{M_t}$ is the transmitted symbols matrix for the training phase. Below, we represent the formula in (5.21) in a vectorized form to exploit the sparse nature of the mmWave channels:

$$\begin{aligned} \mathbf{y}_v &= \text{vec}(\bar{\mathbf{W}}^H\mathbf{H}\bar{\mathbf{F}}) + \text{vec}(\mathbf{Q}) \\ &= (\bar{\mathbf{F}}^T \otimes \bar{\mathbf{W}}^H)(\mathbf{A}_{\text{BS}}^* \circ \mathbf{A}_{\text{MS}})\boldsymbol{\alpha} + \mathbf{n}_Q, \end{aligned} \tag{5.22}$$

which, based on the Kronecker product properties, can be rewritten as follows

$$\mathbf{y}_v = (\bar{\mathbf{F}}^T\mathbf{A}_{\text{BS}}^* \otimes \bar{\mathbf{W}}^H\mathbf{A}_{\text{MS}})\boldsymbol{\alpha} + \mathbf{n}_Q, \tag{5.23}$$

where $\mathbf{A}_{\text{BS}}$ and $\mathbf{A}_{\text{MS}}$ are dictionary matrices of size $M_t \times N$ and $M_r \times N$, respectively, and $\boldsymbol{\alpha} \in \mathcal{C}^{N^2 \times 1}$ is the vector containing the path gains of the corresponding quantized directions. Each column of these matrices has the form $(\bar{\mathbf{a}}_t(\theta_i^t)^* \otimes \bar{\mathbf{a}}_r(\theta_i^r))$, where $i \in \{0, 1, \ldots, N-1\}$ represents the corresponding AoAs/AoDs taken from a uniform grid of N points over $[0, 2\pi)$, and assuming the grid quantization error is negligible. We propose a DFT beamforming vector design for the codebook/dictionary matrices $(\mathbf{A}_{\text{BS}}$ and $\mathbf{A}_{\text{MS}})$. Thus, we can generate the beamformers as follows:

$$\mathbf{A}_{\text{BS}} = [\mathbf{a}_{\text{ULA}}(\theta_0^t), \mathbf{a}_{\text{ULA}}(\theta_1^t), \ldots, \mathbf{a}_{\text{ULA}}(\theta_{N-1}^t)], \tag{5.24}$$

$$\mathbf{A}_{\text{MS}} = [\mathbf{a}_{\text{ULA}}(\theta_0^r), \mathbf{a}_{\text{ULA}}(\theta_1^r), \ldots, \mathbf{a}_{\text{ULA}}(\theta_{N-1}^r)]. \tag{5.25}$$

In adaptive CS, the training process is divided into a number of stages. In this method, the training precoding and measurement matrices are not determined a priori, but rather with respect to the output of the earlier stages. Suppose the training phase is designed to be acquired in Ψ stages, then the training precoders and combiners for stage ψ, namely $\bar{\mathbf{F}}_{(\psi)}$ and $\bar{\mathbf{W}}_{(\psi)}$ are only dependent on the received signal of stages $\{1, 2, \ldots, \psi-1\}$. More specifically, the vectorized received signals of these stages are:

$$\begin{aligned}
\mathbf{y}_{(1)} &= (\bar{\mathbf{F}}_{(1)}^T \mathbf{A}_{\text{BS}}^* \otimes \bar{\mathbf{W}}_{(1)}^H \mathbf{A}_{\text{MS}})\boldsymbol{\alpha} + \mathbf{n}_1 \\
\mathbf{y}_{(2)} &= (\bar{\mathbf{F}}_{(2)}^T \mathbf{A}_{\text{BS}}^* \otimes \bar{\mathbf{W}}_{(2)}^H \mathbf{A}_{\text{MS}})\boldsymbol{\alpha} + \mathbf{n}_2 \\
&\vdots \\
\mathbf{y}_{(\Psi)} &= (\bar{\mathbf{F}}_{(\Psi)}^T \mathbf{A}_{\text{BS}}^* \otimes \bar{\mathbf{W}}_{(\Psi)}^H \mathbf{A}_{\text{MS}})\boldsymbol{\alpha} + \mathbf{n}_\Psi.
\end{aligned} \tag{5.26}$$

The channel estimation algorithm starts by dividing the vector $\boldsymbol{\alpha}$ in (5.26) into a number of intervals, which is equivalent to dividing the AoAs/AoDs grid into a number of intervals, and designs the precoding and combining matrices of the first stage, $\bar{\mathbf{F}}_{(1)}$ and $\bar{\mathbf{W}}_{(1)}$, to sense those intervals. In other words, the received signal $\mathbf{y}_{(1)}$ is used to determine those intervals that have non-zero elements. In later stages, these intervals will be divided into smaller gaps to detect the non-zero elements. If the BS and user both use $M_t = M_r = M$ precoding vectors in each stage of the channel estimation, then the number of stages that adaptive CS requires to detect the AoAs/AoDs within an N-point grid equals $\Psi = \lceil \log_M N/N_p \rceil$. The value of M is a design parameter.

Now, given the proposed analog dictionary matrices $\mathbf{A}_{\text{BS}}$ and $\mathbf{A}_{\text{MS}}$, we create the training precoding and combining matrices $\bar{\mathbf{F}}$ and $\bar{\mathbf{W}}$ at the BS and user in (5.24) as follows:

$$\bar{\mathbf{F}} = (\mathbf{A}_{\text{BS}} \mathbf{A}_{\text{BS}}^H)^{-1} \mathbf{A}_{\text{BS}}, \tag{5.27}$$

$$\bar{\mathbf{W}} = (\mathbf{A}_{\text{MS}} \mathbf{A}_{\text{MS}}^H)^{-1} \mathbf{A}_{\text{MS}}, \tag{5.28}$$

which will be used as an input to Algorithm 5.1 for $\mathbf{F}_{\text{opt}}$ (or $\mathbf{W}_{\text{opt}}$ at the receiver).

5.3.1 Channel Estimation Algorithm for mmWave Channels

Given the received training signals in (5.21), a multipath channel implies that vector $\boldsymbol{\alpha}$ has multiple non-zero elements each associated with one single path. Finding the location of the non-zero elements is essentially equivalent to determining the AoAs/AoDs, and the values of those elements are the channel path gains. The channel estimation algorithm operates as follows: In the initial stage, the BS and the user calculate the MN_p beamforming vectors defined previously to divide the AoD and AoA ranges each into MN_p sub-intervals. Then, the algorithm, after M^2 precoding-combining steps of the first stage, compares the power of the received signal on each interval to determine the one with the maximum received power. The selection of the maximum received power is associated with a certain range of the quantized AoAs/AoDs which means selection of the interval of the quantized AoAs/AoDs that is highly likely to contain at least one path of the channel. Then, the user feeds back the selected subset of the BS precoders to the BS to use in the next stage. As the beamforming vectors of the following stages gain higher resolution, the AoA/AoD ranges are further refined. Therefore, the algorithm proceeds by selecting the maximum received signal power to determine N_p intervals that carry the dominant paths of the channel. This process continues until the desired resolution is achieved. At each stage, the contribution of paths that have already been estimated in the previous stages are projected out before determining the AoA/AoD ranges of newer paths. This process continues until the N_p paths are found.

5.4 Simulation Results

In this subsection, we numerically evaluate the performance of the proposed hybrid precoding-combining algorithm and the proposed DFT beamforming reference codebook for channel estimation purposes. In our Monte Carlo simulations with 10000 iterations, we consider $N_t = 144$, $N_r = 36$, $N_{\text{Rf}}^t = N_{\text{Rf}}^r = N_s = 3$, $N_p = 3$, and $\sigma_\alpha^2 = 1$. The average path loss is $\gamma = 105.4$ dB, where the distance between the BS and user is $l_0 = 50$ m. The average total transmitted power is set to $\rho = 1$. The antenna arrays are ULAs with half-wavelength element spacing, and hence potential coupling between antenna elements can be assumed negligible. The system is assumed to operate at a carrier frequency of 28 GHz. The channel estimation is done in $\Psi = 6$ stages with $M_t = M_r = M = 2$ beamforming vectors at each stage, resulting in a resolution parameter of $N = 192$ points for the AoA/AoD quantized grid. The threshold value in Algorithm 5.1 is set to $\epsilon = 0.001$. In this simulation, we define SNR as equal to ρ/σ^2.

Fig. 5.3 shows the spectral efficiency achieved when the proposed hybrid precoding and combining matrices are calculated using mmWave channel estimation via the DFT beamforming reference codebook, and compares it with the spectral efficiency achieved when the channel estimation uses the RF codebook proposed in [99]. The proposed DFT-based mmWave channel estimation algorithm outperforms the algorithm proposed in [99], which results from the better beamforming reference patterns obtained using the DFT codebook. For example, at -10 dB SNR, our algorithm provides a spectral efficiency of 5.4 bits/sec/Hz, which is more than double compared to 2.4 bits/sec/Hz for the codebook from [99].

Fig. 5.3 also demonstrates the performance of our proposed hybrid precoding algorithm with perfect CSI. The performance of the proposed hybrid precoding algorithm when using CSI estimated with our proposed DFT beamforming codebook is quite close to the case where perfect CSI is known to the transmitter. For SNRs up to -15 dB, the maximum spectral efficiency loss of using estimated CSI relative to perfect CSI is about 14%. This loss increases with further increasing SNR though; at 0 dB SNR, using estimated CSI provides about 73% of the spectral efficiency of using perfect CSI.

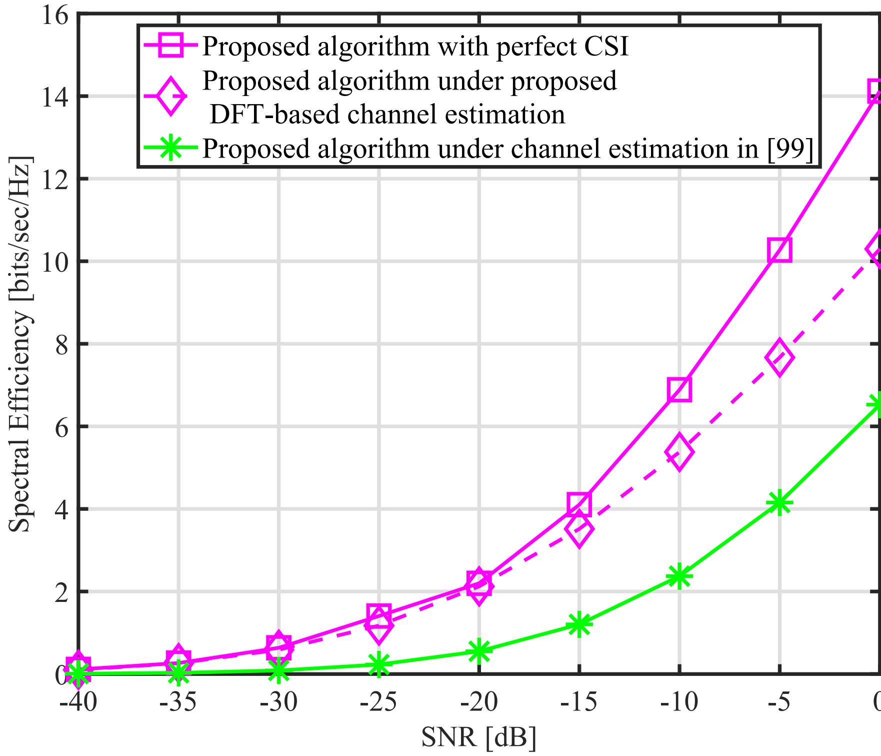

Figure 5.3: Spectral efficiency vs. SNR, comparing different channel estimation methods; $N_t = 144$, $N_r = 36$, $N_{\text{RF}}^t = N_{\text{RF}}^r = 3$, $N_s = 3$, and $N_p = 3$.

In Fig. 5.4, we compare the performance of our proposed hybrid precoding and channel estimation with the algorithms introduced in [99]. As seen, the scheme proposed in [99], despite using a fully-connected antenna array structure and having 16 RF chains at the transmitter and 8 RF chains at the receiver, still shows a poorer performance compared to our algorithm, even when our number of RF chains is considerably lower than the number of antennas at both sides. The spectral efficiency is about 2.4 bits/sec/Hz smaller (or about 46% less) at -10 dB SNR.

For reference, Fig. 5.4 also shows the spectral efficiency possible when using an optimal digital precoder with perfect CSI. There is a notable gap between that case and the

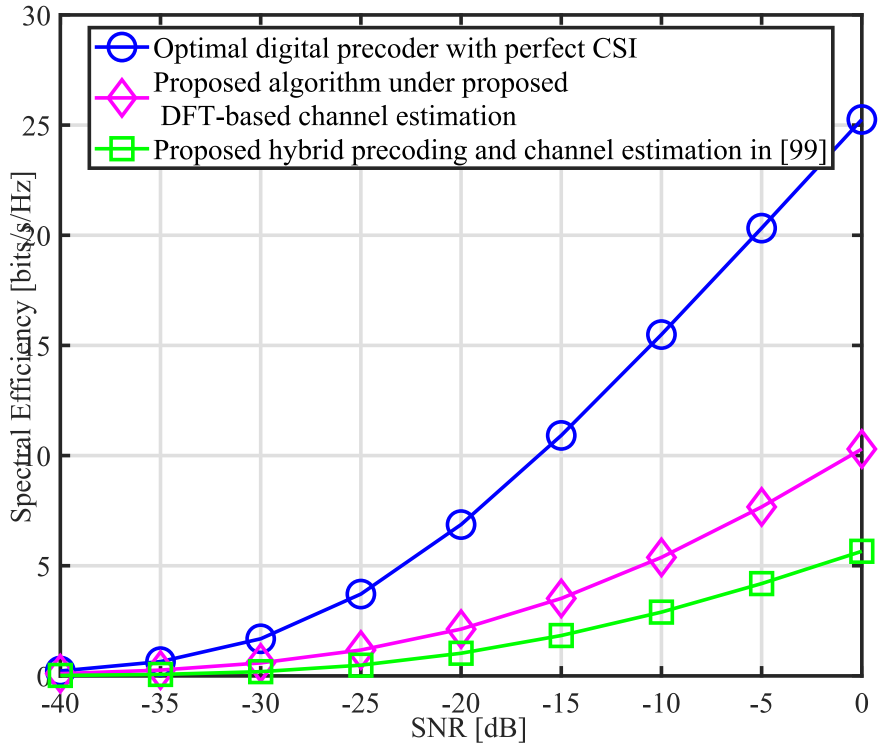

Figure 5.4: Spectral efficiency vs. SNR, comparing various precoding and channel estimation schemes; $N_t = 144$, $N_r = 36$, $N_s = 3$, and $N_p = 3$.

performance of our proposed scheme. For instance, the optimal digital precoder provides about 2.8 times higher spectral efficiency at -10 dB SNR than our scheme. However, our scheme also uses only $1/48$ of the number of RF chains at the transmitter (and $1/12$ of the number at the receiver), and a partially-connected structure. Thus, the relative savings in hardware complexity and energy efficiency resulting from the absence of those components more than balance out the resulting relative loss in spectral efficiency.

5.5 Summary

In this chapter, we have introduced a projection hybrid precoding algorithm for a hybrid precoding-combining transceiver in mmWave MIMO systems with a partially-connected structure. We have also proposed a channel estimation algorithm based on DFT beamforming reference vectors. The DFT-based channel estimation has the limitation of only being applicable to uniform linear antenna arrays, whereas the proposed transceiver structure and precoder optimization algorithm can be applied to any arbitrary type of antenna array. We have evaluated the performance of the proposed hybrid precoding algorithm under both perfect CSI and estimated CSI obtained via the proposed DFT-based mmWave channel estimation algorithm. The simulations results have illustrated that the system using the proposed projection hybrid precoding and channel estimation algorithms approaches the spectral efficiency achievable when perfect channel knowledge is available.

Chapter 6

Hybrid Beamforming for mmWave Massive MIMO Systems Employing DFT-Assisted User Clustering

In [106], we propose a matrix factorization approach to tackle the problem of hybrid precoding-combining design as two separate optimization subproblems. The proposed approach supports both the fully-connected and partially-connected structures described in the previous chapter. We also take advantage of the simplicity of the DFT-based user clustering algorithm introduced in Chapter 3 to further reduce the complexity of the design process. We propose solutions for a multiuser massive MIMO system at mmWave frequencies (although the solutions have the potential for use at sub-6 GHz as well). We also formulate the system design problem for frequency-selective channels employing orthogonal frequency division multiplexing (OFDM).

6.1 System Model

Let us consider the downlink of a cellular system, where a BS equipped with N_t antennas communicates with U non-cooperative mobile users, with user u deploying $N_{r,u}$ antennas. Moreover, the number of RF chains at the BS and at user u are N^t_{RF} and $N^r_{\text{RF},u}$, respectively, with $N_{\text{RF}}^t \leq N_t$ and $N_{\text{RF},u}^r \leq N_{r,u}$. Several independent data streams $N_{s,u} \leq N_{\text{RF},u}^r$ for each user are simultaneously transmitted. We assume the total number of data streams N_s for all the users is smaller than the number of RF chains at the BS, i.e., $\sum_{u=1}^{U} N_{s,u} = N_s \leq N_{\text{RF}}^t$.

We assume a frequency-selective channel, which will be described in the following. In this work, we assume OFDM modulation, with a cyclic prefix large enough to avoid inter-symbol interference. The transmitted data for user u at subcarrier k can be written as $\mathbf{s}_u[k] \in \mathcal{C}^{N_{s,u} \times 1}$ where $\mathbb{E}[\mathbf{s}_u[k]] = \mathbf{0}$, and $\mathbb{E}[\mathbf{s}_u[k]\mathbf{s}_u[k]^H] = \frac{1}{N_{s,u}}\mathbf{I}_{N_{s,u}}$. Focusing on the downlink transmission, the transmitted signal for user u at subcarrier k is:

$$\mathbf{x}_u[k] = \mathbf{F}_{\text{RF}}\mathbf{F}_{\text{BB},u}[k]\mathbf{s}_u[k], \tag{6.1}$$

where the transmitter is assumed to apply a digital baseband precoder $\mathbf{F}_{\text{BB},u}[k] \in \mathcal{C}^{N_{\text{RF}}^t \times N_{s,u}}$ followed by an analog RF precoder $\mathbf{F}_{\text{RF}} \in \mathcal{C}^{N_t \times N_{\text{RF}}^t}$. Note in particular that the same analog RF precoder is used for all subcarriers, since the analog precoding is a post-IFFT processing and the signal of all subcarriers can only share one common analog precoder. Also note that all users share the same analog RF precoder $\mathbf{F}_{\text{RF}}$. This is due to the structure of the transceiver where the output of each RF chain is mapped to each antenna through either all (fully-connected) or some (partially-connected) of the phase shifters. Hence, each stream propagates to all the transmit antennas, so no dedicated RF path for any given user can be assumed.

The receiver at user u uses an analog RF combining matrix $\mathbf{W}_{\text{RF},u} \in \mathcal{C}^{N_{r,u} \times N_{\text{RF},u}^r}$ (again, the same for all subcarriers), and a digital baseband decoder $\mathbf{W}_{\text{BB},u}[k] \in \mathcal{C}^{N_{\text{RF},u}^r \times N_{s,u}}$ at subcarrier k to obtain the received downlink signal $\mathbf{y}_u[k] \in \mathcal{C}^{N_{s,u} \times 1}$:

$$\begin{aligned}\mathbf{y}_u[k] = \sqrt{\rho}\mathbf{W}_{\text{BB},u}^H[k]\mathbf{W}_{\text{RF},u}^H\mathbf{H}_u[k]\sum_{n=1}^{U}\mathbf{F}_{\text{RF}}\mathbf{F}_{\text{BB},n}[k]\mathbf{s}_n[k] \\ +\mathbf{W}_{\text{BB},u}^H[k]\mathbf{W}_{\text{RF},u}^H[k]\mathbf{n}[k],\end{aligned} \tag{6.2}$$

where ρ stands for the average transmitted power, $\mathbf{H}_u[k] \in \mathcal{C}^{N_{r,u} \times N_t}$ is the channel matrix for subcarrier k, and $\mathbf{n} \sim \mathcal{CN}(\mathbf{0}, \sigma^2 \mathbf{I}_{N_{r,u}})$ is the $N_{r,u} \times 1$ additive white Gaussian noise (AWGN) vector corrupting the received signal.

6.1.1 Channel Model

As aforementioned, we assume a frequency-selective channel $\mathbf{H}_{u,d} \in \mathcal{C}^{N_{r,u} \times N_t}$ with d taps of delay at subcarrier k for user u that can be expressed as follows:

$$\mathbf{H}_{u,d} = \beta_u \sum_{p=1}^{N_p} \alpha_{u,p} p_{rc}(dT_s - \tau_{u,p}) \mathbf{a}_{u,k}(\phi_{u,p}) \mathbf{a}_{BS,k}^H(\theta_{u,p}), \tag{6.3}$$

where $\beta_u = \sqrt{\frac{N_t N_{r,u}}{\gamma_P N_p}}$, N_p is the number of multipath components, γ_P is the path loss, and $\mathbf{a}_{u,k}(\phi_{u,p})$ and $\mathbf{a}_{BS,k}^H(\theta_{u,p})$ represent the receive and transmit antenna array response vectors at the corresponding angles of arrival $\phi_{u,p}$ and departure $\theta_{u,p}$ at the k-th subcarrier. $p_{rc}(\cdot)$ denotes the raised-cosine pulse function [107], T_s is the sampling interval, $\tau_{u,p}$ is the time delay of the path, and $\alpha_{u,p}$ is the complex gain of the path. Consequently, the channel response in the frequency domain is:

$$\mathbf{H}_u[k] = \sum_{d=0}^{D-1} \mathbf{H}_{u,d} e^{-j\frac{2\pi k d}{K}}. \tag{6.4}$$

Accordingly, there are K equal-width sub-bands or narrow-band channels, and D is the number of delay taps, where the d-th channel delay tap at the k-th subcarrier index is expressed in (6.3).

The receive and transmit antenna array response vectors are functions of the array structures. However, the proposed algorithm and the results are applicable to any arbitrary antenna array. In this work, we assume both a uniform linear array (ULA) and a uniform planar array (UPA). Given an N-element ULA composed of N isotropic antenna elements, the array response vector is

$$\mathbf{a}_{\text{ULA}}(N, \theta) = \frac{1}{\sqrt{N}} \left[1, e^{j\kappa q \sin(\theta)}, \ldots, e^{j\kappa q (N-1)\sin(\theta)}\right]^T, \tag{6.5}$$

where $\kappa = \frac{2\pi}{\lambda}$, λ is the wavelength, and q is the distance between two adjacent elements. Similarly, for a UPA we can define an $L \times V$-element array response as follows:

$$\mathbf{a}_{\text{UPA}}(\theta, \phi) = \frac{1}{\sqrt{LV}} \begin{bmatrix} 1 \\ e^{j\kappa q(l\sin(\theta)\sin(\phi)+v\cos(\phi))} \\ \vdots \\ e^{j\kappa q((L-1)\sin(\theta)\sin(\phi)+(V-1)\cos(\phi))} \end{bmatrix}, \tag{6.6}$$

where $0 \leq l < L-1$, $0 \leq v < V-1$, and θ and ϕ are the azimuth and elevation angle of departure (arrival), respectively.

6.1.2 Achievable Spectral Efficiency

Let us consider a Gaussian signaling model, therefore the achievable spectral efficiency (in bits/s/Hz, normalized to the entire bandwidth of the system) over the downlink is given by:

$$\begin{aligned} R = \sum_{u=1}^{U} R_u = \frac{1}{K} \sum_{u=1}^{U} \sum_{k=1}^{K} \log_2 \det(\mathbf{I}_{N_{s,u}} + \mathbf{Z}_u^{-1}[k] \\ \times \mathbf{W}_u^H[k]\mathbf{H}_u[k]\mathbf{F}_u[k]\mathbf{F}_u^H[k]\mathbf{H}_u^H[k]\mathbf{W}_u[k]), \end{aligned} \tag{6.7}$$

where $\mathbf{Z}_u[k] = \sum_{i \neq u} \mathbf{W}_i^H[k]\mathbf{H}_u[k]\mathbf{F}_i[k]\mathbf{F}_i^H[k]\mathbf{H}_u^H[k]\mathbf{W}_i[k] + \mathbf{W}_u^H[k]\mathbf{n}[k]\mathbf{W}_u[k]$ is the covariance of the interference plus noise at the receiver after combining, and the combiners and the precoders are $\mathbf{W}_u[k] = \mathbf{W}_{\text{RF},u}\mathbf{W}_{\text{BB},u}[k] \in \mathcal{C}^{N_{r,u} \times N_{s,u}}$ and $\mathbf{F}_u[k] = \mathbf{F}_{\text{RF}}\mathbf{F}_{\text{BB},u}[k] \in \mathcal{C}^{N_t \times N_{s,u}}$, respectively.

6.1.3 Problem Formulation

In this study, the goal is to design a set of hybrid precoders and combiners that maximizes the spectral efficiency expression given in (6.7). As it can be seen, the solution to this problem seeks a joint optimization over four matrices, namely $\mathbf{F}_{\text{RF}}, \mathbf{F}_{\text{BB},u}[k], \mathbf{W}_{\text{RF},u}$ and $\mathbf{W}_{\text{BB},u}[k]$, for each user u and each subcarrier k. However, the global optimum for such an optimization problem due to similar joint constraints is considered to be intractable [100], [101]. For the sake of simplicity in transceiver design, we decouple the joint optimization of the transmitter and receiver, and only focus on the design of the precoder used at the BS, i.e., the RF precoder $\mathbf{F}_{\text{RF}}$ and the baseband precoder $\mathbf{F}_{\text{BB},u}[k]$ for user u at subcarrier k, $\forall u, k$. Hereafter, we focus on designing the hybrid precoders at the transmitter, however the proposed methodology also is applicable to the decoder/combiner design at the receiver. The corresponding problem formulation is given as follows:

$$\begin{array}{ll} \min\limits_{\mathbf{F}_{\text{RF}}, \{\mathbf{F}_{\text{BB},u}[k]\}} & \sum\limits_{u=1}^{U} \sum\limits_{k=1}^{K} \|\mathbf{F}_{\text{FD},u}[k] - \mathbf{F}_{\text{RF}}\mathbf{F}_{\text{BB},u}[k]\|_F^2 \\ \text{s.t.} & \mathbf{F}_{\text{RF}} \in \mathcal{A}, \\ \text{s.t.} & \|\mathbf{F}_{\text{RF}}\mathbf{F}_{\text{BB},u}[k]\|_F^2 = N_{s,u}, \forall u, k, \end{array} \tag{6.8}$$

where $\mathcal{A}$ is the set of feasible analog RF precoders, and $\mathbf{F}_{\text{FD},u}[k] \in \mathcal{C}^{N_t \times N_{s,u}}$ is the target FD precoder for user u on subcarrier k. In [108], it is shown that unconstrained digital BD beamforming is a suboptimal precoder for multiuser MIMO systems when users are equipped with multiple antennas[1]. Based on full channel information of $\mathbf{H}[k] = \left[\mathbf{H}_1[k]^T, \cdots, \mathbf{H}_U[k]^T\right]^T$ for all users, we can use BD to design the FD beamforming matrices for throughput maximization, as fully explained in [108]. The design of BD matrices for each user can be summarized in three steps: 1) given $\mathbf{H}[k]$, create the channel matrix $\tilde{\mathbf{H}}_u[k]$ vertically concatenating all the users' channel matrices except for that of user u; 2) find basis vectors $\tilde{\mathbf{V}}_u^0[k]$ for the null space of $\tilde{\mathbf{H}}_u[k]$, e.g., by singular value decomposition (SVD) $\tilde{\mathbf{H}}_u[k] = \tilde{\mathbf{U}}_u[k]\tilde{\mathbf{\Sigma}}_u[k]\tilde{\mathbf{V}}_u[k]^H$ and using the rightmost right-singular vectors in $\tilde{\mathbf{V}}_u[k]$; 3) perform an SVD of $\tilde{\mathbf{H}}_u[k]\tilde{\mathbf{V}}_u^0[k] = \mathbf{G}_u[k] = \mathbf{U}_{\mathbf{G}_u}[k]\mathbf{\Sigma}_{\mathbf{G}_u}[k]\mathbf{V}_{\mathbf{G}_u}[k]^H$, from which the FD precoder $\mathbf{F}_{\text{FD},u}[k]$ for user u on subcarrier k is obtained from $N_{s,u}$ the leftmost right-singular vectors. In other words,

$$\mathbf{F}_{\text{FD},u}[k] = \text{first } N_{s,u} \text{ columns of } \mathbf{V}_{\mathbf{G}_u}[k]. \tag{6.9}$$

The problem formulation (6.8) is intrinsically a matrix factorization problem which

[1]BD can still be used with single-antenna users, in which case the "block" size of the equivalent channels that are formed becomes 1×1, i.e., a scalar.

involves $\mathbf{F}_{\mathrm{RF}}$ and the set of matrix variables $\{\mathbf{F}_{\mathrm{BB},u}[k]\}, \forall u, k$, whose designs can be different based on the architecture of the transceivers. In this work, we consider both fully-connected and partially-connected structures.

6.1.4 DFT-Based User Clustering Algorithm

In this study, we incorporate the DFT-based user clustering algorithm first introduced in [87], wherein we tackle the problem of user clustering for sparse beam-space massive MIMO channels. A simplified scheme partitions the set of users into clusters each corresponding to the angular bins that they occupy. In this approach, we examine each angular bin, which is connected to a set of user nodes via edges (resolvable paths). Users that receive a signal from the same angular bin are grouped together. This way, one no longer needs to consider the "full" channel matrix, but rather the sparse beam-space representation, which has a limited number of paths.

Given the connectivity matrix $\mathbf{C}$, we adopt the bipartite graph representation and simply cluster users according to the angular bins that they occupy. This algorithm takes advantage of the sparsity of massive MIMO channels to achieve spatial multiplexing and cope with the interference resulting from overlapping multipath components. Specifically, the DFT beamformer creates orthogonality among clusters of users in the beam-space domain to combat inter-beam interference (see Appendix B for more details). The vectors for the beamformer are taken from the columns of the $N_t \times N_t$ DFT matrix. Meanwhile, a linear MU-MIMO precoder achieves spatial multiplexing within groups of users. In this algorithm, the size of user clusters is not fixed. However, within the concept of hybrid beamforming, the sum of the number of users in all clusters must be at most equal to the number of RF chains at the BS[2], N_{RF}^t. Fig. 3 illustrates the user clustering methodology.

[2]In the case that the sum of the number of users in all clusters is larger than the number of RF chains at the transmitter, the system would need to employ some form of user scheduling, which is out of the scope of this work.

Without loss of generality, we assume that the AoD of any path lies in the interval $[-\pi/3, \pi/3]$, which is uniformly spaced into N_t disjoint intervals, which we call angular bins, $\mathcal{B}_i$. The angular bin i for $1 \leq i \leq N_{\text{RF}}^t$ is the following interval:

$$\mathcal{B}_i = \left\{ \theta \middle| -\frac{\pi}{3} + \frac{2\pi}{3} \frac{i-1}{N_t} \leq \theta \leq -\frac{\pi}{3} + \frac{2\pi}{3} \frac{i}{N_t} \right\}. \tag{6.10}$$

With this approach, we quantize the AoD such that if it lies in the angular bin i, it would be represented by the central angle $\hat{\theta}_i = -\frac{\pi}{3} + \frac{\pi}{3N_t} + \frac{2\pi}{3} \frac{i}{N_t}$ for that bin. DFT beamformers are only used to determine the AoDs for clustering users.

Building upon on our work in [87], once these user clusters are formed, we can split up the overall optimization problem to just find the set of analog and digital precoders for each cluster. This reduces the complexity of the subproblems per cluster, allowing the solution(s) to converge faster.

6.2 Hybrid Precoding For Fully-Connected Structure

A fully-connected structure, where each RF chain is connected to all transmit antennas, restricts every entry in the analog precoding matrix to be a complex number of unit modulus. This restriction makes the design of the precoder intractable. However, inspired by [109], the Frobenius norm in the first line of (6.8) can be made exactly zero if the condition $N_{\text{RF}}^t \geq 2N_s$ holds.

6.2.1 Digital Baseband Precoder Design

The design of the digital baseband precoder with the assumption of a fixed analog RF precoder $\mathbf{F}_{\text{RF}}$ can be reformulated as:

$$\min_{\{\mathbf{F}_{\text{BB},u}[k]\}} \sum_{k=1}^{K} \|\mathbf{F}_{\text{FD},u}[k] - \mathbf{F}_{\text{RF}}\mathbf{F}_{\text{BB},u}[k]\|_F^2, \tag{6.11}$$

that has a well-known least squares solution of $\mathbf{F}_{\text{BB},u}[k] = \mathbf{F}_{\text{RF}}^{\dagger}\mathbf{F}_{\text{FD},u}[k]$ [110]. The power constraint is temporarily relaxed and will be dealt with later.

We know that the columns of the unconstrained FD precoding matrix $\mathbf{F}_{\text{FD}}[k] = [\mathbf{F}_{\text{FD},1}[k], \cdots, \mathbf{F}_{\text{FD},U}[k]]$ are mutually orthogonal in order to mitigate the interference between the multiplexed streams. Given this, we also impose a similar constraint on the design of digital baseband precoder, where the columns of the precoding matrix should be mutually orthonormal, i.e.,

$$\mathbf{F}_{\text{BB},u}^{H}\mathbf{F}_{\text{BB},u} = \mathbf{I}_{N_{s,u}}. \tag{6.12}$$

Adding this constraint creates simplicity when designing the analog RF precoder, which will be discussed in the following subsection.

6.2.2 Analog RF Precoder Design with DFT-Assisted User Clustering

For the fully-connected structure, the feasible set of analog RF precoders for each subcarrier can be specified as the set of all $N_t \times N_{\text{RF}}^{t}$ matrices where $|(\mathbf{F}_{\text{RF}})_{i,j}| = 1, \forall i, j$, given each RF chain is connected to all antennas. In this stage, we consider a fixed digital baseband precoder $\mathbf{F}_{\text{BB},u}[k]$ for each user and subcarrier, and seek a solution to the following optimization problem that finds the optimal solution for the analog RF precoder:

$$\begin{aligned} \min_{\mathbf{F}_{\text{RF}}} \quad & \sum_{k=1}^{K} \|\mathbf{F}_{\text{FD}}[k] - \mathbf{F}_{\text{RF}}\mathbf{F}_{\text{BB}}[k]\|_F^2 \\ \text{s.t.} \quad & |(\mathbf{F}_{\text{RF}})_{i,j}| = 1, \forall i, j, \end{aligned} \tag{6.13}$$

where $\mathbf{F}_{\text{BB}}[k] = [\mathbf{F}_{\text{BB},1}[k], \cdots, \mathbf{F}_{\text{BB},U}[k]]$.

As mentioned before, the unit modulus constraint is the main obstacle that causes the problem to be non-convex. However, since the RF precoders are realized by phase shifters (which only adjust the phase of the signal), the set of feasible RF precoders can be simply defined using just the phases of their complex-valued elements. In fact, thanks to the orthogonality of the digital precoders, the phases of the analog RF precoders $\mathbf{F}_{\text{RF}}$ can be extracted from an equivalent precoder which is constructed from the digital baseband precoders $\mathbf{F}_{\text{BB},u}[k]$ and the unconstrained FD precoders $\mathbf{F}_{\text{FD},u}[k]$. Thus, the closed form solution can be written as:

$$\arg(\mathbf{F}_{\text{RF}}) = \arg\left(\sum_{k=1}^{K} \mathbf{F}_{\text{FD}}[k]\mathbf{F}_{\text{BB}}^{H}[k]\right), \tag{6.14}$$

where arg$(\mathbf{A})$ generates a matrix of phases of the entries of $\mathbf{A}$. It is important to mention that this solution reduces the complexity at the cost of performance loss. This performance loss stems from the constraint we impose on the design of the digital precoders, therefore instead of minimizing the original objective in (6.13), we minimize $\sum_{k=1}^{K} \|\mathbf{F}_{\text{FD}}[k]\mathbf{F}_{\text{BB}}^{H}[k] - \mathbf{F}_{\text{RF}}\|_F^2$.

As mentioned above, by the having knowledge of each user's AoDs in the beam-space domain, clusters of users can be formed. Let $\mathcal{B}_c$ be the union of the angular bins for all users in cluster c. Thus, the entries of arg$(\mathbf{F}_{\text{RF}})$ for each user cluster c can be equal to angles within the angular bins (e.g., the quantized central angle for the bin) in $\mathcal{B}_c$. However, these entries can deviate from those of the AoDs in a cluster due to the disjoint interval definition that we have for our bins.

Suppose U users are grouped into C clusters where $\mathcal{U}_c$ (with cardinality U_c) is the subset of users in cluster c. For the υ-th user in $\mathcal{U}_c$, let $N_{r,\upsilon}^{c}$ denote its number of receive antennas, $N_{s,\upsilon}^{c}$ denote the number of streams it receives, and $\mathbf{H}_{\upsilon}^{c}$ denote its channel matrix. Then, let $\mathbf{H}^{c}[k] = \left[\mathbf{H}_1^{c}[k]^T, \cdots, \mathbf{H}_{U_c}^{c}[k]^T\right]^T$ of size $\sum_{\upsilon=1}^{U_c} N_{r,\upsilon}^{c} \times N_t$ denote the aggregate vertically concatenated channel matrix for users in cluster c. The system can then calculate precoders for each cluster in parallel, using per-cluster variables $\mathbf{F}_{\text{FD},\upsilon}^{c}[k]$, $\mathbf{F}_{\text{BB},\upsilon}^{c}[k]$, and $\mathbf{F}_{\text{RF}}^{c}$, which have smaller dimensions. Pseudocode for the overall parallelized optimization is provided in Algorithm 6.1. The algorithm alternates between fixing $\mathbf{F}_{\text{RF}}^{c}$ and solving for $\mathbf{F}_{\text{BB},\upsilon}^{c}[k]$, then fixing $\mathbf{F}_{\text{BB},\upsilon}^{c}[k]$ and solving for $\mathbf{F}_{\text{RF}}^{c}$. The iterations continue until $\|\mathbf{F}_{\text{FD},\upsilon}^{c}[k] - \mathbf{F}_{\text{RF}}^{c}\mathbf{F}_{\text{BB},\upsilon}^{c}[k]\|_F^2$ drops below some specified convergence threshold ϵ.

Algorithm 6.1: User Clustering-Based Precoder Optimization for Fully-Connected Hybrid Transceivers

For all clusters c in parallel
  Calculate unconstrained BD of $\mathbf{H}^c[k], \forall k$ for users υ in cluster c as explained in Section 6.1.3;
  Set $i = 0$ and $\mathbf{F}^c_{\text{FD},\upsilon}[k], \forall k$ as in (6.9);
  Set value of threshold ϵ;
  Construct $\mathbf{F}^{c,(0)}_{\text{RF}}$ with random phases uniformly distributed in interval $\mathcal{B}_c$;
  Repeat
    Fix $\mathbf{F}^{c,(i)}_{\text{RF}}$, find $\mathbf{F}^{c,(i)}_{\text{BB},\upsilon}[k] = \mathbf{F}^{c,(i)\dagger}_{\text{RF}}\mathbf{F}^c_{\text{FD},\upsilon}[k], \forall k, \upsilon$;
    Fix $\mathbf{F}^{c,(i)}_{\text{BB},\upsilon}[k], \forall k$, find $\mathbf{F}^{c,(i+1)}_{\text{RF}}$ using (6.14);
    $i = i + 1$;
  Until $\|\mathbf{F}^c_{\text{FD},\upsilon}[k] - \mathbf{F}^c_{\text{RF}}\mathbf{F}^c_{\text{BB},\upsilon}[k]\|^2_F < \epsilon, \forall k, \upsilon$
End For

6.2.3 Complexity

In this subsection, we briefly discuss the complexity of the proposed user clustering-based hybrid precoding algorithm. Considering the user clustering problem, there is a bipartite graph with a number of vertices (from the sets of user nodes and angular bins) and a number of paths among these vertices. The graph has N_t+U vertices and N_tU edges in total. However, we are able to exploit the sparsity of the graph, since we are only interested in edges with a value of 1 in the connectivity matrix $\mathbf{C}$. (Determining the value is just a simple binary check, whose relatively simple complexity compared to other floating-point operations can easily be neglected.) From our system model, there are only UN_p edges with a value of 1 in $\mathbf{C}$; the rest are zero.

As for the fully-connected structure, the updating rules of the digital precoders are given by closed-form solutions. Furthermore, in the hybrid precoding system, the dimension of the analog precoder is much higher than that of the digital precoder, which makes the complexity of the algorithms dominated by the analog part. In each iteration of Alg. 6.1, the update of the analog precoder is simply realized by a phase extraction operation of the matrix $\sum_k \mathbf{F}^c_{\text{FD}}[k](\mathbf{F}^c_{\text{BB}}[k])^H$ in (6.14), whose dimension is $N_t \times N^t_{\text{RF}}$. The analog precoder update complexity is dominated more by the K matrix multiplications and additions to obtain this matrix, which on the whole over all clusters have an order of complexity of $\mathcal{O}(KN_tN^t_{\text{RF}}N_s)$ [92].

The pseudo-inverse in Alg. 6.1 can be found with $\mathcal{O}(N_t(N^t_{\text{RF}})^2)$ complex operations to find $(\mathbf{F}^c_{\text{RF}})^H\mathbf{F}^c_{\text{RF},}$, the product $((\mathbf{F}^c_{\text{RF}})^H\mathbf{F}^c_{\text{RF}})^{-1}(\mathbf{F}^c_{\text{RF}})^H$ can be computed efficiently by means of LDL decomposition of $(\mathbf{F}^c_{\text{RF}})^H\mathbf{F}^c_{\text{RF}}$ with $\mathcal{O}((N^t_{\text{RF}})^3)$ operations for the decomposition and $\mathcal{O}(N_t(N^t_{\text{RF}})^2)$ operations for matrix multiplications [74]. There is then a multiplication by $\mathbf{F}_{\text{FD},v}[k]$ to update the digital precoder $\mathbf{F}^c_{\text{BB},v}[k]$ on each subcarrier, for complexity $\mathcal{O}(KN^t_{\text{RF}}N_tN^c_{s,v})$. All of these updates are performed for each user v for the number of iterations that Alg. 6.1 requires. Determining if the algorithm has converged requires calculating the squared Frobenius norm near the end of Alg. 6.1 for each user and subcarrier. This requires $\mathcal{O}(N_tN^t_{\text{RF}}N^c_{s,v})$ operations for the matrix multiplication and $\mathcal{O}(N_tN^c_{s,v})$ operations for the subtraction and for the norm itself.

For calculating the FD precoder $\mathbf{F}^c_{\text{FD},v}[k]$, the computational complexity is dominated by the complex-valued SVD. The number of operations for a real-valued SVD operation is given in [92], and [111] shows the number of operations required for an $m \times n$ complex-valued SVD operation is equivalent to that for its extended $2m \times 2n$ real-valued matrix. For an SVD of the $m \times n$ complex-valued matrix $\mathbf{A} = \mathbf{U}_A\mathbf{\Sigma}_A\mathbf{V}^H_A$ with $m \geq n$, if only $\mathbf{U}_A$ and $\mathbf{\Sigma}_A$ are required from the SVD, then $32m^2n - 64mn^2$ operations are required. If $m \leq n$ and $\mathbf{V}_A$ is required instead of $\mathbf{U}_A$, then an SVD of $\mathbf{B} = \mathbf{A}^H$ can be done instead with $32n^2m - 64nm^2$ operations, where $\mathbf{U}_B$ will equal $\mathbf{V}_A$. Hence, for the SVD to find $\mathbf{F}^c_{\text{FD},v}[k]$, since $N_t \gg N^c_{s,v}$, the complexity will be $\mathcal{O}(N^2_tN^c_{s,v})$ for each user and subcarrier, or $\mathcal{O}(KN^2_tN_s)$ overall.

6.3 Hybrid Precoding For Partially-Connected Structure

For a partially-connected structure, only N_t/N_{RF}^t antennas are connected to each of N_{RF}^t chains[3] at the transmitter. Now the benefit of deploying a partially-connected structure with the user clustering algorithm is that the system can still exploit the full beamforming gain. In particular, each subset of RF chains can be dedicated to a certain cluster of users. With the focus only on the design of the hybrid precoders for user u at subcarrier k in cluster c, the optimization function that we seek to maximize is given in (6.8), except with the variables replaced with their per-cluster versions. Furthermore, the analog RF precoder $\mathbf{F}_{\text{RF}}^c$ is block-diagonal and composed of a set of vectors $\mathcal{A}_p = \{\mathbf{p}_1, \mathbf{p}_2, \ldots, \mathbf{p}_{N_{\text{RF}}^t}\}$, each with length N_t/N_{RF}^t. These vectors have elements with unit modulus that are essentially the phase of each phase shifter. Thus, the analog RF precoder $\mathbf{F}_{\text{RF}}^c$ is given by

$$\mathbf{F}_{\text{RF}}^c = \text{diag}\left[\mathbf{p}_1, \mathbf{p}_2, \ldots, \mathbf{p}_{N_{\text{RF}}^t}\right], \tag{6.15}$$

where $\mathbf{p}_i = \left[\exp\left(j\phi_{(i-1)N_t/N_{\text{RF}}^t+1}\right), \ldots, \exp\left(j\phi_{iN_t/N_{\text{RF}}^t}\right)\right]^T$, and ϕ_q is the phase of the q^{th} phase shifter. The special structure of the analog RF precoder $\mathbf{F}_{\text{RF}}^c$ leads to the following power constraint for the optimization problem as follows:

$$\|\mathbf{F}_{\text{RF}}^c \mathbf{F}_{\text{BB},\upsilon}^c[k]\|_F^2 = \frac{N_t}{N_{\text{RF}}^t}\|\mathbf{F}_{\text{BB},\upsilon}^c[k]\|_F^2 = \sum_{\upsilon=1}^{U_c} N_{s,\upsilon}^c = N_s^c. \tag{6.16}$$

Now, the optimization problem for the analog RF precoder design can be written as follows:

$$\begin{aligned}
\min_{\mathbf{F}_{\text{RF}}^c} \quad & \sum_{k=1}^{K} \|\mathbf{F}_{\text{FD}}[k] - \mathbf{F}_{\text{RF}}^c \mathbf{F}_{\text{BB}}^c[k]\|_F^2 \\
\text{s.t.} \quad & \mathbf{F}_{\text{RF}}^c = \text{diag}\left[\mathbf{p}_1, \mathbf{p}_2, \ldots, \mathbf{p}_{N_{\text{RF}}^t}\right], \\
\text{s.t.} \quad & \mathbf{p}_i \in \mathcal{A}_p, i = 1, 2, \ldots, N_{\text{RF}}^t.
\end{aligned} \tag{6.17}$$

[3] In the event that there are significant differences in the number of users per cluster, possibly additional antennas or RF chains could be dedicated to the larger clusters of users. This would be similar to the adaptive structure in [20]. In this work, the propagation environment for different users is balanced enough so large imbalances among clusters do not occur. Hence, such redistribution is unnecessary.

Given the structure of the analog RF precoder, the problem in (6.17) can also be written as

$$\min_{\phi_i} \sum_{k=1}^{K} \|(\mathbf{F}_{\text{FD}}^c[k])_{i,:} - \exp(j\phi_i)(\mathbf{F}_{\text{BB}}^c[k])_{l,:}\|_2^2, \tag{6.18}$$

where $i = 1, 2, \ldots, N_t$ and $l = \lceil iN_{\text{RF}}^t/N_t \rceil$. The problem in (6.18) is equivalent to finding those non-zero elements of $\mathbf{F}_{\text{RF}}^c$ whose phases are equal to

$$\arg\{(\mathbf{F}_{\text{RF}}^c)_{i,l}\} = \arg\left\{\sum_{k=1}^{K}(\mathbf{F}_{\text{FD}}^c[k])_{i,:}\left[(\mathbf{F}_{\text{BB}}^c[k])_{l,:}\right]^H\right\}. \tag{6.19}$$

As it can be seen in (6.19), the design of the analog RF precoder $\mathbf{F}_{\text{RF}}^c$ is only dependent on the phase of the phase shifters, therefore the unit modulus constraint does not cause any intractability in the problem and is met in the partially-connected structure. Given the user clustering algorithm introduced in [87], the initial phases of the phase shifters for the optimization are set uniformly randomly in the interval $\mathcal{B}_c$. Each user cluster can be allocated to a specific set of RF chains.

Now, we can design the digital baseband precoder $\mathbf{F}_{\text{BB},\upsilon}^c[k]$. Based on (6.13), the design problem can be written by

$$\begin{aligned} \min_{\{\mathbf{F}_{\text{BB},\upsilon}^c[k]\}} \quad & \|\mathbf{F}_{\text{FD},\upsilon}^c[k] - \mathbf{F}_{\text{RF}}^c\mathbf{F}_{\text{BB},\upsilon}^c[k]\|_F^2 \\ \text{s.t.} \quad & \|\mathbf{F}_{\text{BB},\upsilon}^c[k]\|_F^2 = \tfrac{N_{s,\upsilon}^c N_{\text{RF}}^t}{N_t}, \forall \upsilon, k. \end{aligned} \tag{6.20}$$

Obviously, the objective function and the constraint in the optimization problem in (6.20) are both quadratic. This means that the design of digital baseband precoder $\mathbf{F}_{\text{BB},\upsilon}^c[k]$ is a quadratic constraint quadratic programming (QCQP) problem and a non-convex optimization problem [102].

In the literature, different methods have been proposed to solve a non-convex QCQP problem. In [103], it has been shown that by applying the S-lemma, the following homogeneous QCQP formula is achieved:

$$
\begin{array}{ll}
\min\limits_{\mathbf{F}} & \operatorname{tr}(\mathbf{A}\mathbf{F}) \\
\text{s.t.} & \operatorname{tr}(\mathbf{A}_1\mathbf{F}) = \frac{N_{s,v}^c N_{\text{RF}}^t}{N_t}, \\
\text{s.t.} & \operatorname{tr}(\mathbf{A}_2\mathbf{F}) = 1, \\
\text{s.t.} & \text{rank}(\mathbf{F}) = 1, \\
\text{s.t.} & \mathbf{F} \succeq \mathbf{0}.
\end{array}
\tag{6.21}
$$

In the problem in (6.21), we try to find a square $n \times n$ matrix $\mathbf{F}$ where $n = N_{\text{RF}}^t N_{s,v}^c + 1$, $\mathbf{F} = \mathbf{f}\mathbf{f}^H$, $\mathbf{f} = [\{\text{vec}(\mathbf{F}_{\text{BB},v}^c[k])\}^T, z]^T$ with an auxiliary variable z, $\mathbf{g} = \text{vec}(\mathbf{F}_{\text{FD},v}^c[k])$, and

$$
\mathbf{A}_1 = \begin{bmatrix} \mathbf{I}_{n-1} & \mathbf{0} \\ \mathbf{0} & 0 \end{bmatrix}, \tag{6.22}
$$

$$
\mathbf{A}_2 = \begin{bmatrix} \mathbf{0}_{n-1} & \mathbf{0} \\ \mathbf{0} & 1 \end{bmatrix}, \tag{6.23}
$$

$$
\mathbf{A} = \begin{bmatrix} (\mathbf{I}_{N_{s,v}} \otimes \mathbf{F}_{\text{RF}}^c)^H (\mathbf{I}_{N_{s,v}} \otimes \mathbf{F}_{\text{RF}}^c) & -(\mathbf{I}_{N_{s,v}} \otimes \mathbf{F}_{\text{RF}}^c)^H \mathbf{g} \\ -\mathbf{g}^H (\mathbf{I}_{N_{s,v}} \otimes \mathbf{F}_{\text{RF}}^c) & \mathbf{g}^H \mathbf{g} \end{bmatrix}. \tag{6.24}
$$

When solving the problem in (6.21), the most difficult constraint to satisfy is the rank constraint. However, this can be relaxed by a semi-definite programming (SDP) relaxation [104], as follows:

$$
\begin{array}{ll}
\min\limits_{\mathbf{F}} & \operatorname{tr}(\mathbf{A}\mathbf{F}) \\
\text{s.t.} & \operatorname{tr}(\mathbf{A}_1\mathbf{F}) = \frac{N_{s,v}^c N_{\text{RF}}^t}{N_t}, \\
\text{s.t.} & \operatorname{tr}(\mathbf{A}_2\mathbf{F}) = 1, \\
\text{s.t.} & \mathbf{F} \succeq \mathbf{0}.
\end{array}
\tag{6.25}
$$

Now, we can iteratively solve the relaxed SDP optimization problem in (6.25) using Algorithm 6.2 to find the digital baseband precoder $\mathbf{F}_{\text{BB},v}^c[k]$. This problem can be solved by standard convex optimization tools such as those described in [102]. Algorithm 6.2 provides a step-by-step pseudocode summary of the user clustering-based precoder optimization algorithm for the partially-connected structure. The algorithm alternates between solving for $\mathbf{F}_{\text{BB},v}^c[k]$ and solving for $\mathbf{F}_{\text{RF}}^c$ in the same manner as Alg. 6.1.

Algorithm 6.2: User Clustering-Based Precoder Optimization for Partially-Connected Hybrid Transceivers

For all clusters c in parallel
  Calculate unconstrained BD of $\mathbf{H}^c[k], \forall k$ for users υ in cluster c as explained in Section 6.1.3;
  Set $i = 0$ and $\mathbf{F}^c_{\text{FD},\upsilon}[k], \forall k$ as in (6.9);
  Set value of threshold ϵ;
  Construct $\mathbf{F}^{c,(0)}_{\text{RF}}$ with random phases uniformly distributed in interval $\mathcal{B}_c$;
  Repeat
    Fix $\mathbf{F}^{c,(i)}_{\text{RF}}$, find $\mathbf{F}^{c,(i)}_{\text{BB},\upsilon}[k]$ using convex optimization tool (see e.g. [102]) and relaxed SDP problem in (6.25);
    Fix $\mathbf{F}^{c,(i)}_{\text{BB},\upsilon}$, find $\mathbf{F}^{c,(i+1)}_{\text{RF}}$ using (6.19);
    $i = i + 1$;
  Until $\|\mathbf{F}^c_{\text{FD},\upsilon}[k] - \mathbf{F}^c_{\text{RF}}\mathbf{F}^c_{\text{BB},\upsilon}[k]\|^2_F < \epsilon, \forall k, \upsilon$
End For

6.3.1 Complexity

In the proposed algorithm for the partially-connected structure, the digital precoders are updated by the relaxed optimization problem in (6.25), which is a computationally efficient approximation approach to a QCQP problem and has polynomial-time complexity in the problem size $n = N^t_{\text{RF}}N^c_{s,\upsilon} + 1$. Updating the analog RF precoder is realized by a phase extraction of the complex scalar value $\sum_k (\mathbf{F}^c_{\text{FD}}[k])_{i,:} [(\mathbf{F}^c_{\text{BB}}[k])_{l,:}]^H$ in (6.19). Each of the N_t non-zero values requires $\mathcal{O}(KN^c_s)$ flops to calculate. Other operations are done similarly to Alg. 6.1, again for each user u and each subcarrier k for the number of iterations that the Alg. 6.2 requires. The complexity of these operations is ostensibly the same as for Alg. 6.1, but the block-diagonal structure of $\mathbf{F}^c_{\text{RF}}$ can be exploited to reduce the required computations.

6.4 Simulation Results and Discussion

In this section, we numerically evaluate the performance of our proposed DFT-assisted user clustering and hybrid precoding-combining algorithm for fully-connected and partially-connected structures. The performance of a mmWave MIMO-OFDM system having frequency-selective channels is examined. In our Monte Carlo simulations with 10000 iterations, we consider a BS equipped with N_t antennas that communicates with U single-antenna users via only one stream per user. Therefore the total number of streams in the system is equal to the number of UEs, i.e., $N_s = U$. The average total transmitted power is set to $\rho = 1$, so different signal-to-noise ratios (SNRs) are set by adjusting the variance of the AWGN. The complex paths' gains $\alpha_{u,p}$ are distributed $\sim \mathcal{CN}(0, 1)$, which models Rayleigh small-scale fading of the gains. The antenna arrays are ULAs with half-wavelength element spacing; hence, potential coupling between antenna elements can be assumed to be negligible. The system is assumed to operate at a carrier frequency of 28 GHz with a sampling frequency of $f_s = 0.25$ GHz and a total bandwidth of $B = 500$ MHz. The number of OFDM subcarriers is set to 32. The raised-cosine pulse function has a roll-off factor of 0.8. Also, the sampling interval is assumed to be $1/f_s$, and delay paths are chosen uniformly from $[0, (D-1)T_s]$. The number of tap delays in the frequency-selective channel is assumed to be 3, which is equal to the assumed number of channel paths per tap. The value of ϵ is set to 0.001 for both algorithms.

6.4.1 Spectral Efficiency

Fig. 6.1 plots the system spectral efficiency (normalized to the total system bandwidth) achieved by both the fully-connected and partially-connected structures and their associated proposed algorithms, for the two cases when the number of the RF chains is equal to 4 and 8, with $N_t = 144$ and $U = N_{\text{RF}}^t$. We see that the curves of the low-complexity partially-connected algorithm almost coincide with those of the

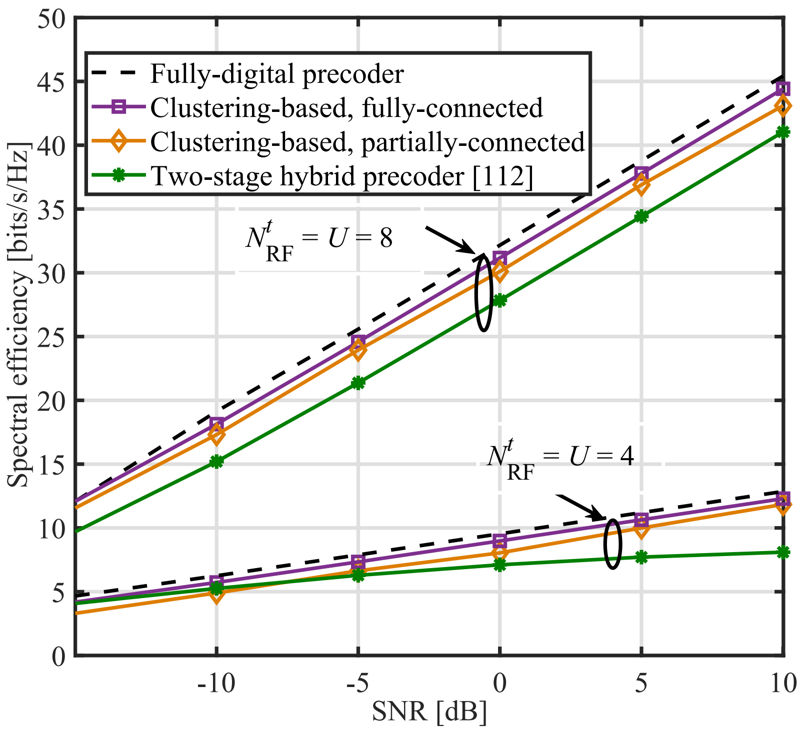

Figure 6.1: Spectral efficiency versus SNR, comparing different precoding methods; $N_t = 144$, $U = N^t_{\text{RF}}$.

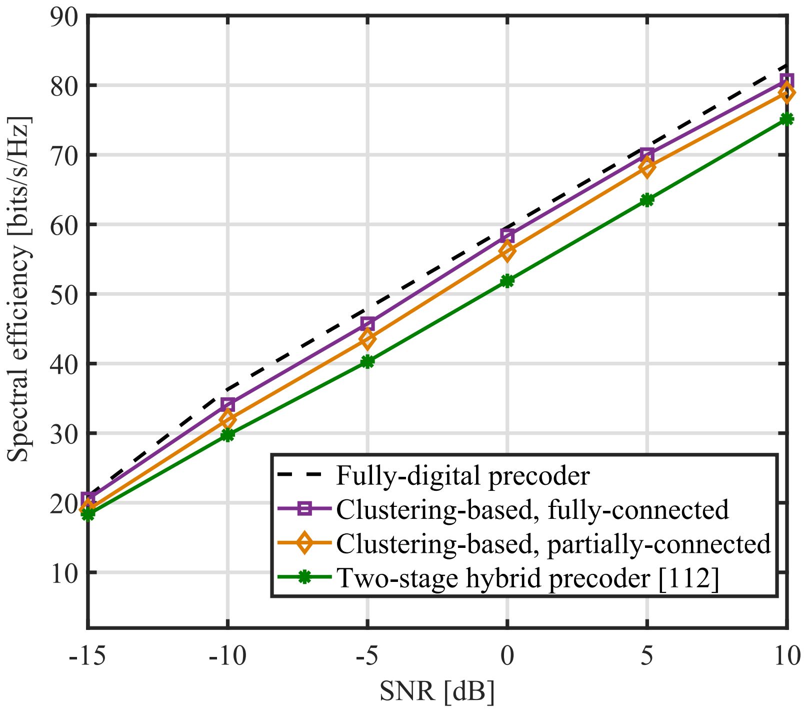

Figure 6.2: Spectral efficiency versus SNR, comparing precoding methods; $N_t = 144$, $U = 16$, $N_{\text{RF}}^t = 17$.

fully-connected algorithm. This result implies that Alg. 6.2 can closely achieve the performance of the higher-complexity (in terms of hardware) Alg. 6.1, by adopting the lower-complexity structure when $N_{\text{RF}}^t = U$. Under this system setup, the partially-connected algorithm serves as an excellent candidate for the hybrid precoder design, achieving both good performance and low complexity. In contrast, the two-stage hybrid precoding algorithm in [112] performs relatively poorly when $N_{\text{RF}}^t = U$, especially as the SNR increases.

Fig. 6.2 plots the spectral efficiency achieved by the proposed algorithms for fully-connected and partially-connected structures compared to the two-stage hybrid precoding method proposed in [112], with $N_t = 144$, $U = 16$, and $N_{\text{RF}}^t = 17$. We also compare with FD precoding. As the figure shows, with 17 RF chains (one RF chain more than the number of users), similar to what we have observed in Fig. 6.1, the solution for the fully-connected structure is close to the performance of the FD precoder. Interestingly, it can be seen that for all the SNR values, the low-complexity algorithm for the partially-connected structure achieves higher spectral efficiency than that of the algorithm in [112], even when the former has fewer paths between antennas and RF chains (in other words, [112] uses a fully-connected structure). This demonstrates that the extra orthogonality achieved between the clusters also has an impact on spectral efficiency in mmWave OFDM systems. This indicates that the proposed algorithm can serve as a more suitable candidate for low-complexity hybrid precoding, both in narrowband and broadband OFDM systems, when the transceivers only have limited RF chains available.

Next we investigate the impact of the number of RF chains, with $N_t = 144$, $U = 8$, and SNR = 0 dB. Fig. 6.3 compares different algorithms assuming 8 data streams are transmitted. Since the solution in the $N_{\text{RF}}^t \geq 2N_s$ region has been fully developed in [109], here we focus on the region $N_{\text{RF}}^t \in [8, 18]$, with particular emphasis on $N_{\text{RF}}^t \leq 16$. We see that the performance of the proposed algorithm for the fully-connected structure starts to coincide with the performance of FD precoding when $N_{\text{RF}}^t \geq 16$. This result demonstrates that when $N_{\text{RF}}^t \geq 2N_s$, as expected our proposed algorithm can achieve the FD spectral efficiency, which, however, cannot be achieved by the two-stage precoding algorithm in [112]. Fig. 6.3 gives us insight into the amount of loss in performance that our system will experience in case of deploying either structure. For example, at $N_{\text{RF}}^t = 12$, the fully-connected structure achieves about 0.5% less spectral efficiency relative to the FD precoder, whereas the partially-connected structure and the algorithm in [112] experience about 5% and 12% less spectral efficiency, respectively. The comparison between our two hybrid precoding schemes shows that the partially-connected scheme, using fewer phase shifters, does entail some non-negligible performance loss when compared with the fully-connected scheme.

In Fig. 6.4, we investigate the impact of ULA and UPA antenna structures on the performance of the system. For the UPA, we assume an 8×8 antenna array with its elements separated by $q = \lambda/2$. As seen, with either transceiver structure, the spectral efficiency achieved for the ULA and UPA are very close, but especially so for the fully-connected structure.

6.4.2 Energy Efficiency

The main difference between the two hybrid precoding structures considered in this work is the number of phase shifters N_{PS} in use for given numbers of data streams, RF chains, and antennas. In terms of spectral efficiency, the fully-connected structure provides more design degrees of freedom in the RF domain and thus will outperform the partially-connected one. However, when taking power consumption into consideration, it is important to know which structure has better energy efficiency. Energy efficiency is defined as the ratio between the data rate and total power consumption in the massive MIMO communication system:

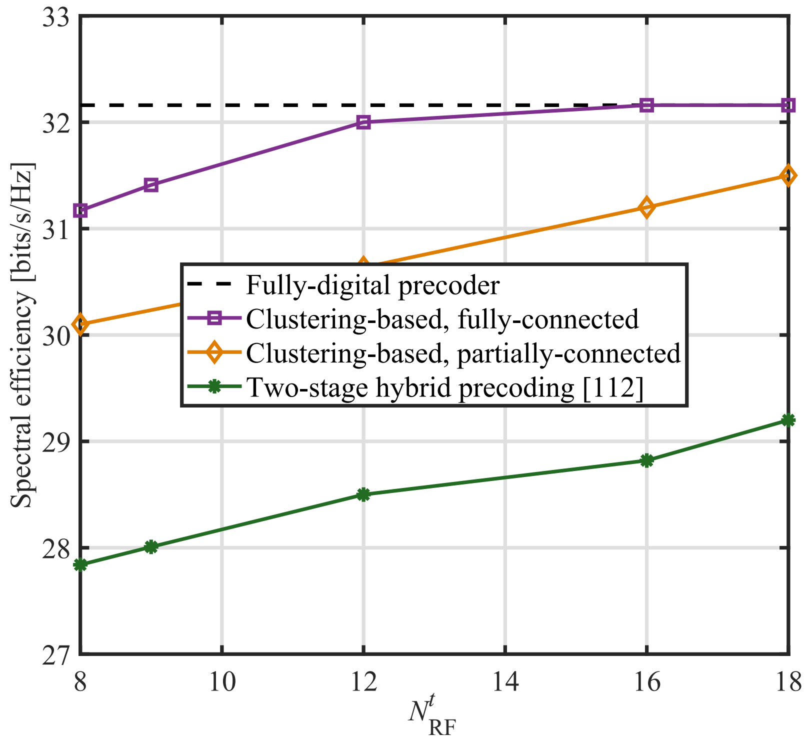

Figure 6.3: Spectral efficiency versus number of RF chains N_{RF}^{t}, comparing various precoding algorithms; $N_t = 144$, $U = 8$, and SNR = 0 dB.

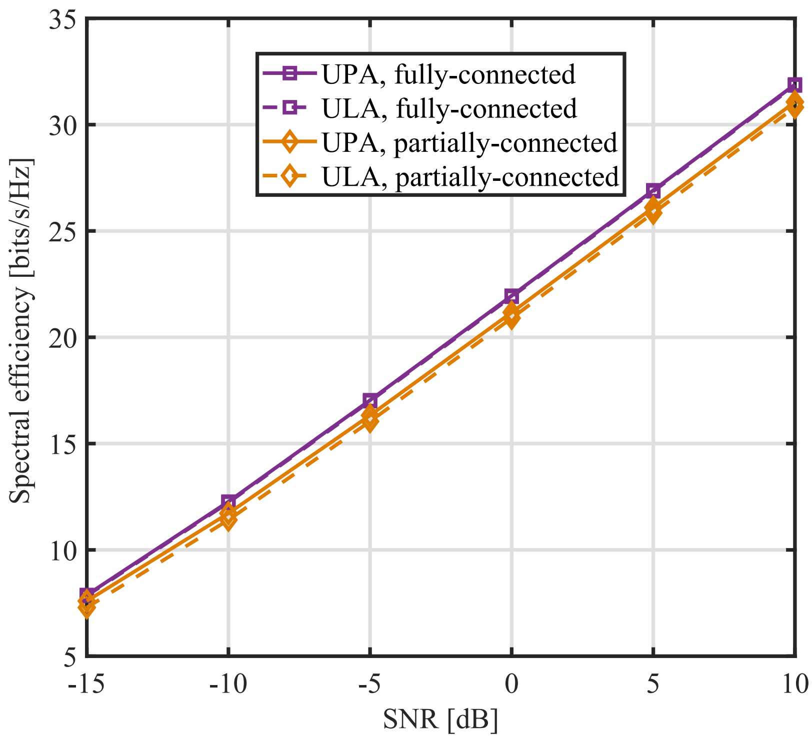

Figure 6.4: Spectral efficiency versus SNR, comparing antenna arrays; $N_t = 64$ (UPA: 8×8), $U = 8$, $N_{\text{RF}}^t = 8$.

$$\xi = \frac{BR}{P_{\text{common}} + N_{\text{RF}}^t P_{\text{RF}} + N_t P_{\text{PA}} + N_{\text{PS}} P_{\text{PS}}} \tag{6.26}$$

where the unit of ξ is bits/s/W (or bits/Joule), R is the sum spectral efficiency from (6.7), and B is the system bandwidth. P_{common} is the common power of the transmitter, accounting for the digital baseband board. P_{RF}, P_{PS}, and P_{PA} are the power of each RF chain, phase shifter, and power amplifier (PA) that are used to transmit data, respectively. We assume a PA is connected to each transmit antenna. The energy consumed by each PA is $P_{\text{PA}} = P_{\text{out}}/\eta$, where P_{out} is the output power and η is the efficiency of the PA. The number of phase shifters N_{PS} can be expressed as follows:

$$N_{\text{PS}} = \begin{cases} N_{\text{RF}}^t N_t, & \text{fully-connected structure;} \\ N_t, & \text{partially-connected structure.} \end{cases} \tag{6.27}$$

A numerical comparison of energy efficiency is illustrated in Fig. 6.5, when $U = 8$, $N_t = 144$, $P_{\text{common}} = 10$ W, $P_{\text{RF}} = 100$ mW, and $P_{\text{PS}} = 10$ mW. Considering an average transmit power of 1 W for the transmitter with 144 antennas, the average output power per PA is $P_{\text{out}} = 6.94$ mW, while we assume an efficiency of $\eta = 12.8\%$ [38]. The figure shows substantially different behaviors for the two structures. Since the number of phase shifters scales linearly with N_{RF}^t and N_t in the fully-connected structure, the power consumption will increase substantially when increasing N_{RF}^t. As illustrated in Fig. 6.3, however, the spectral efficiency achieved by the fully-connected algorithm is sufficiently close or exactly equal to the FD spectral efficiency once $N_{\text{RF}}^t = 2N_s = 16$, and will not increase further as N_{RF}^t increases. Based on these two facts, the power consumption grows much faster than the spectral efficiency, which gives rise to the dramatic decrease in energy efficiency.

For the partially-connected structure, since the number of phase shifters is independent of N_{RF}^t, the dominant part of the total power consumption remains almost unchanged over the investigated range of the number of RF chains. Meanwhile, the spectral efficiency gradually approaches that of the FD precoder when increasing N_{RF}^t. The improvement of the spectral efficiency and the almost unchanged power consumption together account for the rise in the energy efficiency with increasing N_{RF}^t in the partially-connected structure. However, although not shown in the figure, we can expect the energy efficiency of the partially-connected structure to eventually drop again with further increasing N_{RF}^t. Once the system reaches the same maximum spectral efficiency as that provided by the FD precoder, no further gains would be achieved by adding more RF chains, leading to wasted power consumption and decreased energy efficiency.

In the same figure, the energy efficiency of the FD precoder and the two-stage hybrid precoder in [112] is illustrated, where the former assumes the number of RF chains is constant and equal to the number of antenna elements. The algorithm in [112] performs similarly to our fully-connected algorithm, but with lower energy efficiency stemming from its lower spectral efficiency achieved with about the same power consumption.

More importantly, Fig. 6.5 shows that there is an intersection point, i.e., between $N_{\text{RF}} = 8$ and 9, of the energy efficiency for the two hybrid precoding structures. In particular, the fully-connected structure enjoys higher energy efficiency with a small number of RF chains, whereas the partially-connected one is more energy efficient when the transceivers employ a relatively large number of RF chains. This trade-off offers valuable insights for the RF chain implementation in hybrid precoding structures. As we observed in Fig. 6.3, the fully-connected structure can approach the performance of the FD precoder when the number of RF chains is slightly larger than that of the data streams. Therefore, there is no need to add more RF chains considering the energy efficiency. On the other hand, with a low-complexity hardware implementation, it is beneficial for the partially-connected structure to leverage the larger number of RF chains to improve both spectral and energy efficiency.

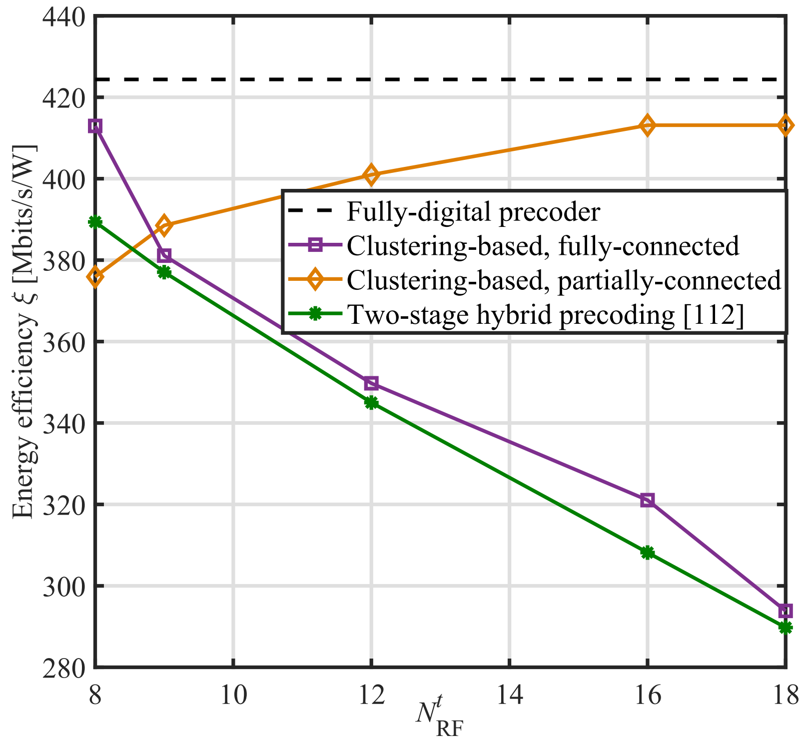

Figure 6.5: Energy efficiency versus number of RF chains N_{RF}^{t}; fully-connected and partially-connected, $N_t = 144$, $U = 8$, SNR = 0 dB.

6.5 Summary

In this chapter, we have proposed a DFT-assisted user clustering hybrid precoding algorithm for an analog-digital hybrid precoding-combining transceiver in mmWave MIMO systems. There are two possible structures for a hybrid architecture, namely fully-connected and partially-connected. We have proposed algorithms to find near-optimal digital baseband and analog RF precoders for both structures. The algorithms make use of DFT-based user clustering to simplify the design of the analog Rf precoders, and add extra orthogonality to the system that improves the spectral efficiency compared to existing methods. The improved performance has been demonstrated by system simulations. We have also examined the energy efficiency of the system using our algorithms. Simulations have demonstrated that the fully-connected structure is the most energy efficient when only a few RF chains are employed; otherwise, the partially-connected structure is more efficient.

Chapter 7

Robust Precoder Design for Massive MIMO with Peak Total Power Constrained Single-RF-Chain Transmitters

The performance of massive MIMO systems relies on the availability of sufficiently accurate channel state information (CSI) at the transmitter. However, due to estimation errors and delay this CSI is imperfect. Additionally, the use of many RF chains to drive a large number of antennas at the transmitter quickly becomes impractical when that number increases. In [113] we discuss the design of a precoder for massive MIMO with a single-RF-chain transmitter having an instantaneous total power constraint that is robust under channel uncertainty. We consider a bounded channel error to model the channel uncertainty [114, 115] and minimize the mean-square error (MSE) of the received signal for all the users under the worst-case channel uncertainty.

7.1 System Model

Assuming downlink of a MU-MIMO system, where the BS is equipped with N_t antennas serving K single-antenna users, the complex-valued received signal y_k at user k is given by

$$y_k = \mathbf{h}_k^T \mathbf{x} + n_k, \tag{7.1}$$

where $\mathbf{x} \in \mathcal{C}^{N_t}$ is the transmitted signal vector from the BS, $n_k \sim \mathcal{CN}(0, \sigma^2)$ is the complex Gaussian noise at user terminal k and $\mathbf{h}_k \in \mathcal{C}^{N_t}$ represents the channel vector of user k. The entries of $\mathbf{h}_k$ are zero-mean complex Gaussian random variables with unity variance. Let P_t denote the instantaneous peak total power constraint at the transmitter. Then, the instantaneous power of the transmitted signal must satisfy the condition $\mathbf{x}^H \mathbf{x} \leq P_t$. We use the strategy of minimizing the MSE of the received signal to design the precoder for massive MIMO with a single-RF-chain transmitter. We assume that a real-valued constant design parameter $1/f$ is applied at all user terminals as an equalizer, thus the received signal of user k after equalization becomes $r_k = y_k/f$. We treat $1/f$ as a tuning parameter available to system designers, which can be optimized for the given performance metric and system configuration. In the MMSE precoding design [114], the objective is to minimize the power of the error $|r_k - u_k|$ for all users, where u_k is the complex-valued desired data for user k embedded in $\mathbf{x}$. The channel uncertainty region for user k can be expressed as

$$\mathbf{h}_k = \widetilde{\mathbf{h}}_k + \boldsymbol{\delta}_k, \tag{7.2}$$

where $\boldsymbol{\delta}_k \in \mathcal{C}^{N_t}$ represents the error, whose norm is less than ε_k, i.e. $\|\boldsymbol{\delta}_k\| \leq \varepsilon_k$. The BS knows the channel estimates $\{\widetilde{\mathbf{h}}_k\}$ and the precoder depends on these channel estimates.

Fig. 7.1 shows the block diagram of the single-RF chain transmitter. It includes a single power amplifier, which outputs a constant-envelope sinusoid, and parallel two-port load modulator components for each antenna element, which are denoted as N_i for antenna element i [55]. These load modulators are adjustable to give the desired currents or signals on the radiating antenna elements based on the desired signaling format coming from the baseband processor. It is worth mentioning that since all the antenna elements are

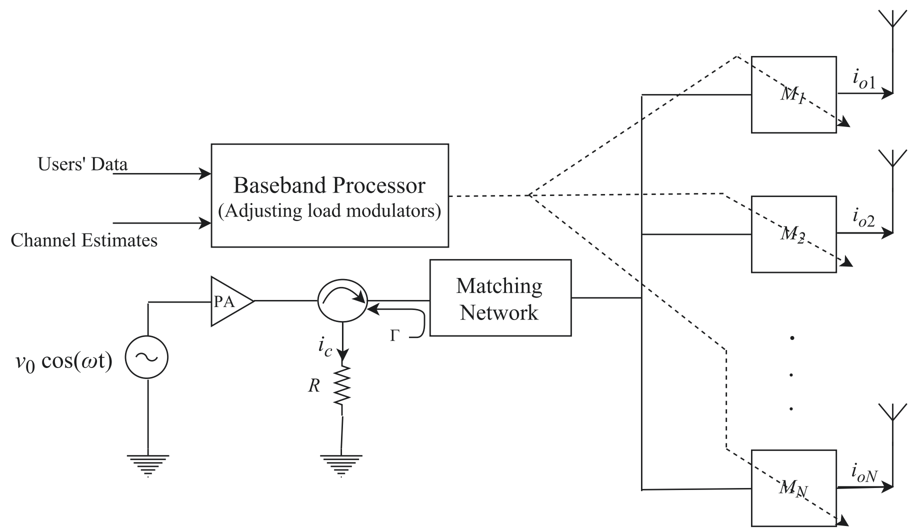

Figure 7.1: The block diagram of the single-RF-chain transmitter (see [55]).

connected to a common source that generates a fixed sinusoid carrier wave, the use of a non-linear power amplifier such as a class F amplifier is possible [58].

7.2 Robust Precoding Design

Our objective in robust precoding design is to minimize the MSE between the desired received signal and its estimate for all users under the worst-case channel uncertainty [69]. Casting this strategy as an optimization problem yields

$$\mathcal{M}_1 = \begin{cases} \min\limits_{\mathbf{x}} \max\limits_{k} \max\limits_{\boldsymbol{\delta}_k} & \mathbb{E}\left[|\frac{1}{f}(\mathbf{h}_k^T\mathbf{x} + n_k) - u_k|^2\right] \\ \\ \text{s.t.} & \|\mathbf{x}\|^2 \leq P_t, \end{cases} \tag{7.3}$$

where the expectation is over the noise. Taking this expectation, the optimization problem in (7.3) becomes

$$\mathcal{M}_1 = \begin{cases} \min\limits_{\mathbf{x}} \max\limits_{k} \max\limits_{\boldsymbol{\delta}_k} & |\frac{1}{f}(\widetilde{\mathbf{h}}_k^\mathsf{T} + \boldsymbol{\delta}_k^\mathsf{T})\mathbf{x} - u_k|^2 \\ \\ \text{s.t.} & \|\mathbf{x}\|^2 \leq P_t. \end{cases} \tag{7.4}$$

Note that the optimization problem $\mathcal{M}_1$ is not convex. Also, the maximization over $\boldsymbol{\delta}_k$ in (7.3) is itself an optimization problem with the constraint on the norm of $\boldsymbol{\delta}_k$. The following lemma can be used to simplify further the optimization problem (7.4). The objective function of the following constrained maximization problem

$$\mathcal{P} = \begin{cases} \max_{\boldsymbol{\delta}_k} & |\frac{1}{f}(\widetilde{\mathbf{h}}_k + \boldsymbol{\delta}_k)\mathbf{x} - u_k|^2 \\ \text{s.t.} & \|\boldsymbol{\delta}_k\| \le \varepsilon_k \end{cases} \tag{7.5}$$

has maximum

$$g_{\max} = \left| \left| \frac{1}{f}\widetilde{\mathbf{h}}_k\mathbf{x} - u_k \right| + \frac{1}{|f|}\varepsilon_k\|\mathbf{x}\| \right|^2. \tag{7.6}$$

Proof. See Appendix C. ■

Using Lemma 7.2, , the problem (7.3) can be simplified to

$$\mathcal{M}_1 = \begin{cases} \min\limits_{\mathbf{x}} \max\limits_{k} & \left| \left| \frac{1}{f}\widetilde{\mathbf{h}}_k^T\mathbf{x} - u_k \right| + \frac{1}{|f|}\varepsilon_k\|\mathbf{x}\| \right|^2 \\ \text{s.t.} & \|\mathbf{x}\|^2 \le P_t. \end{cases} \tag{7.7}$$

Finally, by introducing the slack variable b, as an auxiliary variable to reduce our optimization problem, into (7.7), the following convex optimization problem results

$$\mathcal{M}_2 = \begin{cases} \min\limits_{\mathbf{x},b} & b^2 \\ \text{s.t.} & \left| \frac{1}{f}\widetilde{\mathbf{h}}_k^T\mathbf{x} - u_k \right| + \frac{1}{|f|}\varepsilon_k\|\mathbf{x}\| \le b, \forall k \\ \text{s.t.} & \|\mathbf{x}\|^2 \le P_t. \end{cases} \tag{7.8}$$

Problem $\mathcal{M}_2$ can be solved by well-known interior-point methods [102]. We use `cvx` software [105] to solve this convex problem. Note that at each channel use this optimization problem is solved and the corresponding minimizing solution $\mathbf{x}$ determines the configuration of the load modulators. Furthermore, this optimization algorithm involves interior-point methods. Roughly speaking, this algorithm has $\sqrt{N_t}$ Newton steps and each step involves inversion of $N_t \times N_t$ matrices. Therefore, the complexity of the robust technique is roughly $\mathcal{O}({N_t}^3\sqrt{N_t})$. Although this technique is more complex than the non-robust one, it still has polynomial complexity, making its implementation feasible in a practical setting [92].

7.3 Performance Metrics

To evaluate the performance of the proposed robust precoder, we define three performance metrics: power efficiency, SINR and peak-to-average power ratio (PAPR). To be more precise, let T denote the number of channel uses. Then the power efficiency of the transmitter is defined as

$$\eta_t = \eta_a \frac{\frac{1}{T}\sum_{i=1}^{T} \mathbf{x}_i^H \mathbf{x}_i}{P_t}, \tag{7.9}$$

where η_a is the power efficiency of the power amplifier and $\mathbf{x}_i \in \mathcal{C}^{N_t}$ is the transmitted signal vector at channel use i, obtained as the solution of the optimization problem in (7.8). Here, we assume $\eta_a = 0.8$, which according to [116] is a typical value for a class F amplifier. In the calculation of the power efficiency, we assume that the power reflected back from the matching network is negligible. Instances of power being dissipated in the load modulators are exhibited in cases when $\mathbf{x}_i^H \mathbf{x}_i$ is less than P_t. The SINR at the user terminal is defined as

$$\text{SINR} = \frac{\frac{1}{T}\sum_{i=1}^{T} \|\mathbf{u}_i\|^2}{\frac{K}{f^2}\sigma^2 + \frac{1}{T}\sum_{i=1}^{T} \|\frac{1}{f}\mathbf{H}_i \mathbf{x}_i - \mathbf{u}_i\|^2}, \tag{7.10}$$

where $\mathbf{u}_i \in \mathcal{C}^K$ is the data vector of K users and $\mathbf{H}_i = [\mathbf{h}_{1,i}\ \mathbf{h}_{2,i}\ \cdots\ \mathbf{h}_{K,i}]^T \in \mathcal{C}^{K \times N_t}$ is the aggregate concatenated downlink channel matrix at channel use i; $\mathbf{h}_{k,i} \in \mathcal{C}_t^N$ is the channel vector for user k at channel use i. The PAPR is defined as

$$\text{PAPR} = \frac{\max_i \mathbf{x}_i^H \mathbf{x}_i}{\frac{1}{T}\sum_{i=1}^{T} \mathbf{x}_i^H \mathbf{x}_i}. \tag{7.11}$$

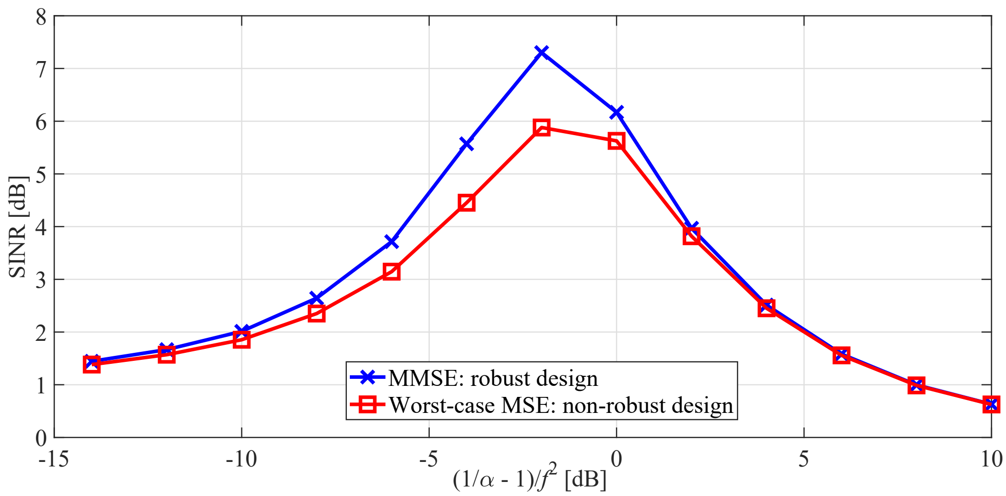

Figure 7.2: SINR for the robust and non-robust precoder vs. $(1/\alpha - 1)/f^2$ in the presence of worst-case channel uncertainty. $K = 40$, $N_t = 80$, $\varepsilon_k = 0.1$ for all $k \in \{1, 2, \cdots, K\}$ and $10\log_{10}(1/\sigma^2) = 8$ dB.

7.4 Simulation Results

Here, first we compare the robust design with the non-robust ones in Figs. 7.2 and 7.3 for the worst-case channel error. Fig. 7.2 shows the SINR in terms of $(1/\alpha - 1)/f^2$ for the robust and non-robust precoders for the worst-case channel uncertainty. We observe that the robust design outperforms the non-robust one. The maximum SINR of the the robust precoder is 1.15 dB higher that of the non-robust precoder. Note that changing $1/f$, which represents the equalizer parameter, changes the trade-off between interference and noise levels. Decreasing $1/f$ increases the interference, while decreasing the noise level. On the other hand, increasing $1/f$ decreases the interference, while increasing the noise level [60]. Since α is a constant for the figure, the peak value of SINR occurs at the optimum value of $1/f$ for the robust design with the given simulation parameters. Fig. 7.3 shows the MSE of the received signal with robust and non-robust precoder in the presence of the worst-case channel uncertainty for $T = 2500$. Again we observe that the robust

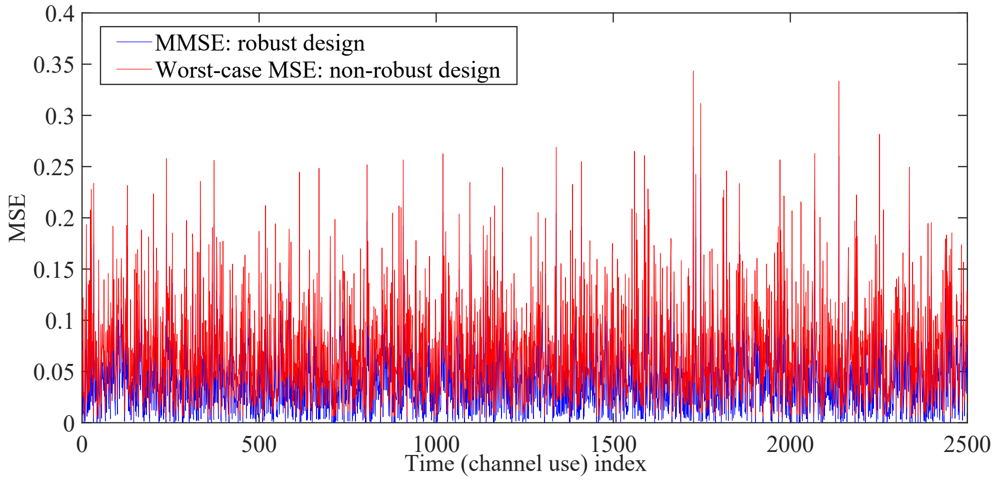

Figure 7.3: MSE of the received signal with the robust and non-robust precoder vs. channel use index in the presence of worst-case channel uncertainty. $K = 40$, $N_t = 80$, $\varepsilon_k = 0.1$ for all $k \in \{1, 2, \cdots, K\}$ and $10 \log_{10}(1/\sigma^2) = 8$ dB.

design exhibits lower MSE at all channel uses in the presence of the worst-case channel error.

Fig. 7.4 shows the SINR and power efficiency for the robust precoder in terms of $(1/\alpha - 1)/f^2$ for different noise power levels. We observe that there again exists an optimal value for $1/f$, at which SINR reaches its maximum. The existence of this optimal value is due to the trade-off between interference and noise levels as we mentioned before. As we decrease σ^2, which means higher SNR at the receiver, the maximum SINR is achieved at a higher $1/f$ value. This is intuitive since lowering the noise level means also lowering the level of interference, which corresponds to a higher $1/f$ value [60].

Fig. 7.5 shows the SINR and power efficiency for the robust precoder in terms of $(1/\alpha - 1)/f^2$ for different numbers of transmit antennas N_t. As the number of antennas increases, the power gain increases as well, which again corresponds to a higher level of $1/f$. Fig. 7.5 confirms the intuition that increasing the number of transmit antennas N_t results in a higher SINR, which implies better performance. Additionally, power efficiency

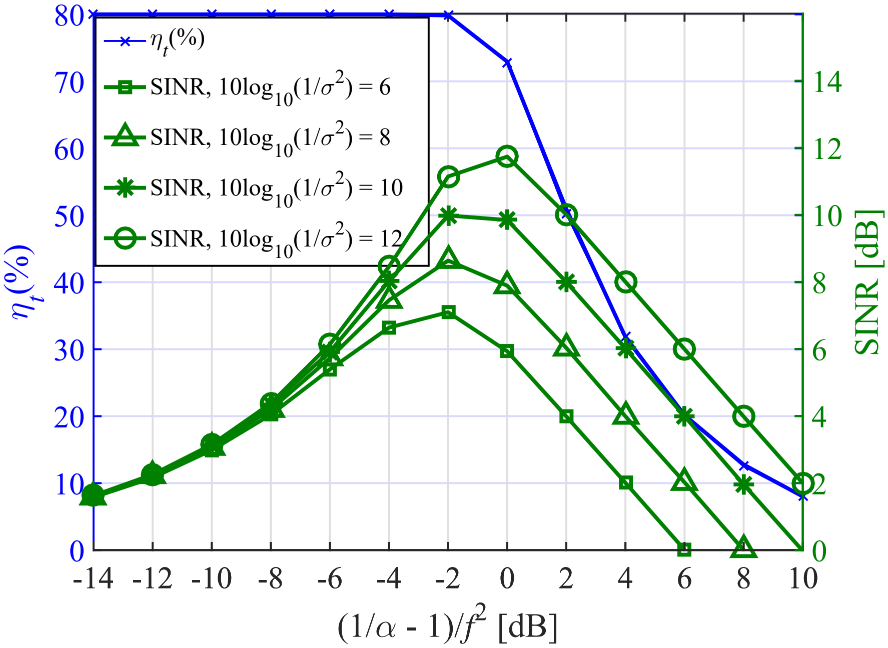

Figure 7.4: SINR and power efficiency for the robust precoder vs. $(1/\alpha - 1)/f^2$ for different noise powers, $K = 40$, ε_k=0.1 for all $k \in \{1, 2, \cdots, K\}$ and $M = 80$.

drops when the equalization parameter $1/f$ takes on a very high value, because in this case the power of the transmitted signal is reduced to minimize the MSE of the received signal. We observe from Fig. 7.5 that power efficiency is slightly less than 80% for $N_t = 200$ when SINR reaches its maximum value at 13.8 dB.

Fig. 7.6 shows the SINR and power efficiency for the robust precoder in terms of $(1/\alpha - 1)/f^2$ for different numbers of users K, while we keep $\alpha = K/N_t = 1/4$. We observe that both the SINR and the power efficiency are approximately the same irrespective of the number of users as we increase both the number of transmit antennas and the number of users keeping their ratio constant. Fig. 7.7 shows the SINR and PAPR for the robust precoder in terms of N_t/K. The instantaneous peak power at the transmitter is set to 1. In this analysis, we solve the optimization problem in (7.8) for different values of N_t/K. For each value of N_t/K we also find the optimal value of $1/f$, for which

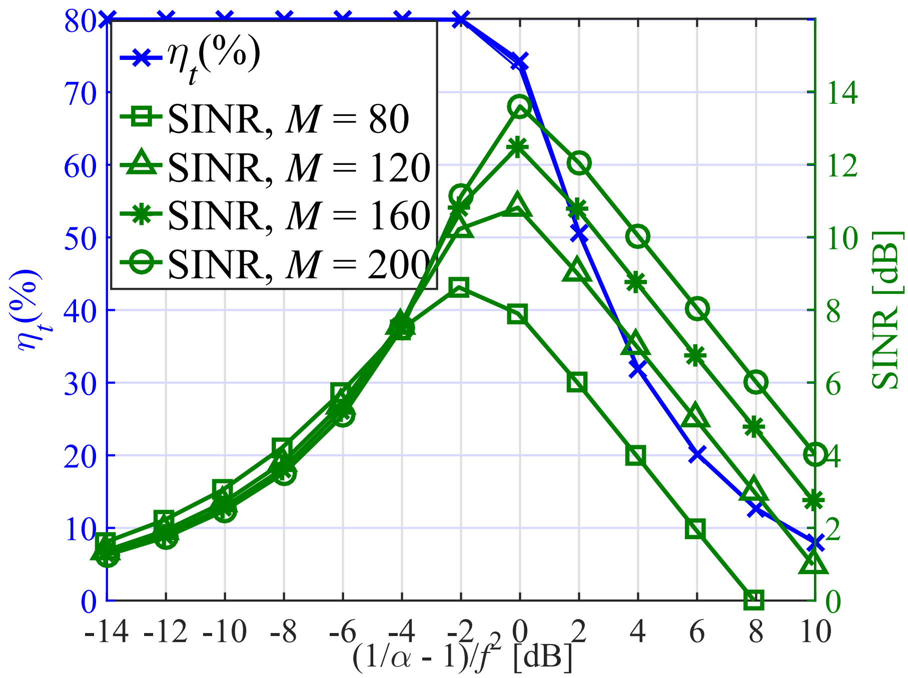

Figure 7.5: SINR and power efficiency for the robust precoder vs. $(1/\alpha - 1)/f^2$ for different numbers of transmit antennas N_t. $K = 40$, $\varepsilon_k = 0.1$ for all $k \in \{1, 2, \cdots, K\}$ and $10\log_{10}(1/\sigma^2) = 8$ dB.

the SINR reaches its maximum. Those maximal SINRs are shown in Fig. 7.7. The PAPR that is achieved by using that same $1/f$ value is also shown for each specific value of N_t/K. The curves in Fig. 7.7 demonstrate that the proposed precoder reaches high SINR values as we increase the ratio of the number of transmit antennas to the number of users, while maintaining a very low PAPR of less than about 0.61 dB. The proposed precoder reduces PAPR significantly at the price of slightly reduced performance; for the conventional MMSE precoder PAPR is between 8 dB and 12 dB [60]. The SINR in dB increases almost exactly logarithmically with N_t/K (i.e. SINR [dB] vs. $\log(N_t/K)$ is linear, so the linear (non-decibel) value of the SINR vs. N_t/K is also linear). Meanwhile, the PAPR in dB increases somewhat faster than that, but still slower than linearly with

N_t/K.

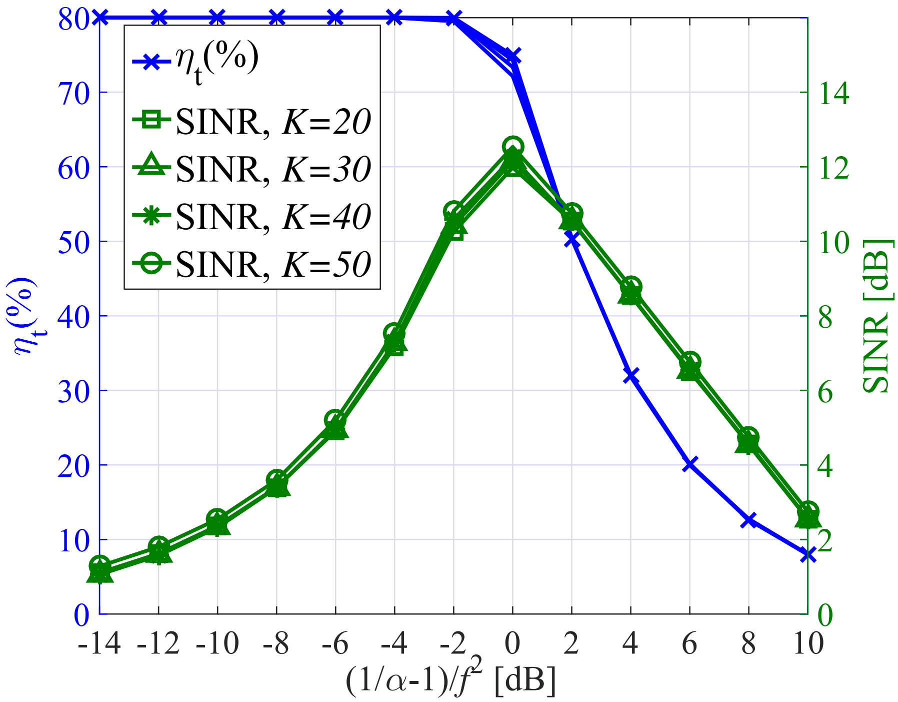

Figure 7.6: SINR and power efficiency for the robust precoder vs. $(1/\alpha - 1)/f^2$ for different numbers of users K. $\alpha = 1/4$, $\varepsilon_k = 0.1$ for all $k \in \{1, 2, \cdots, K\}$ and $10\log_{10}(1/\sigma^2) = 8$ dB.

7.5 Summary

We have introduced in this chapter a precoding technique for massive MIMO robust under the worst-case channel uncertainty. We have considered the peak power constraint in the design of the precoder, which is more relevant to actual implementation than the average power constraint. The proposed robust precoding technique has been applied to a single-RF-chain transmitter with only one power amplifier, in which the modulation is performed by a network of load modulators generating the desired signals on the antenna

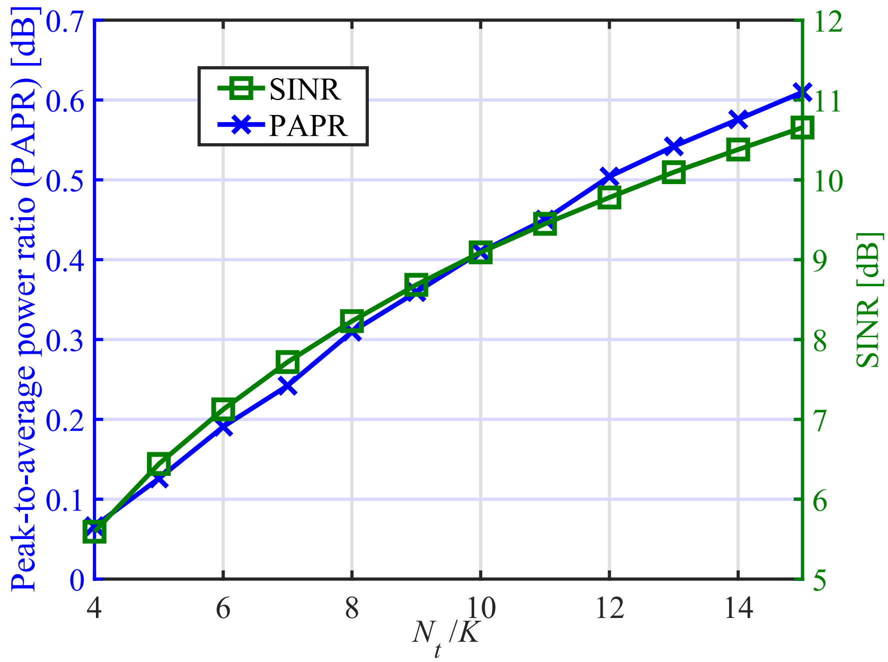

Figure 7.7: SINR and PAPR for the robust precoder vs. N_t/K. $K = 10$, $\varepsilon_k = 0.1$ for all $k \in \{1, 2, \cdots, K\}$ and $10\log_{10}(1/\sigma^2) = 0$ dB.

elements. The robust design attempts to minimize the MSE of the received signals at the user terminals for the worst-case channel uncertainty. We have assumed that the channel uncertainty is confined to a bounded region. We have demonstrated how to transform the resulting non-convex optimization problem of the precoder design into a convex problem, when a simple fixed equalizer is used at all user terminals. The simulation results have shown that the robust design achieves high power efficiency and SINR, as well as low PAPR, in the presence of the worst-case channel uncertainty.

Chapter 8

Conclusion

This chapter summarizes the major contributions of the thesis and gives directions for possible future work. The focus of the thesis is the development of reduced-complexity transmitter/receiver signal processing techniques and algorithms for evolving future broadband cellular systems. In particular, the focus of the thesis is on cost-efficient, implementable signal processing for massive MIMO systems, including hybrid precoding and exploitation of sparsity of channels to reduce complexity of implementation. These techniques display performance that is robust to implementation imperfections and channel uncertainty.

8.1 Summary of Contributions

First, in Chapter 3 we proposed a simplified path selection algorithm for massive MIMO channel, especially at mmWave frequencies, leveraging the sparse nature of the channel matrix. The proposed solution was designed based on a bipartite graph representing the AoDs between the BS and the users. The angular spread of AoDs was divided into N_t disjoint intervals. In the setup of angular bin concept, each bin was associated with one or more AoDs. The establishment of DFT beamforming vectors for each angular bin with orthogonal properties, guaranteed inter-beam interference cancellation. Then, the sum rate maximization function was formulated as an optimization problem where selected paths maximized the sum rate and reduced the inter-beam interference. Since the original problem formulation was not convex, we proposed a greedy approach to solve the optimization problem. In contrast to conventional coarse user selection algorithms discussed in literature, our proposed path selection method achieved higher throughput by taking advantage of multipath and multiuser diversity.

Inspired by the concept of path selection and bipartite graph, we proposed a two-layer beamforming scheme for massive MU-MIMO downlink channels in Chapter 4. The first layer employed a bipartite graph to dynamically group users in the beam-space domain; the aim was to minimize inter-user interference while significantly reducing the effective channel dimensionality. Then, with a focus on maximizing spatial multiplexing gain and system throughput, in the second layer a MU-MIMO linear precoding is performed within each group, which is a function of the effective channel.

We proposed a projection-based hybrid precoding algorithm for a hybrid precoding-combining transceiver in mmWave MIMO systems in Chapter 5. The algorithm was designed for the partially-connected structure employing fewer phase shifters; it reduced complexity and improved energy efficiency. Inspired by the principle of matrix factorization, we used projection algorithms to greatly simplify the design problem of digital baseband and analog RF precoders by dividing the design problem into two optimization subproblems, whose optimal solutions can be found. Additionally, we proposed a DFT-based mmWave channel estimation algorithm that efficiently detected the different parameters of the mmWave channel with a low training overhead, by leveraging the sparse nature of the mmWave channels.

In Chapter 6 we proposed a DFT-assisted user clustering hybrid precoding algorithm for an analog-digital hybrid precoding-combining transceiver. In this investigation, we considered a frequency-selective channel with an OFDM-based system. There are two possible structures for a hybrid architecture, namely fully-connected and partially-connected. We proposed algorithms to find near-optimal digital baseband and analog RF precoders for both structures. The algorithms made use of DFT-based user clustering to simplify the design of the analog RF precoders, and to add extra orthogonality to the system that improved the spectral efficiency compared to existing methods. The improved performance was demonstrated by system simulations. We also examined the energy efficiency of the system using our algorithms. Simulations demonstrated that the fully-connected structure was the most energy efficient when only a few RF chains were employed; otherwise, the partially-connected structure was more efficient.

Since the use of many RF chains to drive a large number of antennas at the transmitter quickly becomes impractical when that number of antennas increases, reducing the number of RF chains in massive MIMO systems is essential to reduce the system complexity and cost. In Chapter 7, considering a massive MIMO system with a single-RF-chain transmitter, we introduced a precoding technique that is robust in the presence of channel uncertainty. To make our design more realistic we considered the peak total transmitted power rather than the average power constraint. Also, we considered imperfect CSI with a bounded uncertainty region. In this transmitter structure, there was only one power amplifier and load modulation was used rather than voltage modulation to generate the desired signals on the antenna elements. We demonstrated that when a very simple fixed equalizer is used at all user terminals, the problem of minimizing the mean-square error of the received signals at user terminals under the worst-case channel uncertainty can be transformed into a convex optimization problem. We provided simulation results and demonstrated that the proposed robust precoding technique outperformed non-robust techniques in terms of power efficiency and signal-to-interference-plus-noise ratios.

8.2 Future Work

The multiplicative structure of the proposed simplified user grouping algorithm in Chapter 4 makes it suitable for application in hybrid architecture implementations. While we highlighted a simplified user grouping algorithm for this implementation, several open problems still need careful investigation. For example, it is important to develop novel and optimized solutions for implementing the inter-cell interference avoidance stage in the RF beamforming. One initial way to do that is by employing antenna elements that have electrically controlled directional patterns [117]. Further research is required to optimize this solution and facilitate its implementation, however. Another important challenge with hybrid architecture based multi-layer precoding is the channel knowledge acquisition. In Chapter 5, we outlined a DFT codebook design for a channel knowledge acquisition procedure to obtain the required channel knowledge for training a hybrid precoding transceiver. Implementation of this procedure with hybrid architecture will require further research. Estimation of the elevation interference covariance matrix when the channel is seen through an embedded RF lens [118] needs to be addressed in this context. Therefore, extending the hybrid architecture based channel estimation solution in Chapter 5 to the multi-layer precoding will be an important problem that future work may examine.

There are several possible directions for future research for mmWave channel estimation. In Chapter 5, we proposed a low-complexity mmWave channel estimation algorithm that leverages the sparse nature of the channel alongside adaptive compressed sensing tools. Extending this solution to multi-user system, however, is non-trivial. This is mainly due to the adaptive nature of the solution that causes the training overhead to scale with the number of users. One way to handle this scaling is by adopting random beamforming/measurement vectors [119]. Random beamforming and measurement allow all users to simultaneously estimate the channels, and hence decreases the associated training overhead. Therefore, it would be interesting to develop random compressed sensing based channel estimation algorithms for mmWave systems leveraging the sparse formulation developed in Chapter 5. Additionally, channel estimation with hybrid MIMO architectures with the beam-squint effect, that appears when the system bandwidth is very large, is another interesting research topic [120]. Under this effect, different subcarriers in an OFDM system will "see" distinct angles of arrival (AoAs) for the same path.

This thesis has focused on hybrid architecture based precoding and channel estimation algorithms that assume that RF circuit components and antennas are both ideal. Practical circuits and antennas, however, have non-ideal characteristics that can affect the real world performance of our algorithms. Thus, it is important to study the impact of hardware impairments on the performance of massive MIMO systems. For example, it is known that the fully-connected hybrid architecture has an array gain over the partially/dynamically-connected structure, but it is not clear what the net gain is if the insertion losses in the power dividers, combiners, and phase shifters are taken into consideration. Analyzing different hybrid architectures under practical RF circuit models is critical to provide an accurate evaluation of the different architectures. It would also be interesting to develop impairment-aware precoding and channel estimation solutions. Based on the insights that will be obtained from analyzing hybrid architectures under practical circuit models, it might be possible to design new optimized hybrid architectures, precoding, and channel estimation solutions that take these insights into consideration. An extension of the proposed hybrid precoding-combining technique, in Chapter 6, for when CSI is not perfect will require further investigation. Lastly, our proposed algorithms can be applicable to a wide range of mobile and vehicular communications. The performance of the proposed algorithms is dependent on the availability of CSI and AoDs/AoAs. However, [121] has demonstrated that the channel in a massive MIMO system can be tracked fairly accurately even at vehicular speeds. Consequently, our algorithm can be also applied in such scenarios.

Further, developing solutions that are more robust to the hardware impairments can boost the actual performance of hybrid architectures under practical conditions. Therefore, developing such hybrid architectures and associated signal processing solutions and analyzing their performance is important for future mmWave and massive MIMO systems.

Bibliography

[1] G. L. Stüber, *Principles of Mobile Communication*. Springer International Publishing, Cham, Switzerland, 4th edn., 2017.

[2] X. Foukas, G. Patounas, A. Elmokashfi, M. K. Marina, “Network slicing in 5G: survey and challenges,” *IEEE Commun. Mag.*, vol. 55, no. 5, pp. 94–100, May 2017.

[3] M. Agiwal, A. Roy, and N. Saxena, ”Next generation 5G wireless networks: a comprehensive survey,” *IEEE Commun. Surveys & Tutorials*, vol. 18, no. 3, pp. 1617–1655, Feb. 2016.

[4] F. Jejdling *et al.*, “Ericsson mobility report,” Ericsson, Stockholm, Sweden, Jun. 2019.

[5] *Measuring digital development: Facts and figures*, ITU Publications, 2019. [Online]. Available: https://www.itu.int/en/ITU-D/Statistics/Documents/facts/FactsFigures2019.pdf

[6] H. Bölcskei, D. Gesbert, C. Papadias, and A.J. van der Veen, Eds., *Space-Time Wireless Systems: From Array Processing to MIMO Communications*. Cambridge, U.K.: Cambridge Univ. Press, 2006.

[7] G. J. Foschini and M. J. Gans, ”On limits of wireless communications in a fading environment when using multiple antennas,” *Wireless Pers. Commun.*, vol. 6, no. 3, pp. 311–335, Mar. 1998.

[8] İ. E. Telatar, "Capacity of multi-antenna Gaussian channels," *Eur. Trans. Telecommun.*, vol. 10, no. 6, pp. 585–595, Nov./Dec. 1999.

[9] D.N.C. Tse and P. Viswanath, *Fundamentals of Wireless Communications*. Cambridge University Press, 2005.

[10] D. Gesbert, M. Kountouris, R.W. Heath Jr., C. Chae, and T. Salzer, "Shifting the MIMO Paradigm," *IEEE. Signal Process. Mag.*, vol. 24, no. 5, pp. 36–46, Sep. 2007.

[11] L. Zheng and D. Tse, "Communication on the Grassmann manifold: a geometric approach to the non-coherent multiple-antenna channel," *IEEE Trans. Inf. Theory*, vol. 48, no. 2, pp. 359–383, Feb. 2002.

[12] T. Marzetta and B. Hochwald, "Capacity of a mobile multiple-antenna communication link in Rayleigh flat fading," *IEEE Trans. Inf. Theory*, vol. 45, no. 1, pp. 139–157, Jan. 1999.

[13] M.K. Karakayali, G.J. Foschini, and R.A. Valenzuela, "Network coordination for spectrally efficient communications in cellular systems," *IEEE Wireless Commun. Mag.*, vol. 13, no. 4, pp. 56-–61, Aug. 2006.

[14] S. Jing, D.N.C. Tse, J.B. Soriaga, J. Hou, J.E. Smee, and R. Padovani, "Downlink macro-diversity in cellular networks," in *Proc. IEEE Int. Symp. on Inf. Theory (ISIT'07)*, Nice, France, June 2007, pp. 1–5.

[15] D. Gesbert, S. Hanly, H. Huang, S. Shamai Shitz, O. Simeone, and W. Yu, "Multi-cell MIMO cooperative networks: A new look at interference" *IEEE J. Sel. Areas Commun.*, vol. 28, no. 9, pp. 1380–1408, Dec. 2010.

[16] M. Sawahashi, Y. Kishiyama, A. Morimoto, D. Nishikawa, and M. Tanno, "Coordinated multipoint transmission/reception techniques for LTE-advanced

[coordinated and distributed MIMO]," *IEEE Wireless Commun.*, vol. 17, no. 3, pp. 26–34, June 2010.

[17] D. Lee, H. Seo, B. Clerckx, E. Hardouin, D. Mazzarese, S. Nagata, and K. Sayana, "Coordinated multipoint transmission and reception in LTE-advanced: deployment scenarios and operational challenges," *IEEE Commun. Mag.*, vol. 50, no. 2, pp. 148–155, Feb. 2012.

[18] J.G. Andrews, S. Buzzi, W. Choi, S.V. Hanly, A. Lozano, A.C.K. Soong, and J.C. Zhang, "What will 5G be?," *IEEE J. Sel. Areas Commun.*, vol. 32, no. 6, pp. 1065–1082, Jun. 2014.

[19] Peter Clarke. "Homepage." pedroc.co.uk. https://pedroc.co.uk (Jul. 5, 2020).

[20] LINKSYS. linksys.com. https://www.linksys.com/ca/p/P-EA9500 (Jul. 5, 2020).

[21] N. Jindal and A. Goldsmith, "Dirty-paper coding versus TDMA for MIMO broadcast channels," *IEEE Trans. Inf. Theory*, vol. 51, no. 5, pp. 1783–1794, May 2005.

[22] G. Caire and S. Shamai, "On achievable rates in a multi-antenna broadcast downlink," in *Proc. 38th Annu. Allerton Conf. Commun., Control and Comput.*, Monticello, IL, Oct. 2000.

[23] G. Caire and S. Shamai (Shitz), "On the achievable throughput of a multiantenna Gaussian broadcast channel," *IEEE Trans. Inf. Theory*, vol. 49, no. 7, pp. 1691–1706, Jul. 2003.

[24] M. Tomlinson, "New automatic equaliser employing modulo arithmetic," *Electron. Lett.*, vol. 7, no. 5, pp. 138–139, 25 1971.

[25] H. Harashima and H. Miyakawa, "Matched-transmission technique for channels with intersymbol interference," *IEEE Trans. Commun.*, vol. 20, no. 4, pp. 774–780, Aug. 1972.

[26] B. M. Hochwald, C. B. Peel, and A. L. Swindlehurst, "A vector-perturbation technique for near-capacity multiantenna multiuser communication-Part II: perturbation," *IEEE Trans. Commun.*, vol. 53, no. 3, pp. 537–544, Mar. 2005.

[27] A. Dabbagh and D. Love, "Precoding for multiple antenna Gaussian broadcast channels with successive zero-forcing," *IEEE Trans. Signal Process.*, vol. 55, no. 7, pp. 3837–3850, July 2007.

[28] T.L. Marzetta, "Non-cooperative cellular wireless with unlimited numbers of base station antennas," *IEEE Trans. Wireless Commun.*, vol. 9, no. 11, pp. 3590–3600, Nov. 2010.

[29] F. Rusek, D. Persson, B.K. Lau, E.G. Larsson, T.L. Marzetta, O. Edfors, and F. Tufvesson, "Scaling up MIMO: Opportunities and challenges with very large arrays," *IEEE Signal Process. Mag.*, vol. 30, no. 1, pp. 40–60, Jan. 2013.

[30] E.G. Larsson, O. Edfors, F. Tufvesson, and T. L. Marzetta, "Massive MIMO for next generation wireless systems," *IEEE Commun. Mag.*, pp. 186–195, Feb. 2014.

[31] E. Björnson, E.G. Larsson, and T. L. Marzetta, "Massive MIMO: ten myths and one critical question," *IEEE Commun. Mag.*, vol. 54, no. 2, pp. 114–123, Feb. 2016.

[32] J. Jose, A. Ashikhmin, T.L. Marzetta, and S. Vishwanath, "Pilot contamination and precoding in multi-cell TDD systems," *IEEE Trans. Wireless Commun.*, vol. 10, no. 8, pp. 2640–2651, Aug. 2011.

[33] F. Fernandes, A. Ashikhmin, and T. Marzetta, “Inter-cell interference in non-cooperative TDD large scale antenna systems,” *IEEE J. Sel. Areas Commun.*, vol. 31, no. 2, pp. 192–201, 2013.

[34] A. Ashikhmin and T. Marzetta, “Pilot contamination precoding in multi-cell large scale antenna systems,” in *Proc. IEEE International Symposium on Information Theory (ISIT’12)*, Cambridge, USA, Jul. 2012, pp. 1137–1141.

[35] R.R. Müller, L. Cottatellucci, and M. Vehkaperä, “Blind pilot decontamination,” *IEEE J. Sel. Topics Signal Process.*, vol. 8, no. 5, pp. 773–786, Oct. 2014.

[36] H.Q. Ngo and E. Larsson, “EVD-based channel estimation in multicell multiuser MIMO systems with very large antenna arrays,” in *Proc. IEEE International Conference on Acoustics, Speech and Signal Processing (ICASSP’12)*, Kyoto, Japan, March 2012, pp. 3249–3252.

[37] T.S. Rappaport, G.R. MacCartney, Jr., M.K. Samimi, and S. Sun, “Wideband millimeter-wave propagation measurements and channel models for future wireless communication system design,” *IEEE Trans. Commun.*, vol. 63, no. 9, pp. 3029–3056, Sept. 2015.

[38] T.S. Rappaport, R.W. Heath Jr., R.C. Daniels, and J.N. Murdock, *Millimeter Wave Wireless Communications*. Upper Saddle River, NJ: Prentice Hall, 2014.

[39] A. Ghosh, R. Ratasuk, B. Mondal, N. Mangalvedhe, and T. Thomas, “LTE-advanced: next-generation wireless broadband technology,” *IEEE Wireless Commun.*, vol. 17, no. 3, pp. 10–22, Jun. 2010.

[40] T.S. Rappaport, S. Sun, R. Mayzus, H. Zhao, Y. Azar, K. Wang, G.N. Wong, J.K. Schulz, M. Samimi, and F. Gutierrez, “Millimeter wave mobile communications for 5G cellular: It will work!,” *IEEE Access*, vol. 1, pp. 335–349, May 2013.

[41] Y. Niu, Y. Li, D. Jin, L. Su, and A.V. Vasilakos, "A survey of millimeter wave communications (mmWave) for 5G: opportunities and challenges," *Wireless Netw.*, vol. 21, no. 8, pp. 2657–2676, Nov. 2015.

[42] Y. Azar, G.N. Wong, K. Wang, R. Mayzus, J.K. Schulz, H. Zhao, F. Gutierrez, Jr.D. Hwang, and T.S. Rappaport, "28 GHz propagation measurements for outdoor cellular communications using steerable beam antennas in New York City," in *Proc. IEEE Int. Conf. Commun. (ICC)*, Budapest, Hungary, Jun. 2013, pp. 5143–5147.

[43] R.W. Heath Jr., N. Gonzalez-Prelcic, S. Rangan, W. Roh, and A.M. Sayeed, "An overview of signal processing techniques for millimeter wave MIMO systems," *IEEE J. Sel. Topics Signal Process.*, vol. 10, no. 3, pp. 436–453, Apr. 2016.

[44] V. Venkateswaran and A.-J. van der Veen, "Analog beamforming in MIMO communications with phase shift networks and online channel estimation," *IEEE Trans. Signal Process.*, vol. 58, no. 8, pp. 4131–4143, Aug. 2010.

[45] L. Chen, Y. Yang, X. Chen, and W. Wang, "Multi-stage beamforming codebook for 60GHz WPAN," in *Proc. 6th Int. ICST Conf. Commun. Netw. in China (CHINACOM)*, Harbin, China, Aug. 2011, pp. 361–365.

[46] Y.M. Tsang, A.S.Y. Poon, and S. Addepalli, "Coding the beams: Improving beamforming training in mmWave communication system," in *Proc. IEEE Global Commun. Conf. (GLOBECOM)*, Houston, TX, USA, Dec. 2011, pp. 1–6.

[47] S. Hur, T. Kim, D.J. Love, J.V. Krogmeier, T.A. Thomas, and A. Ghosh, "Millimeter wave beamforming for wireless backhaul and access in small cell networks," *IEEE Trans. Commun.*, vol. 61, no. 10, pp. 4391–4403, Oct. 2013.

[48] X. Gao, O. Edfors, F. Tufvesson, and E.G. Larsson, "Massive MIMO in real propagation environments: Do all antennas contribute equally?" *IEEE Trans. Commun.*, vol. 63, no. 11, pp. 3917–3928, Nov. 2015.

[49] O. El Ayach, S. Rajagopal, S. Abu-Surra, Z. Pi, and R.W. Heath, Jr., "Spatially sparse precoding in millimeter wave MIMO systems," *IEEE Trans. Wireless Commun.*, vol. 13, no. 3, pp. 1499–1513, Mar. 2014.

[50] Z. Ni, J. A. Zhang, K. Yang, F. Gao and J. An, "Low-complexity subarray-based RF precoding for wideband multiuser millimeter wave systems," *IEEE Trans. Veh. Tech.*, vol. 69, no. 7, pp. 8028–8033, July 2020.

[51] H. Zhang, H. Zhang, W. Liu, K. Long, J. Dong and V. C. M. Leung, "Energy efficient user clustering, hybrid precoding and power optimization in terahertz MIMO-NOMA systems," *IEEE J. Sel. Areas Commun.*, vol. 38, no. 9, pp. 2074–2085, Sept. 2020.

[52] A.F. Molisch, V.V. Ratnam, S. Han, Z. Li, S.L.H. Nguyen, L. Li, and K. Haneda, "Hybrid beamforming for massive MIMO: A survey," *IEEE Commun. Mag.*, vol. 55, no. 9, pp. 134–141, Sept. 2017.

[53] A. Adhikary, J. Nam, J.-Y. Ahn, and G. Caire, "Joint spatial division and multiplexing—The large-scale array regime," *IEEE Trans. Inf. Theory*, vol. 59, no. 10, pp. 6441–6463, Oct. 2013.

[54] A. Adhikary, E. Al Safadi, M. k. Samimi, R. Wang, G. Caire, T. S. Rappaport, and A. F. Molisch, "Joint spatial division and multiplexing for mmWave channels," *IEEE J. Sel. Areas Commun.*, vol. 32, no. 6, pp. 1239–1255, Jun. 2014.

[55] M.A. Sedaghat, R.R. Müller, and G. Fischer, "A novel single-RF transmitter for massive MIMO," in *Proc. 18^{th} ITG Workshop on Smart Antennas*, Erlangen, Germany, March 2014, pp. 1–8.

[56] R.R. Müller and M.A. Sedaghat, "RF MIMO transmitter with load modulation." European Patent Application WO 2015001116 A1, filed July 2014.

[57] R.R. Müller, M.A. Sedaghat, and G. Fischer, "Load modulated massive MIMO," in *Proc. IEEE Global Conf. Signal and Information Process.*, Atlanta, USA, Dec. 2014, pp. 622–626.

[58] M.A. Sedaghat, V.I. Barousis, R.R. Müller, and C.B. Papadias, "Load modulated arrays: A low-complexity antenna," *IEEE Commun. Mag.*, vol. 54, no. 3, pp. 46–52, March 2016.

[59] K. Lee, I.-D. Choi, and J. Lee, "Design of impedance loading board supporting load-modulated beamspace MIMO single RF system," in *Proc. IEEE Int. Symp. Antennas and Propagation USNC/URSI National Radio Science Meeting*, Vancouver, Canada, July 2015, pp. 131–132.

[60] M.A. Sedaghat, R.R. Müller, and G. Fischer, "Broadcast precoding for massive MIMO subject to an instantaneous total power constraint," in *Proc. IEEE Global Commun. Conf.*, Austin, USA, Dec. 2014, pp. 1637–1641.

[61] D. Gesbert, M. Kountouris, R. W. Heath Jr., C. B. Chae, and T. Sälzer, "Shifting the MIMO paradigm," *IEEE Signal Process. Mag.*, vol. 24, no. 5, pp. 36–46, Sept. 2007.

[62] M. Costa, "Writing on dirty paper," *IEEE Trans. Inf. Theory*, vol. 29, no. 3, pp. 439–441, 1983.

[63] S. Vishwanath, N. Jindal, and A. Goldsmith, "Duality, achievable rates, and sum-rate capacity of Gaussian MIMO broadcast channels," *IEEE Trans. Inf. Theory*, vol. 49, no. 10, pp. 2658–2668, Oct. 2003.

[64] N. Jindal, S. Vishwanath, and A. Goldsmith, "On the duality of Gaussian multiple access and broadcast channels," *IEEE Trans. Inform. Theory*, vol. 50, no. 5, pp. 768–783, May 2004.

[65] P. Viswanath and D.N. Tse, "Sum capacity of the vector Gaussian channel and uplink-downlink duality,“ *IEEE Trans. Inform. Theory*, vol. 49, no. 8, pp. 1912–1921, Aug. 2003.

[66] H. Weingarten, Y. Steinberg, and S. Shamai (Shitz), "The capacity region of the Gaussian multiple-input multiple-output broadcast channel," *IEEE Trans. Inf. Theory*, vol. 52, no. 9, pp. 3936–3964, Sept. 2006.

[67] N. Jindal, W. Rhee, S. Vishwanath, S. A. Jafar, and A. Goldsmith, "Sum power iterative water-filling for multi-antenna Gaussian broadcast channels," *IEEE Trans. Inf. Theory*, vol. 51, no. 4, pp. 1570–1580, Apr. 2005.

[68] M. Joham, W. Utschick and J. A. Nossek, "Linear transmit processing in MIMO communications systems," *IEEE Trans. Signal Process.*, vol. 53, no. 8, pp. 2700–2712, Aug. 2005.

[69] C. B. Peel, B. M. Hochwald and A. L. Swindlehurst, "A vector-perturbation technique for near-capacity multiantenna multiuser communication-part I: channel inversion and regularization," *IEEE Trans. Commun.*, vol. 53, no. 1, pp. 195–202, Jan. 2005.

[70] Q. Spencer, A. L. Swindlehurst, and M. Haardt, "Zero-forcing methods for downlink spatial multiplexing in multiuser MIMO channels," *IEEE Trans. Sig. Proc.*, vol. 52, no. 2, pp. 462–471, Feb. 2004.

[71] R. Chen, R. W. Heath Jr., and J. G. Andrews, “Transmit selection diversity for unitary precoded multiuser spatial multiplexing systems with linear receivers,” *IEEE Trans. Sig. Proc.*, vol. 55, no. 3, pp. 1159–1571, March 2007.

[72] E. G. Larsson, O. Edfors, F. Tufvesson and T. L. Marzetta, “Massive MIMO for next generation wireless systems,” *IEEE Commun. Mag.*, vol. 52, no. 2, pp. 186–195, Feb. 2014.

[73] A. Papoulis, and S. U. Pillai *Probability, Random Variables and Stochastic Processes*. McGraw-Hill, New York, USA, 4th edn., 2001.

[74] E. Björnson, J. Hoydis, and L. Sanguinetti, *Massive MIMO Networks: Spectral, Energy, and Hardware Efficiency*, NOW Publishers, 2017.

[75] B. M. Hochwald, T. L. Marzetta, and V. Tarokh, “Multiple-antenna channel hardening and its implications for rate feedback and scheduling,” *IEEE Trans. Inf. Theory*, vol. 50, no. 9, pp. 1893–1909, Sept. 2004.

[76] S. Gunnarsson, J. Flordelis, L. Van der Perre and F. Tufvesson, “Channel hardening in massive MIMO – A measurement based analysis,” in *Proc. 2018 IEEE 19th Int. Workshop on Signal Processing Advances in Wireless Communications (SPAWC 2018)*, Kalamata, Greece, 2018, pp. 1–5.

[77] T. L. Narasimhan and A. Chockalingam, “Channel hardening-exploiting message passing (CHEMP) receiver in large-scale MIMO systems,” *IEEE J. of Sel. Topics Signal Process.*, vol. 8, no. 5, pp. 847–860, Oct. 2014.

[78] Y.-H. Nam, B. L. Ng, K. Sayana, Y. Li, J. Zhang, Y. Kim, and J. Lee, “Full-dimension MIMO (FD-MIMO) for next generation cellular technology,” *IEEE Commun. Mag.*, vol. 51, no. 6, pp. 172–179, June 2013.

[79] Y. Kim, H. Ji, J. Lee, Y.-H. Nam, B. L. Ng, I. Tzanidis, Y. Li, and J. Zhang, "Full dimension MIMO (FD-MIMO): The next evolution of MIMO in LTE systems," *IEEE Wireless Commun. Mag.*, vol 21, no. 2, pp. 26–33, Apr. 2014.

[80] L. Sanguinetti, E. Björnson and J. Hoydis, "Toward massive MIMO 2.0: understanding spatial correlation, interference suppression, and pilot contamination," *IEEE Trans. Commun.*, vol. 68, no. 1, pp. 232–257, Jan. 2020.

[81] E. Björnson, J. Hoydis, M. Kountouris, and M. Debbah, "Massive MIMO systems with non-ideal hardware: Energy efficiency, estimation, and capacity limits," *IEEE Trans. Inf. Theory*, vol. 60, no. 11, pp. 7112–7139, Nov. 2014.

[82] J. Vieira, F. Rusek, and F. Tufvesson, "Reciprocity calibration methods for massive MIMO based on antenna coupling," in *Proc. IEEE Global Commun. Conf. (GLOBECOM)*, Dec. 2014.

[83] X. Chen, S. Zhang and Q. Li, "A review of mutual coupling in MIMO systems," *IEEE Access*, vol. 6, pp. 24706–24719, Apr. 2018.

[84] R. Deng, Z. Jiang, S. Zhou and Z. Niu, "How often should CSI be updated for massive MIMO systems with massive connectivity?," in *Proc. GLOBECOM 2017 - 2017 IEEE Global Communications Conference*, Singapore, 2017, pp. 1-6.

[85] M. Soleimani, M. Mazrouei-Sebdani, W.A. Krzymień, and J. Melzer, "A path selection algorithm for sparse massive MIMO channels," in *Proc. IEEE 50th Asilomar Conf. on Signals, Systems, and Computers*, Pacific Grove, USA, Nov. 2016, pp. 208–212.

[86] A.M. Sayeed, "Deconstructing multiantenna fading channels," *IEEE Trans. Signal Process.*, vol. 50, no. 10, pp. 2563–2579, Oct. 2002.

[87] M. Soleimani, M. Mazrouei-Sebdani, R. C. Elliott, W. A. Krzymień, and J. Melzer, "Simplified user grouping algorithm for massive MIMO on sparse beam-space channels," *IEICE Trans. Commun.*, vol. E102–B, no. 3, pp. 623–631, Mar. 2019.

[88] E. Jacobsen and R. Lyons, "The sliding DFT," *IEEE Signal Process. Mag.*, vol. 20, no. 2, pp. 74–80, Mar. 2003.

[89] T.H. Cormen, C.E. Leiserson, R.L. Rivest, and C. Stein, Introduction to Algorithms, 3rd ed., The MIT Press, Cambridge, MA, USA, 2009.

[90] J. Brady, N. Behdad, and A.M. Sayeed, "Beamspace MIMO for millimeter-wave communications: System architecture, modeling, analysis, and measurements," *IEEE Trans. Antennas Propag.*, vol. 61, no. 7, pp. 3814–3827, Jul. 2013.

[91] M. Soleimani, R. C. Elliott, W. A. Krzymień, J. Melzer, and P. Mousavi, "Hybrid beamforming and DFT-based channel estimation for millimeter wave MIMO systems," in *Proc. 28th Int. Symp. on Personal, Indoor and Mobile Radio Commun. (PIMRC)*, Montreal, Canada, Oct. 2017, pp. 1–7.

[92] G.H. Golub, and C.F. Van Loan, *Matrix computations*. The John Hopkins University Press, Baltimore, USA, 4th edn., 2013.

[93] A.M. Davie and A.J. Stothers, "Improved bound for complexity of matrix multiplication," *Proc. Royal Soc. Edinburgh: Section A Mathematics*, vol. 143, no. 2, pp. 351–369, Apr. 2013.

[94] A. Garcia-Rodriguez, V. Venkateswaran, P. Rulikowski, and C. Masouros, "Hybrid analog-digital precoding revisited under realistic RF modeling," *IEEE Wireless Commun. Lett.*, vol. 5, no. 5, pp. 528–531, Oct. 2016.

[95] D. Mi, M. Dianati, S. Muhaidat, and Y. Chen, “A novel antenna selection scheme for spatially correlated massive MIMO uplinks with imperfect channel estimation,” in *Proc. IEEE 81st Veh. Technol. Conf. (VTC 2015-Spring)*, Glasgow, UK, May 2015, pp. 1–6.

[96] X. Gao, L. Dai, Z. Chen, Z. Wang, and Z. Zhang, “Near-optimal beam selection for beamspace mmWave massive MIMO systems,” *IEEE Commun. Lett.*, vol. 20, no. 5, pp. 1054–1057, May 2016.

[97] J. Nam, A. Adhikary, J.-Y. Ahn, and G. Caire, “Joint spatial division and multiplexing: Opportunistic beamforming, user grouping and simplified downlink scheduling,” *IEEE J. Sel. Topics Signal Process.*, vol. 8, no. 5, pp. 876–890, Oct. 2014.

[98] S. Han, C.-L I, Z. Xu, and C. Rowell, “Large-scale antenna systems with hybrid analog and digital beamforming for millimeter wave 5G,” *IEEE Comm. Mag.*, vol. 53, no. 1, pp. 186–194, Jan. 2015.

[99] A. Alkhateeb, O. El Ayach, G. Leus, and R.W. Heath, Jr., “Channel estimation and hybrid precoding for millimeter wave cellular systems,” *IEEE J. Sel. Topics Signal Process.*, vol. 8, no. 5, pp. 831–846, Oct. 2014.

[100] D.P. Palomar, J. M. Cioffi, and M. A. Lagunas, “Joint Tx-Rx beamforming design for multicarrier MIMO channels: a unified framework for convex optimization,” *IEEE Trans. Signal Process.*, vol. 51, no. 9, pp. 2381–2401, Sept. 2003.

[101] D.P. Palomar and M. Chiang, “A tutorial on decomposition methods for network utility maximization,” *IEEE J. Sel. Areas Commun.*, vol. 24, no. 8, pp. 1439–1451, Aug. 2006.

[102] S. Boyd, and L. Vandenberghe, *Convex optimization*. Cambridge University Press, Cambridge, UK, 2004.

[103] I. Pólik and T. Terlaky, "A survey of the S-lemma," *SIAM Review*, vol. 49, no.3, pp. 371–418, 2007.

[104] A. Beck, "Quadratic matrix programming," *SIAM J. Optimization*, vol. 17, no. 4, pp. 1224–1238, 2007.

[105] M. Grant, and S. Boyd, "CVX: Matlab software for disciplined convex programming," version 2.1, March 2017, http://cvxr.com/cvx.

[106] M. Soleimani, R.C. Elliott, W.A. Krzymień, J. Melzer, and P. Mousavi "Hybrid beamforming for mmWave massive MIMO systems employing DFT-assisted user clustering," *IEEE Trans. Veh. Tech.*, vol. 69, no. 10, pp. 11646-11658, Oct. 2020.

[107] K-L. Du and M. N. S. Swamy, *Wireless Communication Systems: From RF Subsystems to 4G Enabling Technologies.* Cambridge, UK: Cambridge Univ. Press, 2010.

[108] Q. H. Spencer, A. L. Swindlehurst, and M. Haardt, "Zero-forcing methods for downlink spatial multiplexing in multiuser MIMO channels," *IEEE Trans. Signal Process.*, vol. 52, no. 2, pp. 461–471, Feb. 2004.

[109] E. Zhang and C. Huang, "On achieving optimal rate of digital precoder by RF-baseband codesign for MIMO systems," in *Proc. 80th IEEE Veh. Technol. Conf. (VTC 2014-Fall)*, Vancouver, Canada, Sept. 2014, pp. 1–5.

[110] A. F. Molisch, *Wireless Communications*, 2nd ed. Chichester, UK: Wiley, 2011.

[111] K. Zu and R. C. de Lamare, “Low-complexity lattice reduction-aided regularized block diagonalization for MU-MIMO systems,” *IEEE Commun. Lett.*, vol. 16, no. 6, pp. 925–928, Jun. 2012.

[112] A. Alkhateeb, G. Leus, and R. W. Heath, Jr., “Limited feedback hybrid precoding for multi-user millimeter wave systems,” *IEEE Trans. Wireless Commun.*, vol. 14, no. 11, pp. 6481–6494, Nov. 2015.

[113] M. Soleimani, M. Mazrouei-Sebdani, R.C. Elliott, W.A. Krzymień, and J. Melzer, “Robust precoder design for massive MIMO with peak total power constrained single-RF-chain transmitters,” *IET Commun.*, vol. 11, no. 17, pp. 2667–2672, Nov. 2017.

[114] J. Wang, M. Bengtsson, B. Ottersten, D.P. Palomar, “Robust MIMO precoding for several classes of channel uncertainty,” *IEEE Trans. Signal Process.*, vol. 61, no. 12, pp. 3056–3070, Dec. 2013.

[115] A. Tajer, N. Prasad, and X. Wang, “Robust linear precoder design for multi-cell downlink transmission,” *IEEE Trans. Signal Process.*, vol. 59, no. 1, pp. 235–251, Jan. 2011.

[116] A. Grebennikov, and S. Bulja, “High-efficiency Doherty power amplifiers: Historical aspect and modern trends,” *Proc. IEEE*, vol. 100, no. 12, pp. 3190–3219, Dec. 2012.

[117] V. V. Ratnam, A. F. Molisch, O. Y. Bursalioglu and H. C. Papadopoulos, “Hybrid beamforming with selection for multiuser massive MIMO systems,” *IEEE Trans. Signal Process.*, vol. 66, no. 15, pp. 4105–4120, Aug. 2018.

[118] T. Kwon, Y. Lim, B. Min and C. Chae, “RF lens-embedded massive MIMO systems: fabrication issues and codebook design,” *IEEE Trans. Microw. Theory Techn.*, vol. 64, no. 7, pp. 2256–2271, July 2016.

[119] C. Tsai and A. Wu, “Structured random compressed channel sensing for millimeter-wave large-scale antenna systems,” *IEEE Trans. Signal Process.*, vol. 66, no. 19, pp. 5096–5110, Oct. 2018.

[120] J. Rodriguez-Fernandez and N. Gonzalez-Prelcic, “Channel estimation for frequency-selective mmWave MIMO systems with beam-squint,” in *Proc. 2018 IEEE Global Communications Conference (GLOBECOM)*, Abu Dhabi, United Arab Emirates, Dec. 2018, pp. 1–6.

[121] P. Harris *et al.*, “Performance characterization of a real-time massive MIMO system with LOS mobile channels,” *IEEE J. Sel. Areas Commun.*, vol. 35, no. 6, pp. 1244–1253, Jun. 2017.

[122] C. Ingemarsson and O. Gustafsson, “On fixed-point implementation of symmetric matrix inversion,” in *Proc. 2015 Europ. Conf. Circuit Theory Design*, Trondheim, Norway, Aug. 2015.

Appendix A

Computational Complexity of Matrix Operations

The exact complexity of a matrix operation depends strongly on the hardware implementation, including the bit width (i.e., the number of binary digits used to represent a number) and the data type (e.g., floating point or fixed point). In this section, we provide first-order approximations by counting the number of complex multiplications and divisions that are needed, while the complexity of additions/subtractions is neglected since these operations are much easier to implement in hardware.

Lemma 1. Consider matrices $\mathbf{A} \in \mathcal{C}^{N_1 \times N_2}$ and $\mathbf{B} \in \mathcal{C}^{N_2 \times N_3}$. The matrix multiplication $\mathbf{AB}$ requires $N_1 N_2 N_3$ complex multiplications. The $\mathbf{AA}^H$ multiplication only requires $\frac{N_1^2+N_1}{2} N_2$ complex multiplications by using the Hermitian symmetry.

Proof. There are $N_1 N_3$ elements in $\mathbf{AB}$ and the computation of each of them involves N_2 multiplications. In the case of $\mathbf{B} = \mathbf{A}^H$, the Hermitian symmetry is only used to compute $\frac{N_1^2+N_1}{2}$ elements which represent the main diagonal and half of the off-diagonal elements.

When the inverse of a matrix is multiplied by another matrix, the $\mathbf{LDL}^H$ decomposition can be used to achieve an efficient hardware implementation, both in terms of computations and memory usage. The matrix $\mathbf{L}$ is a lower triangular with ones on the main diagonal and $\mathbf{D}$ is a diagonal matrix.

Lemma 2. Consider the Hermitian positive semi-definite matrix $\mathbf{A} \in \mathcal{C}^{N_1 \times N_1}$ and

and the matrix $\mathbf{B} \in \mathcal{C}^{N_1 \times N_2}$. The $\mathbf{LDL}^H$ decomposition of $\mathbf{A}$ can be computed using $\frac{N_1^3 - N_1}{3}$ complex multiplications. The matrix $\mathbf{A}^{-1}\mathbf{B}$ can be computed using $N_1^2 N_2$ complex multiplications and N_1 complex divisions if the $\mathbf{LDL}^H$ decomposition of $\mathbf{A}$ is known.

Proof. Efficient algorithms for computing the $\mathbf{LDL}^H$ decomposition and its corresponding number of multiplications can be found in [122]. Note that $\mathbf{A}^{-1}\mathbf{B}$ can be computed by solving N_2 linear systems of equations. If $\mathbf{LDL}^H$ is known it can be used to solve the system of linear equations by forward-backward substitution requires N_1^2 multiplications per system. N_1 additional divisions are required to calculate $\mathbf{D}^{-1}$.

Appendix B

Proof of Orthogonality of Angular Bins

Here, we consider the orthogonality between user clusters and its effect on inter-beam interference. On subcarrier k, let us assume a beamforming matrix $\mathbf{F}_a[k] = \mathbf{F}_{\text{RF}}^{c_a}\mathbf{F}_{\text{BB},a}^{c_a}[k]$ for user a and $\mathbf{F}_b[k] = \mathbf{F}_{\text{RF}}^{c_b}\mathbf{F}_{\text{BB},b}^{c_b}[k]$ for user b, where the two users are in different clusters c_a and c_b, with $c_a \neq c_b$. We focus on a single AoD interval for each group (i.e., one angular bin) and a single subcarrier k; the extension to multiple intervals/bins is trivial, and the discussion is applicable to any subcarrier. Let the interval be $[\theta_a - \Delta, \theta_a + \Delta]$ for user a and $[\theta_b - \Delta, \theta_b + \Delta]$ for user b. Since the users are in different clusters, their AoD intervals are disjoint. As we have stated in Section 6.2.2 (discussing fully-connected structures), the phases for an analog RF precoder $\mathbf{F}_{\text{RF}}^{c}$ can be made equal to angles in the angular bins for cluster c. The same argument holds for $\mathbf{F}_{\text{RF}}^{c}$ with partially-connected structures (discussed in Section 6.3).

An indication of the amount of interference between user groups can be found by

$$\frac{1}{N_t}\left\|\left(\mathbf{F}_a[k]\right)^H \mathbf{F}_b[k]\right\|_F^2 = \frac{1}{N_t}\left\|\left(\mathbf{F}_{\text{BB},a}^{c_a}[k]\right)^H \left(\mathbf{F}_{\text{RF}}^{c_a}\right)^H \mathbf{F}_{\text{RF}}^{c_b}\mathbf{F}_{\text{BB},b}^{c_b}[k]\right\|_F^2. \tag{B.1}$$

We note the identities $\|\mathbf{A}\|_F^2 = \operatorname{tr}\left(\mathbf{A}\mathbf{A}^H\right)$ and $\operatorname{tr}(\mathbf{AB}) = \operatorname{tr}(\mathbf{BA})$ for $\mathbf{A}$ and $\mathbf{B}$ having compatible dimensions. Furthermore, $\mathbf{A}\mathbf{A}^H$ will be positive semi-definite. If $\mathbf{A}$ and $\mathbf{B}$ are positive semi-definite, then it holds that $\operatorname{tr}(\mathbf{AB}) \leq \operatorname{tr}(\mathbf{A})\operatorname{tr}(\mathbf{B})$. From these facts, we have:

$$
\begin{aligned}
&\left\|(\mathbf{F}_{\text{BB},a}^{c_a}[k])^H(\mathbf{F}_{\text{RF}}^{c_a})^H\mathbf{F}_{\text{RF}}^{c_b}\mathbf{F}_{\text{BB},b}^{c_b}[k]\right\|_F^2 \\
&\quad = \operatorname{tr}\left(\left(\mathbf{F}_{\text{BB},a}^{c_a}[k]\right)^H(\mathbf{F}_{\text{RF}}^{c_a})^H\mathbf{F}_{\text{RF}}^{c_b}\mathbf{F}_{\text{BB},b}^{c_b}[k]\left(\mathbf{F}_{\text{BB},b}^{c_b}[k]\right)^H \times \ (\mathbf{F}_{\text{RF}}^{c_b})^H\,\mathbf{F}_{\text{RF}}^{c_a}\mathbf{F}_{\text{BB},a}^{c_a}[k]\right) \\
&\quad = \operatorname{tr}\left((\mathbf{F}_{\text{RF}}^{c_a})^H\,\mathbf{F}_{\text{RF}}^{c_b}\mathbf{F}_{\text{BB},b}^{c_b}[k]\left(\mathbf{F}_{\text{BB},b}^{c_b}[k]\right)^H(\mathbf{F}_{\text{RF}}^{c_b})^H\,\mathbf{F}_{\text{RF}}^{c_a} \times \mathbf{F}_{\text{BB},a}^{c_a}[k]\left(\mathbf{F}_{\text{BB},a}^{c_a}[k]\right)^H\right) \\
&\quad \leq \operatorname{tr}\left((\mathbf{F}_{\text{RF}}^{c_a})^H\,\mathbf{F}_{\text{RF}}^{c_b}\mathbf{F}_{\text{BB},b}^{c_b}[k]\left(\mathbf{F}_{\text{BB},b}^{c_b}[k]\right)^H(\mathbf{F}_{\text{RF}}^{c_b})^H\,\mathbf{F}_{\text{RF}}^{c_a}\right) \times \operatorname{tr}\left(\mathbf{F}_{\text{BB},a}^{c_a}[k]\left(\mathbf{F}_{\text{BB},a}^{c_a}[k]\right)^H\right) \\
&\quad = \operatorname{tr}\left((\mathbf{F}_{\text{RF}}^{c_b})^H\,\mathbf{F}_{\text{RF}}^{c_a}(\mathbf{F}_{\text{RF}}^{c_a})^H\,\mathbf{F}_{\text{RF}}^{c_b}\mathbf{F}_{\text{BB},b}^{c_b}[k]\left(\mathbf{F}_{\text{BB},b}^{c_b}[k]\right)^H\right) \times \operatorname{tr}\left(\left(\mathbf{F}_{\text{BB},a}^{c_a}[k]\right)^H\mathbf{F}_{\text{BB},a}^{c_a}[k]\right) \\
&\qquad \leq \operatorname{tr}\left((\mathbf{F}_{\text{RF}}^{c_b})^H\,\mathbf{F}_{\text{RF}}^{c_a}(\mathbf{F}_{\text{RF}}^{c_a})^H\,\mathbf{F}_{\text{RF}}^{c_b}\right)\operatorname{tr}\left(\mathbf{F}_{\text{BB},b}^{c_b}[k]\left(\mathbf{F}_{\text{BB},b}^{c_b}[k]\right)^H\right) \times \operatorname{tr}\left(\left(\mathbf{F}_{\text{BB},a}^{c_a}[k]\right)^H\mathbf{F}_{\text{BB},a}^{c_a}[k]\right) \\
&\qquad = \operatorname{tr}\left((\mathbf{F}_{\text{RF}}^{c_a})^H\,\mathbf{F}_{\text{RF}}^{c_b}(\mathbf{F}_{\text{RF}}^{c_b})^H\,\mathbf{F}_{\text{RF}}^{c_a}\right)\operatorname{tr}\left(\left(\mathbf{F}_{\text{BB},b}^{c_b}[k]\right)^H\mathbf{F}_{\text{BB},b}^{c_b}[k]\right) \times \operatorname{tr}\left(\left(\mathbf{F}_{\text{BB},a}^{c_a}[k]\right)^H\mathbf{F}_{\text{BB},a}^{c_a}[k]\right) \\
&\qquad = N_{s,a}N_{s,b}\left\|(\mathbf{F}_{\text{RF}}^{c_a})^H\,\mathbf{F}_{\text{RF}}^{c_b}\right\|_F^2
\end{aligned} \tag{B.2}
$$

where the last line follows from the power constraint in (6.12), so $\operatorname{tr}\left(\left(\mathbf{F}_{\text{BB},u}^{c}[k]\right)^H\mathbf{F}_{\text{BB},u}^{c}[k]\right) = \operatorname{tr}\left(\mathbf{I}_{N_{s,u}}\right) = N_{s,u}$ for any u and c. Hence, overall we have $\left\|(\mathbf{F}_a[k])^H\,\mathbf{F}_b[k]\right\|_F^2 \leq N_{s,a}N_{s,b}\left\|(\mathbf{F}_{\text{RF}}^{c_a})^H\,\mathbf{F}_{\text{RF}}^{c_b}\right\|_F^2$.

We can now focus on the analog RF precoders. Consider also the ULA response vector in (6.5). By letting $N_t \to \infty$, we have:

$$
\begin{aligned}
\Theta_{a,b} &= \lim_{N_t\to\infty}\frac{N_{s,a}N_{s,b}}{N_t}\left\|(\mathbf{F}_{\text{RF}}^{c_a})^H\,\mathbf{F}_{\text{RF}}^{c_b}\right\|_F^2 \\
&= \lim_{N_t\to\infty}\frac{N_{s,a}N_{s,b}}{N_t}\int_{\alpha\in\mathcal{S}_a}\int_{\beta\in\mathcal{S}_b}\delta\left(\alpha-\beta\right)d\alpha d\beta
\end{aligned} \tag{B.3}
$$

where $\mathcal{S}_a = [N_t q\sin(\theta_a-\Delta), N_t q\sin(\theta_a+\Delta)]$, $\mathcal{S}_b = [N_t q\sin(\theta_b-\Delta), N_t q\sin(\theta_b+\Delta)]$, and $\delta(\cdot)$ is the Dirac delta function. In the limit of $N_t \to \infty$, $\Theta_{a,b}$ will be the measure of overlap between the two AoD intervals. Since the intervals are disjoint (as are $\mathcal{S}_a$ and $\mathcal{S}_b$), the result is zero.

A similar derivation can be made for the use of a UPA with the array response given in (6.6) instead of a ULA. In that case, the intervals/bins involve both azimuth and elevation angles θ and ϕ, respectively. The two-dimensional bins will still be disjoint; though two bins may share the same interval for either θ or ϕ, or a portion thereof, they will not share the same intervals for both angles. Consequently, the final result will be the 2-D overlap of the intervals, which is still zero.

Appendix C

Proof of Lemma 7.1

Proof. Its proof is straightforward and is a simple application of Lemma 1 in [115]. For the sake of completeness, we outline the proof here. We can expand the objective function in (7.6) as

$$\left|\frac{1}{f}\left(\widetilde{\mathbf{h}}_k+\boldsymbol{\delta}_k\right)\mathbf{x}-u_k\right|^2=\left|\frac{1}{f}\widetilde{\mathbf{h}}_k\mathbf{x}-u_k\right|^2+\left|\frac{1}{f}\boldsymbol{\delta}_k\mathbf{x}\right|^2+2\left(\frac{1}{f}\boldsymbol{\delta}_k\mathbf{x}\right)\left(\frac{1}{f}\widetilde{\mathbf{h}}_k\mathbf{x}-u_k\right).$$

To get the maximum of the objective function, vector $\boldsymbol{\delta}_k$ must have the maximum norm ε_k and be in the direction of $\mathbf{x}$. Additionally, $\frac{1}{f}\boldsymbol{\delta}_k\mathbf{x}$ must have the same sign as $\frac{1}{f}\widetilde{\mathbf{h}}_k\mathbf{x}-u_k$. Therefore, $\boldsymbol{\delta}_k=\operatorname{sgn}\left(\frac{1}{f}\widetilde{\mathbf{h}}_k\mathbf{x}-u_k\right)\varepsilon_k\frac{\mathbf{x}^H}{\|\mathbf{x}\|}$. Substituting this $\boldsymbol{\delta}_k$ into the optimization problem (7.5) gives the maximum (7.6). ■